RELATIONSHIPS BETWEEN PROCESS VARIATION, NUCLEATION, AND THE MICROSTRUCTURE OF CASTINGS

By

KENNETH JOHN EGER II

Chemical Engineering
University of Cincinnati
Cincinnati, Ohio
1963

Master of Science
University of Cincinnati
Cincinnati, Ohio
1965

Submitted to the Faculty of the Graduate College
of the Oklahoma State University
in partial fulfillment of the requirements
for the Degree of
DOCTOR OF PHILOSOPHY
May, 1976

Thesis
1976D
E29r
Cop. 2

OKLAHOMA STATE UNIVERSITY LIBRARY

RELATIONSHIPS BETWEEN PROCESS VARIATION, NUCLEATION, AND THE MICROSTRUCTURE OF CASTINGS

Thesis Approved:

Thesis Adviser

Dean of the Graduate College

964138

PREFACE

This study is concerned with the mechanisms of nucleation and growth of metal from a melt. Particular emphasis was placed on the effort to define the principles underlying the growth of a population of small randomly oriented crystals in the center of alloy ingots. Enhancing the development of such a population would produce a final product with more desirable properties, and could lead to a better understanding of the processes which take place as a metal solidifies.

Metal specimens were solidified under a variety of circumstances, and then examined microscopically to see the effects of each change.

The author wishes to express his deep appreciation to Dr. C. E. Price, his technical adviser, for direction, insights, encouragement and help. The direction in the mechanics of the study by Dr. J. R. Norton; the assistance of Dr. John B. West; and the lining of copper molds with glass by Professor John H. O'Toole, were also greatly appreciated.

A note of thanks is given to George Cooper, Preston Wilson, and the Mechanical Engineering staff for help in the preparation of molds and fixtures, and to Velda Davis for her help in preparing the final copy.

Finally, a special thank you is due to my wife, Dottie, and our children, Duane and Kathie, for their sacrifice and patience when the work competed with them for my time.

TABLE OF CONTENTS

LIST OF TABLES

LIST OF FIGURES

LIST OF SYMBOLS

a, A	- To designate locations in diagrams; also a constant
b, B	- To designate locations in diagrams
c	- Concentration of solute in the liquid
C	- To designate locations in diagrams
Cp	- Heat capacity
D	- To designate locations in diagrams
E_a	- Activation energy
G	- Gibbs Free Energy
G_s	- Gibbs Free Energy of the solid phase
GLCM	- Glass lined copper mold
H	- Enthalpy
I_s	- Crystal nuclei formation frequency per unit area of catalyst
k	- Rate constant for uni- or bi-molecular reactions
K	- 1/T
L	- Latent Heat of fusion
MCB	- Producer of tin, Matheson, Coleman and Bell
MRC	- Producer of tin, Materials Research Corporation
P	- Log t½
p	- Pressure
r	- Radius of crystal or embryo
r*	- Critical radius of crystal embryo

S - Entropy

t - Time

$t_{1/2}$ - Half-time for the deactivation reaction

T - Temperature

T_B - Bath temperature

T_e - Equilibrium temperature

T_H - Temperature where homogeneous nucleation begins

T_v - Temperature where solidification begins

T_p - Temperature predicted

T_R - Temperature where heterogeneous nucleation begins

U - Empirical energy factor

v - Volume

V - Empirical shape factor

W - Empirical contact factor

x - Area of impurity covered by crystal cap

X - Distance in the X direction

X_o - Initial concentration of solute in the melt

y - Area of crystal cap adjacent to the liquid

σ - Surface energy (joules/cm^2)

$\sigma_{\alpha L}$ - Surface energy of the solid-liquid interface

$\sigma_{\beta L}$ - Surface energy of the impurity-liquid interface

$\sigma_{\alpha\beta}$ - Surface energy of the solid-impurity interface

CHAPTER I

INTRODUCTION

The properties of a metal depend on the strength and direction of the metallic bonds, on the size and shape of the crystals (grains) which make it up, on dislocations within the grains, and on voids, inclusions and other large scale defects. The control of the grain size of a metal is important because dislocations do not move across grain boundries, and the principle mechanism for metal deformation is via the motion of dislocations. Therefore, fine uniform grains, which limit this motion, give the metal added tensile and yield strength, toughness, and hardness.

Experimentation with metals has uncovered many alloying or heat treating techniques which give desired grain sizes and, therefore, these desired properties. Partial grain size control has been achieved in various metal forming fields. In powder metallurgy control is achieved through the selection of a powder of the proper size and the choice of optimum sintering conditions. During electrodeposition grain size control is achieved through variations in current density and agitation. Grain sizes in castings are usually controlled by selecting a special cooling rate or by the addition of materials (grain refiners) which alter the grain size.

The primary emphasis of this work is in the development of a basic understanding of the processes which determine the microstructure of

castings. Significant reductions in grain size have been achieved through enhancing the formation of a fine-grained zone often found in the center of ingets, through nucleation in undercooled melts, and in response to external influences during solidification, such as vibration or stirring. However, the events which favor the nucleation of greater numbers of crystals are not well defined. Many mechanisms have been suggested, each with a measure of experimental evidence. These include showering, chill crystal migration, fragmentation of existing crystals, cavitation in the liquid, homogeneous nucleation, pressure pulses in the solid, constitutional supercooling, and recrystallization.

The purposes of this study were twofold. The first was to review the literature dealing with the mechanisms for solidification and nucleation, and the structural variations which can result. Then an experimental program was carried out based on questions revealed in the literature survey, and issues which remained unresolved. This program was to investigate the mechanisms for forming crystal nuclei that were responsible for the significant grain size reductions observed experimentally.

A better definition of the active mechanisms and the conditions where each is dominant will allow for better selection of the casting process variables and, therefore, better as-cast properties. In addition, in the many cases where casting is followed by processes like annealing and cold working, better as-cast properties mean that fewer additional steps are needed. Costs would be reduced and energy would be saved.

CHAPTER II

SOLIDIFICATION OF A PURE METAL

A liquid solidifies as the temperature is decreased because the free energy of the solid phase becomes less than that of the liquid phase. The free energy may be given by the following expression:

$$G = H - TS \tag{1}$$

H is the enthalpy, T is the absolute temperature, and S is the entropy. The temperature dependence of the free energy G is found by differentiation of Equation (1) (Hamill and Williams, 1959).

$$dG = -vdp - SdT \tag{2}$$

Since vdp is negligible for condensed systems, the temperature normalized change in free energy is proportional to -S.

$$dG/dT = -S \tag{3}$$

Now S for liquids is larger than S for the corresponding solid because there are more statistically independent ways of distributing particles among the available quantum states in the liquid. This dependence of the free energy upon temperature is displayed diagrammatically in Figure 1. Each expression for free energy is shown as a straight line of negative slope, with the slope of the line representing the free energy of the liquid being steeper. At one temperature, $T = T_e$, the free energy of the solid and the liquid are identical. At this equilibrium

temperature both a solid and its melt can coexist. Above this temperature the liquid is stable and any solid present will melt. The opposite is true for $T < T_e$. The solid is stable and any liquid present will freeze.

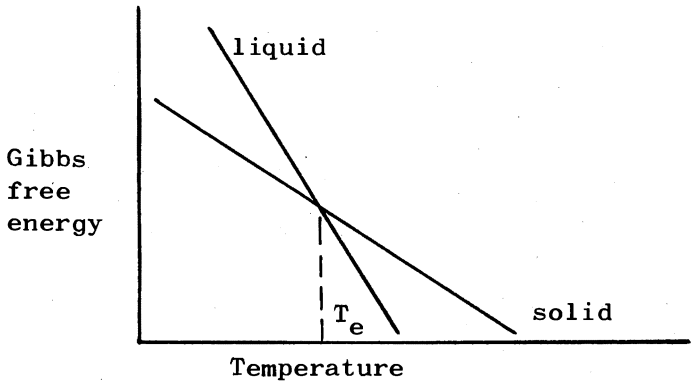

Figure 1. Temperature Dependence of the Gibbs Free Energy for the Solid and Liquid Phase of a Single Substance

When a pure substance in the liquid state is cooled to $T < T_e$ there is a barrier that must be overcome before the first solid can form. This barrier exists because the formation of a solid-liquid interface deprives atoms along that surface of some of their former nearest neighbors. Just as a box packed randomly with spheres has a high void volume along the sides and bottom, there are more spaces between the atoms of liquid at the interface than there are in the bulk liquid. The energy that must be supplied to move atoms from the bulk liquid to form the surface is termed the interfacial energy. It is abbreviated by σ and has the units of joules/cm^2. The total energy

required to form a surface is the product of the interfacial energy and the surface area. Energy which could be used to form the surface is released whenever a solid is formed. This occurs because there is a difference between the potential energy of the solid and the precursor liquid which is released during solidification. The amount of this release varies with the amount of material solidified. The net free energy change, including the energy required to form the surface and the energy released by freezing is given for the ideal case when the solid formed is spherical.

$$\Delta G = 4\pi r^2\sigma - L\Delta T(4\pi r^3)/3T \qquad (4)$$

Here $L\Delta T/T$ is the change in free energy for solidification at T, $\Delta T = T_e - T$, and L is the latent heat of fusion in compatible units. It can be shown from Equation (4) that ΔG will be positive for small ΔT and small r. In this case crystals of solid will not form unless (1) the amount of undercooling is increased, or (2) the radius of the solid crystal formed is large.

Homogeneous Nucleation

Homogeneous nucleation occurs when the undercooling is so great that crystallites already existing in the liquid are big enough to form a stable nucleus. The required size can be defined by differentiation of Equation (4). $d(\Delta G)/dT$ has an extremum

$$r^* = 2\sigma T/L\Delta T \qquad (5)$$

defined by ΔT and r. The r^* in Equation (5) is the critical radius. Crystallites with radii greater than r^* will grow as rapidly as the

latent heat of fusion can be removed. If in a liquid at $T < T_e$ all the crystallites are small ($r < r^*$) solidification will be postponed. Then as the amount of supercooling is increased r^* will decrease until it is less than the radius of some of the crystallites present. The solidification that follows is extremely rapid, and it produces a sample with a very fine grain size.

Experience with many high purity metals shows that undercoolings on the order of $0.2T_e$ can be obtained before homogeneous nucleation takes place. Much of the early work was done by Turnbull and Cech (1950) and Turnbull (1950). Table I shows some of the maximum undercoolings he reported and their relation to the equilibrium temperatures of the metals tested.

TABLE I

MAXIMUM SUPERCOOLINGS FOR VARIOUS METALS*

Metal	Supercooling °C	Equilibrium Temperature °K	Relative Undercooling ($\%T_e$)
Tin	118	505	23
Bismuth	90	544	17
Lead	80	601	13
Antimony	135	904	15
Silver	227	1234	18
	292**	1234	24
Copper	236	1356	17
	277**	1356	20
Nickel	319	1725	18
Iron	295	1808	16

*Turnbull, 1950; Holloman and Turnbull, 1953.

**Scripov, Koverda, and Butorin, 1972.

Heterogeneous Nucleation

Nuclei can be formed from small crystallites if impurities are present. The atoms in the crystallite may form a "cap" on the surface of an impurity particle. The apparent radius of this cap may be greater than the critical radius (Equation (5)) even though the volume of the cap is much smaller than the volume of a sphere having the critical radius. If so, the impurity-plus-cap will serve as a nucleus for crystal growth. In forming a cap such as the one shown in Figure 2 a surface of area x between the liquid and the impurity is replaced by the same area of cap-impurity surface plus a cap-liquid surface of area y. The net change in surface energy is given in Equation (6).

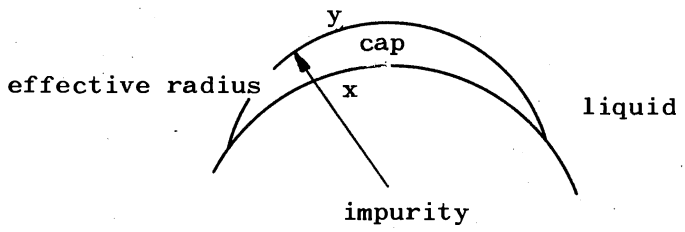

Figure 2. The Creation of a Heterogeneous Nucleus by the Condensation of a Crystallite to Form a Cap

$$\Delta G_s = y\sigma_{\alpha L} + x\sigma_{\alpha\beta} - x\sigma_{\beta L} \qquad (6)$$

If the interfacial energies for tin and lead that are quoted by Crosley and Mondolfo (1951) are used in Equation (6) and areas x and y are assumed to be practically equal, ΔG_s, the change in the free energy of

the surface for cap formation, is negative. Hence, the

$$\Delta G_s = x(33 + 25 - 62) = -4x \qquad (7)$$

cap will form spontaneously for any tin crystallite, no matter what its size. Then if the effective radius is sufficiently large, this capped impurity serves as a nucleus for the growth of a crystal of tin. The effectiveness of an impurity, in this case metallic lead, in catalyzing nucleation in a pure metal (tin) is demonstrated in Table II.

TABLE II

UNDERCOOLING RESULTS REPORTED FOR TIN

Maximum Undercooling °C	Purity	Authors
36	.999 and .99999	This paper
37	.999	Glicksman and Childs (1962)
33	.99999	Iyer and Youdelis (1972)
39*	.99999	Iyer and Youdelis (1972)
105	not specified	Turnbull (1950)
118	not specified	Holloman and Turnbull (1953)
0	lead present	Crosley and Mondolfo (1971)

*rapid cooling

Crosley, Douglas and Mondolfo (1968) and Crosley and Mondolfo (1971) concur in emphasizing the importance of the relative interfacial energies on the formation of a stable heterogeneous nucleus. They were able to demonstrate that nucleation catalysis could not be explained by the relative compatibility of the crystal structures of nucleant and

nucleus. Their work, and subsequent work by Powell and Colligan (1969) showed that nucleation in a binary system is a one-way process; i.e., if one of the components will serve as a nucleant for the other, the second will not nucleate the first. The following empirical expression is reported for predicting the efficiency of a nucleation catalyst:

$$(\Delta T_R/\Delta T_H)^{2/3} = (UV)^{1/3}(1-W(\sigma_{\alpha L} + \sigma_{\beta L} - \sigma_{\alpha\beta})/\sigma_{\alpha L})) \qquad (8)$$

U, V, and W are energy, shape, and contact factors. $\Delta T_R/\Delta T_H$ is the ratio of undercoolings for heterogeneous nucleation to homogeneous nucleation.

The interfacial energy term in Equation (8) is different from the one developed through Equation (6) because the initial conditions are not the same. This term is consistent with the development of a heterogeneous nucleus from a solid embryo and a particle of impurity surrounded by liquid instead of the liquid and impurity alone (Equation (6)). The proper choice is not clear. Chernov (1973) draws a distinction between the structures of crystallites in liquids (clusters) and the structure of the solid (Chernov, 1973). In addition, Leychkis and Mikhaylov (1970) suggest that nucleation occurs in two stages, embryo formation and then deformation to a crystal structure that has long range stability. On the other hand, calculations using Equation (8) predict the undercooling for heterogeneous nucleation reasonably well. This is shown in Table III.

TABLE III

UNDERCOOLINGS FOR HETEROGENEOUS NUCLEATION IN BINARY SYSTEMS -- OBSERVED AND CALCULATED*

System	Solid Crystals Present	Undercooling (°C) Experimental	Calculated
Pb-Sn	Pb	>40	35
Pb-Sn	Sn	0	0
Ag-Cu	Ag	>53	225
Ag-Cu	Cu	29	29

*Crosley and Mondolfo, 1971.

Undercooling

Several methods have been tried to achieve large undercoolings in pure metals. All of the methods were designed to control or eliminate the impurity content, either in the bulk sample or on its surface. One or more of the following experimental techniques were invariably used: the use of high purity metals, the use of samples broken from large pieces of stock, the cleaning of the sample surface by etching, the use of inert atmospheres or vacuum, the use of non-crystalline substrates, immersion in high boiling liquids, or subdivision of the sample into very small pieces.

Turnbull and Cech (1950) were the earliest to systematically achieve supercoolings which correspond to homogeneous nucleation. They used small particles (10 to 100 microns in diameter) and observed their solidification microscopically. They were melted on flakes of freshly blown quartz or pyrex glass in a controlled atmosphere (H_2, He or in vacuum).

Efforts to supercool bulk samples more than $0.1T_e$ have not been so successful. Turnbull attributes this to the increased probability of finding a suitable impurity when the sample is large.

Much work has been done toward identification of the impurities which prevent homogeneous nucleation and the quantification of their effects. Turnbull (1952) used dilatometric techniques to follow the solidification of small mercury droplets, first coated and then dispersed in a fluid. The temperature of isothermal solidification and the particle size distribution were varied and the volume fraction of the mercury that was solidified was determined. Nucleation of mercury coated with mercury laurate was found to be homogeneous. However, droplets coated with mercury acetate solidified at a rate proportional to their surface area. The acetate was concluded to be effective in catalyzing the heterogeneous nucleation of mercury. In addition, Turnbull calculated values for I_s, the frequency of crystal nuclei formation per unit area of catalyst. The behavior of acetate coated droplets was consistent with a constant, I_s; but I_s was variable for drops coated with mercury stearate. Nucleation was heterogeneous since the stearate coated drops solidified about 19° above the temperature for homogeneous nucleation, so the variation in I_s was attributed to the presence of more than one kind of effective catalyst. Vonnegut (1948) had a similar finding. He was unable to explain the solidification rate of oxide coated tin droplets on the basis that a single catalyst was present.

Glicksman and Childs (1962) were able to show that substantial reductions in the amount of supercooling for tin samples could be achieved by the introduction of six substances (Pt, Y, Ag, TiC, MoS, and

Al). Five other substances (SiC, Al_2O_3, CeS, MgO, and C) had no effect. They attributed this to catalysis of heterogeneous nucleation when the equilibrium contact angle between the embryo and the impurity is small (a small contact angle corresponds to a well wetted surface) and/or when $(\sigma_{\alpha L} - \sigma_{\alpha\beta})$ is large.

Takahashi and Tiller (1969) examined small droplets of lead, tin, and bismuth microscopically. High purity metals (99.9999) and a purified hydrogen atmosphere were used. They observed a marked variation in the undercooling when the droplet size was changed. This variation in the log-diameter was better described by $\Delta T/T_s$ than by ΔT alone so surface patches, either the result of the inevitable oxides present, or existing purely for molecular reasons were believed to be the sites where nucleation occurred. The difficulty in achieving a large enough flat patch on a small droplet would then account for the larger supercooling observed.

Powell and Hogan (1968) report recent successes in supercooling bulk samples of several metals (Fe, Ni, and Co) when the samples were solidified under a glass slag. They were able to use a similar technique to undercool 400 gram samples of copper 208°C when others had only been able to achieve a ΔT of 60°. The impurities were believed to be oxidized and then dissolved by the glass slag. Cu_2O was eliminated as the impurity of record when planned Cu_2O additions failed to prevent substantial undercooling of copper; i.e., the copper had undercooled 82°C with solid Cu_2O present. Other papers by Bradshaw et al. (1958) and Powell (1965) also show that nucleation of a metal by its oxide does not occur for small amounts of undercooling.

The undercooling of a pure metal is seen to be dependent on the

most effective catalyst present. While some of these catalysts are removed by routine measures, others have only been eliminated by subdivision or by dissolution in a flux. With all of the catalysts removed, supercooling can be increased to the point where homogeneous nucleation occurs.

External Effects on Undercooling

The effects of superheating on the crystal structure of an ingot are well known. Chalmers (1964) explained that increased superheating caused remelting of the chill crystals formed when hot metal is poured into a cold mold. However, Glicksman and Childs (1962) observed a similar effect when the mold and melt were heated and cooled together. They found a step increase in the supercooling of 8°C (from 1 to 9°C) when the superheating was increased beyond 12°C. Clearly the nucleation events were heterogeneous. The change was ascribed to the deactivation or removal of the most potent catalyst.

According to Crosley and Mondolfo (1971), this effect is now well known. What remains to be determined is the cause. Evidence demonstrating local nucleation and inefficient use of available nucleants suggests that only one part of the nucleant is active. Mascre (1971) explains that size, orientation and a cluster-nucleant coincidence are needed before a nucleant can effect a nucleation event. Crosley and Mondolfo (1971) say that a good nucleant-crystal atomic fit may be needed that can only be achieved if a rarely present high-order crystal plane on the nucleant is available or if vacancies or faults are present. However, experiments showing the deactivation of nucleants by superheating could not be used to select the proper mechanism because

superheating would (1) equilibrate the nucleant surfaces probably destroying any high-order planes, (2) anneal out faults and vacancies, or (3) cause the nucleant to dissolve.

Takahashi and Tiller (1969) reported that there was no evidence that the amount of superheating or the time at superheat had any effect on supercooling. Yet, heterogeneous nucleation did occur, at a supercooling of about 36°C for tin, about 16° for lead, and 42° for bismuth.

A variety of potential nucleants could be present in technical grade metals. Then if the more effective ones had a lower deactivation energy (or a higher solubility) they could be removed easily to achieve moderate undercoolings. Less effective but stable ones, perhaps oxides (Powell and Hogan, 1968 and Bradshaw, Gasper, and Pearson, 1958) would prevent cooling to homogeneous nucleation and resist removal. The high purity metals used by Takahashi and Tiller (1969) could very well be free of the more effective nucleants, and not be free of oxygen.

Crystal Microstructure

The structure formed by the solidification of a pure metal reflects its thermal history. The shape of the crystals formed during solidification depend on the temperature gradient across the solid-liquid interface and the amount of undercooling. The various temperature gradients may be resolved topologically into the two forms shown in Figure 3. In the first case, the heat of fusion is removed by conduction through the solid and the stable interface geometry is a plane. In the second case, the heat is removed in part by conduction into the liquid. Here a planar interface is unstable because the plane is located at the point in the liquid least favorable to growth. Any

perturbation in the plane results in the insertion of part of the solid into a region where growth is faster. Then the growth rate of this part exceeds that of the remainder of the plane. The planar interface is modified by a pencil shaped grain or several such grains protruding from the surface. This kind of growth form, a dendritic crystal structure, is typical of solidification which occurs in a supercooled melt.

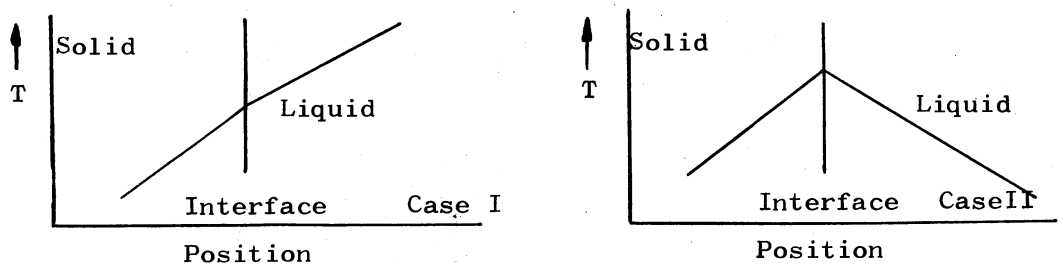

Figure 3. Generalized Temperature Profiles for the Two Mechanisms Applicable to Solidification of Pure Metals

Planar solidification is important in growing single crystals and in zone refining where the controlled addition of heat to the liquid is essential. The dendritic growth mechanism is the predominant form in the initial solidification of castings, as some supercooling nearly always occurs.

Dendritic growth is rapid because the heat sink for the dissipation of the latent heat is the supercooled liquid adjacent to the dendrite itself. Several authors (Rosenberg and Winegard, 1954; Orrok, 1958; and Yesin, Pankin, and Nasyroo, 1971) have reported values for the linear

growth rate of tin dendrites. However, Table IV shows that substantial disagreement exists between them.

TABLE IV

COMPARISON OF DENDRITIC GROWTH RATES IN TIN SUPERCOOLED 11°C

Dendrite Growth Rate cm/sec	Reference
22	Rosenberg and Winegard (1954)
3.8	Orrok (1958)
76	Yesin, Pankin, and Nasyroo (1971)

Whatever the value, there is general agreement that the rate varies as the square of the amount of supercooling. A comparison between the dendrite growth rate and the transfer of heat between a melt and its surroundings shows that this kind of solidification occurs adiabatically. The portion of the liquid that is solidified this way is given by Equation (9).

$$\text{Fraction solidified adiabatically} = (1/L)\int_{T_o}^{T_e} C_p \, dT \qquad (9)$$

T_o is the temperature at which solidification begins. For tin, this fraction increases from zero to about 48 percent. The latter value is for solidification at a supercooling at 118°C, the largest supercooling reported.

The stable form for dendrite growth was determined mathematically to be a paraboloid of revolution by Trivedi (1970). Chernov (1973) disagrees, but uses the paraboloid as the first approximation to the truly stable form.

Unlike planar solidification, dendritic growth direction is determined by the orientation of the planes in the growing crystal. For example, dendrites of metals with face centered cubic structures are known to grow in the [1,0,0] direction. Powell's (1969) observation of this growth direction experimentally in a sample of silver supercooled 127°C helps confirm this belief.

Side arms form on dendrites when the amount of supercooling is small. Tarshis, Walker and Rutter (1971) attribute this to spatial restriction, as dendrites growing in a highly supercooled melt are reported to be longer and closer together. Powell and Hogan (1965) shows columnar growth (dendrites without side arms) in a silver ingot supercooled 175°C. Powell and Hogan (1968) show the same thing in a copper ingot nucleated at a supercooling of 208°C. Faint sidearms are seen in copper formed with an undercooling at 113°C and distinct ones are seen in Cu undercooled 80°C and in Cu_2O undercooled 82°C.

The Number of Crystals

The number of crystals formed during the solidification of a pure metal can be predicted by defining the cooling rate, and the impurity characteristics of the liquid. One model is proposed by the author which relies on the definition of impurities in terms of the supercooling required before they can cause nucleation. Then a distribution

of these potential nucleants can be described for any liquid. Figure 4 shows three such postulated nucleant distributions.

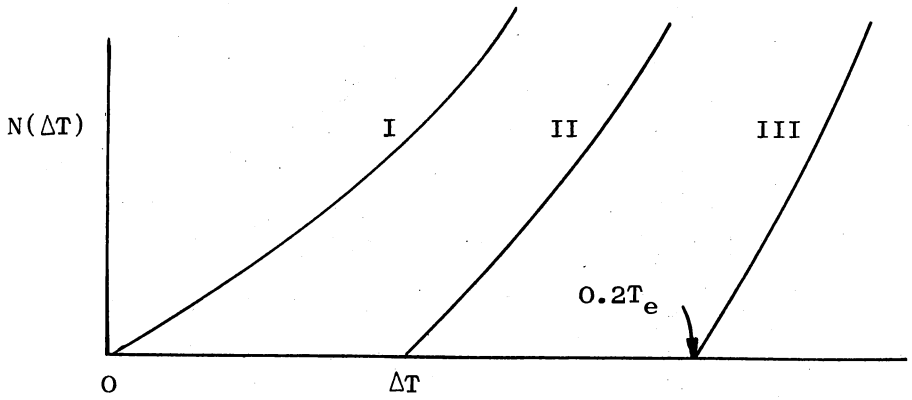

Figure 4. Suggested Distribution of Potential Nucleants in a Sample According to the Temperature at Which They Cause Nucleation

In Case I nucleants are effective at any supercooling. Nucleants in Case II are only effective after some intermediate undercooling. This might correspond to the distribution expected for a oxide coated metal. Nucleants in Case III are the embryos existing in the liquid. Homogeneous nucleation would result.

The use of a model like this to explain the formation of various numbers of crystals can best be understood by considering a cooling liquid. If the cooling rate were very slow the temperature would decrease until the first nucleant became effective. Then all solidification would proceed from that point. For faster cooling rates, the formation of the first crystal would not release enough heat to stop the decrease in temperature immediately. Further supercooling would

occur for a short time allowing some of the slightly less effective nucleants to cause nucleation as well. A polycrystalline ingot would result.

The expected number of crystals predicted by this model would vary in the following way:

- increase for a steeper nucleant distribution
- increase for more rapid cooling, and
- increase when the initial nucleation occurs with less undercooling.

The idea that supercooling can continue even after initial nucleation occurs is consistent with the works of Iyer and Youdelis (1972) and Miroshnickenko and Brekharya (1970). Iyer showed that the cooling rate affects the reversal point in the cooling curve and argued that this point cannot automatically be interpreted as the temperature at which nucleation occurred. Table V summarizes the results. Miroshnickenko cooled samples fast enough to suppress recalsecense. He found that an Al-6.9%Mn alloy would supercool 150°C more when cooled at a rate of 3×10^{5}°C/sec than at a ten times slower rate. Metals of high purity were found to cool less than their technical grade counterparts in the same work. Neither pair of authors reported any crystal size information.

TABLE V

THE EFFECT OF COOLING RATE ON SUPERCOOLING

Metal	Ratio of Cooling Rates °C/min	Increase in Supercooling at the Faster Rate
Sb	238/30	47
Pb	65/55	8
Ag	215/82	8
Bi	40/5	16
Sn	34/30	6
Sb-40%Pb	140/25	20
Sb-70%Pb	140/25	23
Bi-10%Sn	30/5	8
Bi-30%Sn	30/5	35

The experimental works of Powell and Hogan (1968, 1969) are consistent with the predicted increase in the number of crystals with reduced undercooling. Copper samples that had been solidified at supercoolings from 25 to 50°C were examined metallo-graphically and found to have many nucleation sites. In contrast, samples which undercooled more than 50°C (up to 150°C) showed only a single nucleation site. Large columnar crystals were observed to radiate from that site. When silver was undercooled 175°C and nucleated by proding, all the crystals formed were observed to originate at a single site. No samples solidified with smaller undercoolings were examined.

Tarshis, Walker, and Rutter (1971) used vibration to initiate nucleation at various degrees of undercooling. They found fine grained structures in copper-nickel alloys when the undercooling was less than about 60°C. Very coarse grains were observed at supercoolings from 80 to 160°C with mixed grain sizes appearing for intermediate undercoolings.

Although this experiment did not involve nucleation by the cooling of a liquid to the temperature where inherent nucleation catalysts became effective, it still substantiates the model. A constant externally stimulated nucleation rate will produce fewer nuclei in a highly supercooled melt because growth would become dominant sooner. Very fine grain sizes reported from stimulation of melts undercooled more than 160°C can be explained by the following mechanism.

Powell (1965) and Powell and Hogan (1969) establish the proposal that spontaneous recrystallization occurs following solidification if the undercooling is sufficiently large. Metallographic evidence of the recrystallization consisted of (1) small grains inside much larger ones, (2) large angle boundaries separating grains, and (3) the presence of twinned polygonal grains. Factors affecting recrystallization were suggested to be a high dislocation density grown into the solid solution during high-velocity freezing--that would be sensitive to the content of oxygen or other impurity or alloy, cavitation caused by the rapid change in density, or deformation or fracture of dendritic arms from moving liquid or from pressure pulses in the solid (Glicksman, 1965).

The number of grains found in a solidified sample is seen to depend first on the number of nucleation sites which become effective through undercooling, and then on the amount of recrystallization which occurs immediately after solidification is complete.

CHAPTER III

SOLIDIFICATION OF ALLOYS

Single Phase Alloys

The solidification of a metal containing a completely soluble alloying element differs from that of a pure metal in two major ways. First, the alloying element alters the surface energy of the melt and, therefore, affects the temperature at which homogeneous or heterogeneous nucleation occurs. In the second case, solidification of an alloy results in segregation of the solute and constitutional undercooling.

In general, the surface energy of a single component liquid is reduced by the addition of a solute. This can affect nucleation by reducing $\sigma_{\alpha L}$, and/or $\sigma_{\beta L}$ (Equation (6)). Youdelis and Iyer (1973) reported that the amount of undercooling observed depended on alloy composition for all five systems examined. Consideration of either binary component as the solvent permits effects to be noted for ten independent dilute alloys. Of these, five systems showed a decrease in supercooling with an increase in solute concentration. In three cases the opposite was true. There was not enough data for evaluation of the other two cases. Table VI is a tabulation of their results. All of the values of supercoolings for these dilute alloys were small, ranging from 8 to 33°C. Therefore, nucleation was heterogeneous.

TABLE VI

THE EFFECT OF THE ADDITION OF A SOLUTE ON SUPERCOOLING

Solute	Solvent	Change in Supercooling $d(\Delta T)dc$*
Bi	Sn	36
Sn	Bi	80
Sn	Al	83
Pb	Sn	254
Pb	Sb	239
Sb	Pb	-762
Sn	Pb	- 12
Cu	Ag	- 43

*Supercooling (solvent-alloy)°C/fraction minor constituent.

Cech and Turnbull (1951) reported supercoolings corresponding to homogeneous nucleation for the whole range of Ni-Cu alloys.

A possible explanation for the aforementioned data comes by reference to Equation (6)). The value of ΔG_s changes as $\sigma_{\alpha L}$ and $\sigma_{\beta L}$ decrease depending on the comparative rates of decrease. If the decrease in $\sigma_{\alpha L}$ dominates, ΔG_s will decrease and the formation of a nucleus with less undercooling will be favored. This would account for the first five solute-solvent systems listed in Table VI. $\sigma_{\beta L}$ would be dominant, and ΔG_s increase if $\sigma_{\alpha L}$ were low. Since lead and silver have lower surface energies ($\sigma_{\alpha L}$) than tin and copper, respectively (Crosley and Mondolfo, 1971), one could predict the behavior of the final three systems in Table VI. For an alloy nucleating homogeneously, there is no β and the nucleation temperature should vary inversely as $\sigma_{\alpha L}$. Cech and Turnbull (1951) did not observe any effect, but the change in surface energy from 2.55×10^{-5} to 2×10^{-5} joules/cm^2 corresponds closely to

the change in the absolute supercooling of 319°C for nickel to 236°C for copper.

The first solid to form during the solidification of a dilute alloy is solute poor, and the liquid is enriched. The events that follow can be described by three processes, depending on the growth rate of the solid. First, the rate of solidification can be kept slow so that a uniform concentration is maintained in the liquid by diffusion. In the second way, solidification can proceed fast enough to maintain a concentration gradient in the liquid, through rejection of solute, during the whole of the solidification process. Finally, solidification which occurs very rapidly would not result in segregation; rather, the solute would be trapped uniformly in the growing solid.

When the rate of solidification is very slow it can be explained adequately by reference to the equilibrium diagram as shown diagrammatically in Figure 5.

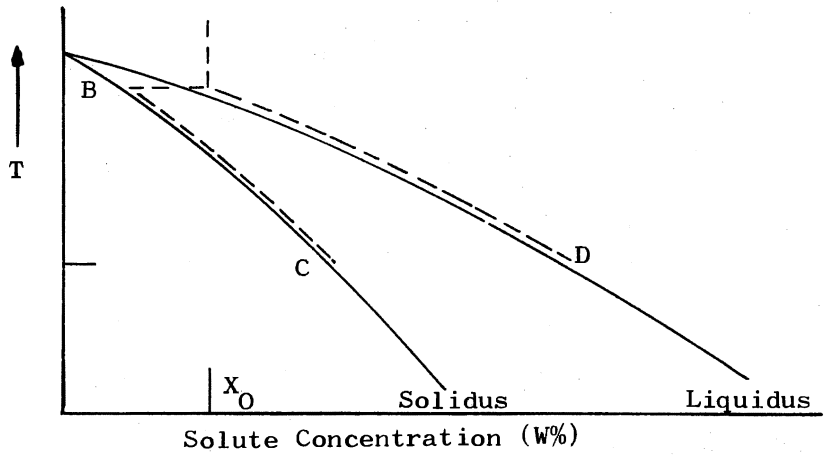

Figure 5. Solidification of a Dilute Alloy Very Slowly

A liquid of concentration X_o is cooled until it reaches the liquidus. Then a solid with a composition corresponding to point B is formed and the liquid becomes richer in solute. As the temperature continues to decrease, more solid is formed changing gradually in composition from B to C. The liquid, as it is consumed, increases in solute concentration from A to D. At the temperature corresponding to CD, solidification is complete. When solidification occurs this way there is a concentration gradient in the final sample. The first material to solidify is poor in solute, and the last is richer in solute than the mother liquor. It is equivalent to solidification when complete mixing of the liquid is achieved continuously. The change in solute concentration as solidification proceeds is shown in Figure 6.

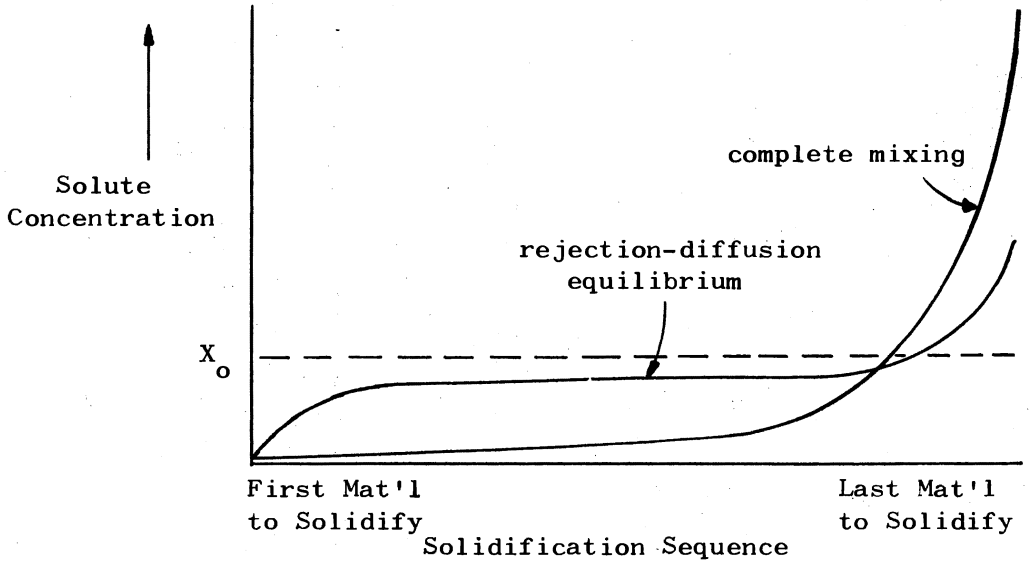

Figure 6. Concentration Gradient Arising From the Solidification of a Dilute Alloy

When the solidification rate is more rapid, rejected solute builds up at the interface until the rate of rejection equals the rate of diffusion away from the interface. The next solid is formed from this neighboring liquid which is artificially rich in solute. The change in concentration of solute from B toward C occurs rapidly at first. Then the rejection diffusion equilibrium is established and solidification of a solid of nearly constant composition (intermediate between B and C) occurs. Finally the remaining liquid can no longer act as a diffusion sink and its solute concentration increases substantially. The solid and liquid compositions change systematically toward C and D again until solidification is complete. This result is also shown in Figure 6 for comparison with the former case. The shape of the curve depends on the solidification rate. A faster rate causes the concentration in the solid to increase more rapidly at first, to reach a higher equilibrium concentration (closer to the original liquid concentration), and to have a smaller and shorter tail. The shape of the liquidus and the solidus curves and the initial concentration of the melt also affect the curve.

The buildup of solute in the liquid in advance of the approaching interface results in a decreased equilibrium temperature (T_e). Solidification is delayed until heat enough is removed to reduce the interface temperature to this value. The combination of the concentration gradient in front of the interface and the thermal gradient due to interface cooling cause some of the neighboring liquid to be cooled to a temperature below its T_e. The interface becomes unstable and dendrites grow into the supercooled region. Figure 7 shows diagrammatically the concentration gradient, the corresponding T_e gradient, and the expected

temperature profile. The shaded region indicates the location of constitutionally undercooled liquid. The dendrites that grow into this region create their own constitutionally undercooled region and branches will occur if solidification is fast enough. Otherwide, the remaining liquid solidifies by growing on the dendrites that are already present.

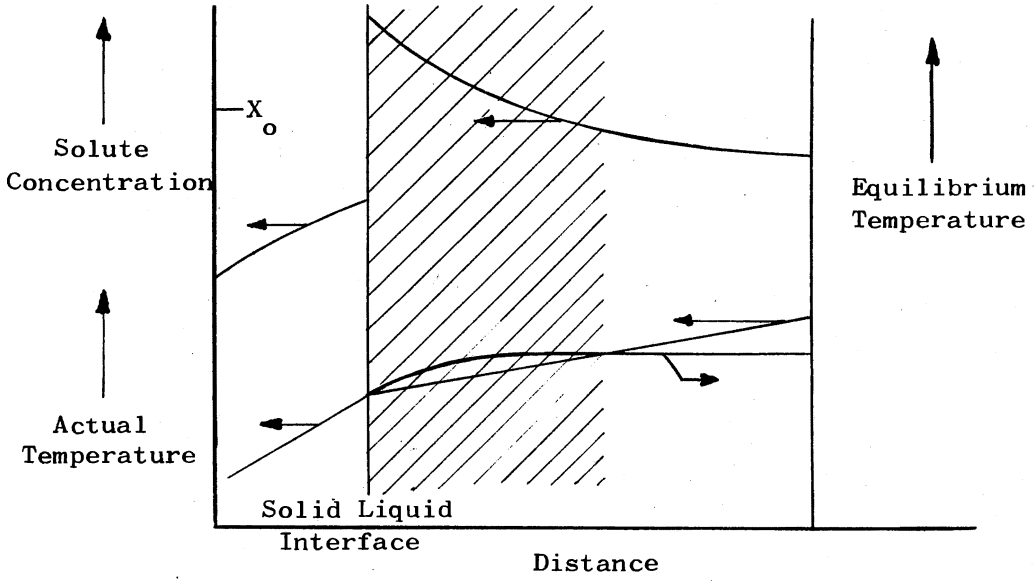

Figure 7. The Formation of a Constitutionally Undercooled Liquid Next to the Solid-Liquid Interface

When the alloy melt is substantially supercooled, the growth of a crystal from a single nucleation site is very rapid. Very little diffusion or external heat transfer is possible in the same time scale. The dendrites grow adiabatically with essentially the same constitution as that of the original bulk liquid. After sufficient dendritic growth

has occurred, the temperature of the half-solidified ingot increases to the equilibrium temperature. From there solidification proceeds according to one of the mechanisms discussed earlier with the existing dendrites serving as growth centers. The composition of the ingot would not be uniform. The original composition in the center would fade into a solute poor region, and the outside (last to solidify) portion would be solute rich.

The number of crystals formed when a dilute alloy solidifies depends on the effect a change in surface energy has on the nucleation temperature. The crystals form in a dendritic pattern with long and arm-less dendrites occurring more often with high thermal and/or constitutional undercooling. Segregation results from the solidification. It is marked at slow cooling rates, but reduced when substantial undercooling proceeds solidification.

Solidification of a Two Phase Alloy

The solidification of a metal to form two identifiable phases has many similarities to the solidification of a single phase alloy. Nucleation and growth of the first phase proceeds in an exactly analogous manner. However, the nucleation of the first phase may be influenced heavily by the presence of the second component because of the wide range in melt composition which leads to two phase alloys. Table VII gives some of the values observed for first phase undercooling.

TABLE VII

THE EFFECT OF ALLOY COMPOSITION ON
FIRST PHASE UNDERCOOLING*

Alloy Composition Weight %	First Phase	Undercooling °C	
		Alloy	Pure Metal
Cu-0.08%O	Cu	218	208
Ag-0.12%O	Ag	250	
Pb-30%Sb	Sb	51	32
Pb-40%Sb	Sb	16	32
Pb-60%Sn	Pb	17	8
Pb-70%Sn	Pb	32	8
Pb-80%Sn	Sn	35	33
Pb-88%Sn	Sn	22	33
Sn-82%Bi	Bi	7	16
Sn-45%Bi	Bi	16	16
Sn-36%Bi	Sn	18	33
Sn-20%Bi	Sn	28	33

*Youdelis and Iyer (1973); Powell and Hogan (1968); and Powell (1965).

Two kinds of behavior shown in Table VII are worth noting. First, undercooling for homogeneous nucleation is not apparently affected by variations in alloy composition. This implies that $\sigma_{\alpha\beta}$ and $\sigma_{\alpha L}$ are of major importance in determining the effectiveness of a nucleation catalyst. Secondly, significant increases in first phase undercooling occur as the eutectic composition is approached in the Pb-Sb and Pb-Sn systems. This does not occur in the Sn-Bi and the Ag-Cu systems, however. No explanation is given for this effect.

In two phase alloys nucleation of the second phase must be done independently from that of the first phase. Sundquist and Mondolfo (1961) and later authors (Crosley and Mondolfo (1971) and Powell and

Colligan (1969) have observed that the presence of first phase crystals effectively causes nucleation the second in half of the cases. However, when a hypereutectic alloy behaves this way, the hypoeutectic alloy does not. Table VIII, as an extension of Table III, gives some of the data reported to show the effect of first phase crystals on nucleation of the second phase.

TABLE VIII

THE EFFECTIVENESS OF THE FIRST PHASE CRYSTALS ON THE NUCLEATION OF THE SECOND PHASE*

First Phase	Second Phase	Undercooling of Second Phase °C
Cu	Cu_2O	19
Cu_2O	Cu	82
Sn	Pb	1
Pb	Sn	$\geq$40
Sb	Pb	6
Pb	Sb	$\geq$21
Sn	Bi	$\geq$17
Bi	Sn	6
Cu	Ag	29
Ag	Cu	$\geq$53

*Powell and Hogan (1968) and Sundquist and Mondolfo (1961).

The growth of the first phase is similar to that in the solidification of a dilute alloy as a dendritic structure and segregation are displayed. The growth of the second phase, usually eutectic, is different. Ideal eutectic solidification leads to a laminar structure. The two components, A saturated with B and B saturated with A grow together

in a way which minimizes the time needed to accommodate the diffusion away of solute rejected during freezing. The diagrams in Figure 8 illustrate this principle. The ability of this growth mechanism to dominate the eutectic solidification process occurs because less interface supercooling is required for growth if the rejected solute is effectively removed from the liquid adjacent to the interface. When the rate of heat removal is increased the laminar spacing decreases. Less diffusion is required to deplete the rejected solute because the sinks and sources are closer together. Cline and Livingston (1969) showed that the laminar spacing varied inversely with the square root of the growth velocity. In addition, Cline (1967) showed that laminar growth is preferred over dendritic growth even in off-eutectic alloys if the solidification rate is high enough.

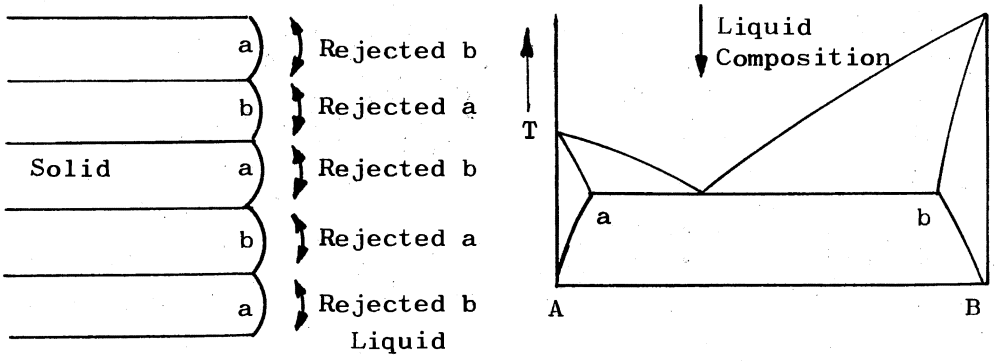

Figure 8. Accommodation of Rejected Solute Through Coupled Growth of a Eutectic Alloy

Anomalous eutectic structures are reported by Jones (1971) and

Kattamis and Flemings (1970). These eutectic structures are characterized by apparent discontinuities in one phase. It was first thought that repeated nucleation of the discontinuous component must be occurring during solidification. But Kattamis and Flemings showed that the second phase was continuous. Jones (1971) attributes the anomaly to solidification of the eutectic from an undercooled melt, and unequal growth rates for the two components.

Bulk Movements in the Melt

Convection in the molten alloy, and gravitational settling in it may cause segregation and/or an increase in the number and distribution of crystals. Convection is important when the density of the solute-rich or cool liquid at the solidification interface is different from that of the bulk liquid. Streat and Weinberg (1974) observed shrinkage trails and pipes in Pb-20%Sn ingots which they attributed to this cause. Convection also occurs when solidification is accompanied by substantial shrinkage. In this case the liquid flows from the casting center toward the outside surfaces. Jaffey (1975) found that this effect, called inverse segregation, is the more important of the two--except when the ingot is large and solidification is slow.

Possible results of the convection are threefold. First, it can cause early homogenization of the melt, reducing the amount of constitutional supercooling and enhancing the growth rate. Secondly, the convection resulting from shrinkage can cause solute-rich liquid to flow into the inter-dendritic spaces and restore in part the overall uniformity in composition originally present in the melt. Finally, convection in the sample can cause dendrite remelting.

Dendrite remelting occurs when a dendritic framework that has grown into a constitutionally supercooled region comes in contact with the bulk liquid. The liquid, which has a temperature higher than the dendrite melting point, caused some of the dendritic material to melt. Fragments removed from the parent structure this way but not completely dissolved are logical sites for the growth of new crystals in the melt.

Streat and Weinberg (1972, 1973) have shown that dendritic frameworks can be dissolved away by the melt if the driving force for convection is sufficiently high. Thus, it is possible that significant grain refinement can be achieved in some systems through the creation of heterogeneous nucleation sites by the remelting of dendrites.

If crystals formed by heterogeneous nucleation in the melt have a different enough density and the opportunity to grow large, settling can occur. Then there would be an increase in the number of small randomly oriented grains in the central part of an ingot, near the bottom if the crystals were heavy, and near the top if they are lighter than the melt. Strangmen and Kattamis (1973), for example, report the formation of a vertical composition gradient in a Pb-46%Sn alloy. It is attributed to the settling of lead dendrites that were the last to melt during reheating.

CHAPTER IV

FORMATION OF THE EQUIAXED ZONE

The equiaxed zone is a volume in the center of an ingot which is comprised of small randomly oriented crystals. The structure is distinct from the columnar zone which surrounds it. The columnar zone is composed of inward growing crystals which originate through nucleation at the surface and survive because a crystallographic direction for rapid growth is nearly antiparallel to the direction of heat removal.

The transition from columnar growth to form the equiaxed zone is one that involves the formation of new crystals. However, the origin of these crystals has not been satisfactorally defined. Two points of view persist. In one, the crystals are understood to grow from pieces of solid previously formed but somehow separated from the bulk of the crystal. The second viewpoint holds that the crystals are nucleated independently in the liquid ahead of the growing columnar zone.

A number of variables are known to affect the transition and the changes they cause help define the factors which alter grain sizes. One of these variables is vibration. Ultrasonic, aural and subaural vibration when applied during solidification cause equiaxed regions to be larger and to have finer grains. A similar effect is observed if the free surface of the liquid is agitated or if the mold is rotated during solidification. The initial superheat and the cooling rate affect the zone. Higher superheats cause a reduction in the extent of the zone and

an increase in the size of the crystals in it. High cooling rates have the opposite effect.

Investigations done to produce fine grained ingots and/or to determine the appropriate mechanisms for grain refinement and the experimenters' interpretations are summarized.

Rotation

Grain refinement can be produced by the rotation of the solidifying liquid. Langenberg, Pestel and Honeycutt (1961) produced grain refinements in stainless steels by solidifying the metal in a rotating magnetic field. The refinement was attributed to fracturing of the solid caused by the relative motion between the solid and the liquid. The broken pieces of solid were deemed responsible for each of the fine grains that comprised the finished ingot.

Crossley, Fisher and Metcalfe (1961) used both magnetic stirring and mechanical rotation to obtain grain refinement in aluminum. Magnetic stirring was accomplished by passing current (DC) through the melt and through a stirring coil. When the stirring coil was shut off, grain coarsening occurred. But the mechanical motion in the liquid caused when both currents were induced caused grain refinement to result. Grain refinement was further enchanced when the stirrer polarity was reversed to make the liquid rotation stop and then proceed in the opposite direction. Mechanical rotation at constant speed was found to increase grain size, but when the rate of rotation was changed, the grain size was reduced. The authors did not propose a mechanism to explain their experimental results. Instead, they concluded that viscous shear in the liquid is important to the nucleation mechanism.

Cole and Bolling (1967) solidified Sn-Zn alloys in a rotating mold to study this effect. A typical ingot structure, having a columnar and an equiaxed zone resulted. The equiaxed zone was found to shrink during slow rotation or when initial superheating was higher. Rotational oscillations were the cause of an increase in the extent of the equiaxed zone. The experimenters observed that slow rotation hinders convection so that the temperature gradient in the liquid remains high. In comparison, convection was supposedly enhanced by the oscillation, and this caused the thermal gradient in the liquid to be small. This difference in the gradient from rotating, to stationary, to oscillating melts, is given as the major reason for the grain refinement observed. However, this effect was reduced when the amount of superheat was varied. Ingots made with less superheating all had extensive equiaxed zones and the effects of motion were comparatively small. A similar effect was observed for ingots made with very high superheats. The equiaxed zone was very small in this case, and did not appear to depend on rotation. Even then, with high superheat and slow rotation some central equiaxed crystals were found. The authors were unable to explain this effect in terms compatible with "breaking-off" theory because of the lack of convective motion in the liquid.

Vibration

Richards and Rostoker (1955) studied the effect of vibration on the solidification of aluminum ingots. Vibrational frequency and amplitude were varied and the change in grain size was observed. Results of their experiments showed refinement of grain size with an increase in vibrational amplitude--up to a point. After that, no further refinement

occurred. They showed, in addition, that the grain coarsening effect of increased superheat was completely eliminated by vibration, that vibration of the liquid before freezing had no effect, and that vibration caused primary intermediate phases to become more coarse. Fragmentation was discounted as the responsible mechanism because broken crystals would be so small that they would be unstable and, therefore, dissolve. Instead, the authors proposed that the nucleation rate was increased because of microscopic pressure changes in the liquid. Then if the rate of nuclei formation was dependent upon the radius of the nucleus (not linearly) the average rate over the cycle would be different than the average rate without vibration. Refinement of metals like bismuth which expand during solidification, as well as the coarsening effect of vibration on intermediate phases could be understood using this idea.

Frawley and Childs (1968, 1969) reported two series of results. The first experiments were done using bismuth and tin alloys. The alloy was undercooled and then solidified by vibration. They found that there was an amplitude effect that (1) had a threshold, (2) caused increased refinement when the amplitude was increased--up to a point, and (3) was ineffective thereafter. Pressure changes caused by cavitation were thought to be responsible for the effects. In the later work, also involving Sn and Bi, they came to adopt the alternate mechanism. Differences in the ability to refine Bi-rich and Sn-rich alloys were attributed to the greater breakability of tin dendrites during the early stages of growth. Cavitation combined with constitutional supercooling was considered, as was dendrite remelting. However, neither

mechanism was felt to be as likely responsible for the refinement as fragmentation.

Southin (1966) studied vibration produced grain refinement and came to a similar conclusion. The effect he observed was interpreted as (1) the breaking of crystals when the growth was dendritic and (2) the erosion of columnar crystals by cavitation when the growth form did not result in thin sections. He worked with alloys of Al, Bi, Cd, Pb, Sn, and Zn.

Russians Leychkis and Mikhaylev (1970) caused nucleation in tin at supercoolings which were too small to produce homogeneous nucleation. In some experiments a seed was used, and in others, vibration in order to initiate the solidificattion process. In both cases, finer crystal sizes corresponded to nucleation at greater undercooling. The effect was not strongly dependent on the temperature, however. Their account of the experiments regards nucleation to be a two step process, first the formation of an embryo and then its deformation to a crystal structure with long range stability. Changes in crystal size caused by vibration or increasing alloy content were attributed to the removal (mechanically, or because of the chemical difference between embryo and substrate) of embryos during the second state of development. Then they serve as the substrate for conversion of a new nucleus from short to long range stability. Very pure metals were not refined this way.

CHAPTER V

EXPERIMENTAL RATIONALE

One finds through a review of the literature on solidification as summarized in Chapters II, III, and IV that significant areas of disagreement still exist. For example, some authors argue that nucleation occurs because of impurities, while others credit planar surface patches. One field of thought says that nucleation is a single step process; another says that there are two steps. Some authors maintain that a good atomic fit is the essential element in heterogeneous nucleation whereas others suggest that the right sized cluster must meet the right sized nucleant with the right orientation. And nearly everybody differs to some degree on the origin of the nuclei that grow in the liquid and eventually cause the columnar to equiaxed transition. Indeed, Fredriksson and Hillert (1972) were very careful to avoid this question in their study on the transition mechanism.

This experimental work, in order to resolve some of these questions, was designed to investigate the underlying principles which have made certain grain refinement techniques successful. These techniques, for modification of the equiaxed zone, for the initiation of nucleation in an undercooled melt, and for vibrating the casting during solidification can be viewed in either of two general ways.

In the first case, success in grain refinement can be described by the breaking-off theory. In it, numerous fragments are assumed to be

broken off from the first material to solidify. Each such fragment is expected to develop into a grain.

In the second case, the grain size reduction results from supercooling and then heterogeneous or homogeneous nucleation. The supercooling is assumed to occur because of constitutional effects, the lack of effective nucleation sites, or modification of the phase diagram because of non-equilibrium conditions.

The conditions required for breaking up of the solid during solidification were to be studied by rotating the sample and mold together during the entire cooling process. In this way a predetermined buoyant force could be applied to the first dendrites to solidify. It could be varied systematically by changing the speed of rotation and/or the alloy composition. Any fragments formed as a result would float (or sink if they were heavier than the melt), and an evaluation of the process could be made by examining the radial distribution of the crystals and their size.

Investigation of the second viewpoint was to be accomplished by the separate examination of several of the variables that influence nucleation and growth. To isolate the sample from external effects which might themselves cause nucleation, the samples were melted and solidifed in glass molds and under the cover of a high-boiling organic liquid. Similarly, the thermocouples were enclosed in thin glass sheaths to prevent the sample from coming in contact with any crystalline surface.

By thus eliminating the opportunity for incidental nucleation, the temperatures of nucleation and recalescense, and the final crystal structure could be studied parametrically. Solidification parameters

which were to be examined included the time and temperature of superheat, the effect of a prefreezing soak at temperatures slightly greater than T_e, and the effect of different cooling rates. The impurity and alloying effects were also to be studied this way, by varying the grades of material used, and the sample composition. Liquid metal baths were chosen for heating and cooling purposes because of the potential for rapid temperature equalization and, hence, a better definition of the experimental conditions. In addition, copper molds with thin glass linings were to be made. This would further improve the heat transfer characteristics of the mold so near-isothermal conditions for solidification could be achieved.

Grain sizes and shapes in the samples solidified as a part of these series would be related to the number of effective nucleants present and the conditions of growth.

CHAPTER VI

EXPERIMENTAL PROCEDURE

Materials

Tin and lead were the major materials chosen for the experimental work. The selection was made because they are readily available in several different grades, and melt at easily obtainable temperatures. In addition, the lead-tin binary phase diagram consists of a simple eutectic and has been thoroughly investigated. Finally, lead and tin have significantly different densities (11.34 and 7.30 g/cm^3, respectively).

Three grades of tin were used, two reagent grades ("Baker", and "Matheson, Coleman, and Bell" (MCB)) and a high purity grade from Materials Research Corporation (MRC). The chemical analyses listed for each grade is shown in Table IX.

Only one grade of lead was used, Fisher No. 8 Lead Shot. Reagent grades of bismuth and cadmium were used.

TABLE IX

ANALYSES OF TIN GRADES USED EXPERIMENTALLY

Constituent	Baker	MCB	MRC
Sn	99.9	99.9	99.999
Nonvolatile in HBr and Br_2	.020	.02	
Sb	.01	.02	
As	.00001	.0001	
Cu	.001		
Fe	.004		
Pb	.003		
Zn	.0004		
Form	Shot	Shot	Ingot

Metallography

Routine treatment of the cast samples consisted of sectioning, sanding, and finally rough and fine polishing. Conventional etching solutions were then used to reveal the microstructure.

This treatment worked well for the whole range of lead-tin alloys, but was unsuccessful for tin-only samples. The structures of tin samples prepared this way consisted of fine equiaxed grains (5 to 25 micrometers in diameter) which had no apparent relationship to the direction or rate of solidification. This structure was attributed to the recrystallization of a surface layer of the tin during the cutting and sanding. Samuels (1971) reports this effect in zinc and gives 3 to 45 micrometers as the thickness of the recrystallized zone. The variation in thickness was attributed to differences in the quality of the grinding. Figure 9 shows this artificial structure.

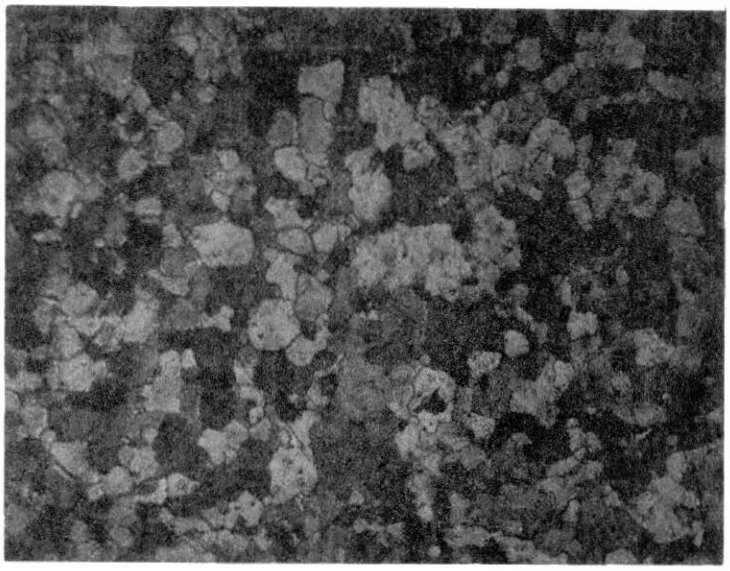

Figure 9. Recrystallized Structure in Tin Caused by Sanding During Sample Preparation. X200

Chemical removal of the recrystallized layer was attempted using concentrated HC1, as recommended by Kehl (1949), without success. However, the application of 5% silver nitrate followed by 2% nital did remove this layer.

A second kind of artifact, mechanical twins was uncovered. The twinned zone had to be eaten away, by repetition of the nitrate-nital treatment. The twins are shown in Figure 10 for comparison of the authentic tin structure of Figure 11.

A summary of the etchants used throughout the work is given in Table X.

Often the mechanical twins were not eliminated, but this did not interfere with the interpretation of the structure.

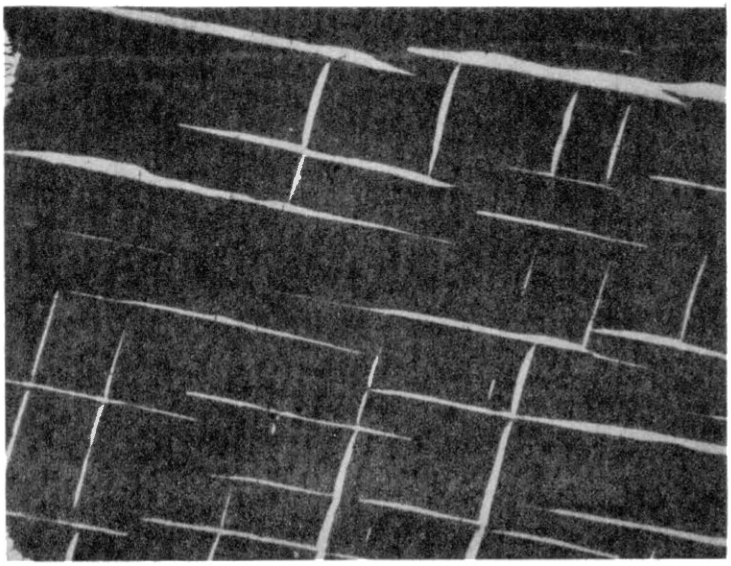

Figure 10. Mechanical Twins Formed in Tin Samples During Preparation for Micro-examination. X50

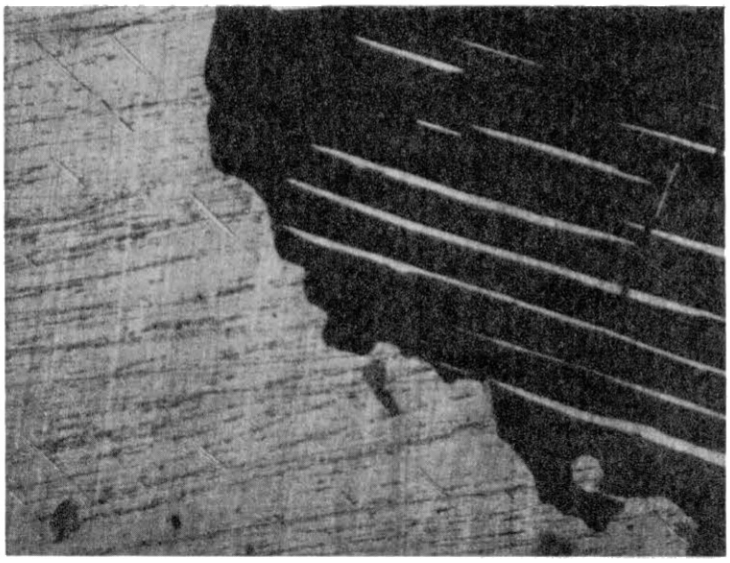

Figure 11. Authentic Tin Structure Obtained by Chemical Removal of the Layers Deformed During Sample Preparation. X50

TABLE X

ETCHANTS USED FOR SAMPLE PREPARATION

Sample Composition	Etchant, and Technique
Tin only	5% $AgNO_3$ followed by 2% Nital. Repolished pieces etched in Nital only.
Tin-dilute lead	Alcoholic $FeCl_3$
Near eutectic Tin-Lead	Mixed Acid (2% HC1 and 5% HNO_3 in methanol)
Tin-Bismuth	2% Nital
Bismuth Cadmium	2% Nital

Solidification in the Rotating Mold

A cylindrical mold was made of stainless steel. It had a cavity 1.75 inches in diameter and one inch deep. The mold was designed so that it could be mounted for rotation around its major axis. The motor and apparatus for spinning the mold could be adjusted so that horizontal and vertical orientations of the axis of rotation were possible. The vertical position was used when the speed of rotation was less than 1800 rpm.

The temperature was controlled by installing a heating coil around the mold and insulating bricks around the coil. A Variac was used to vary the amount of resistance heating in the coil. Figure 12 shows a diagram of the mold and Figure 13 shows the mode of operation.

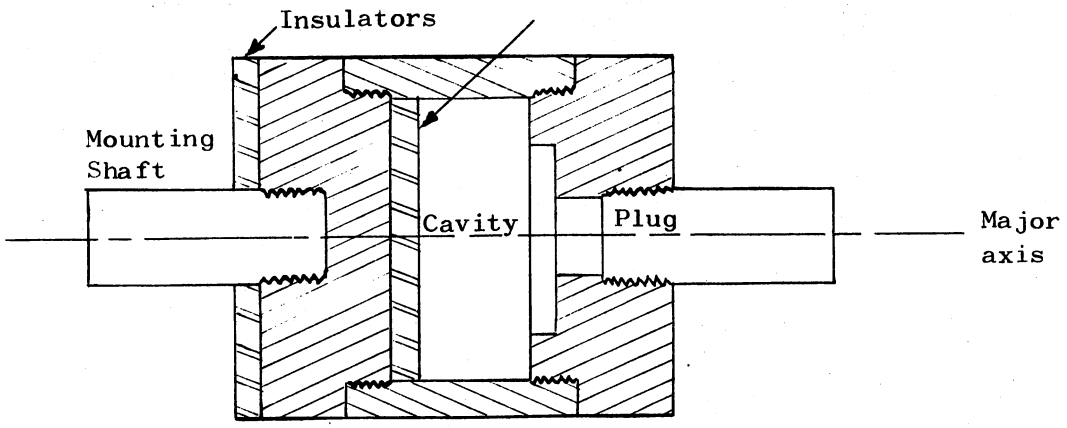

Figure 12. Cross-Section of the Mold Assembled Prior to Rotation

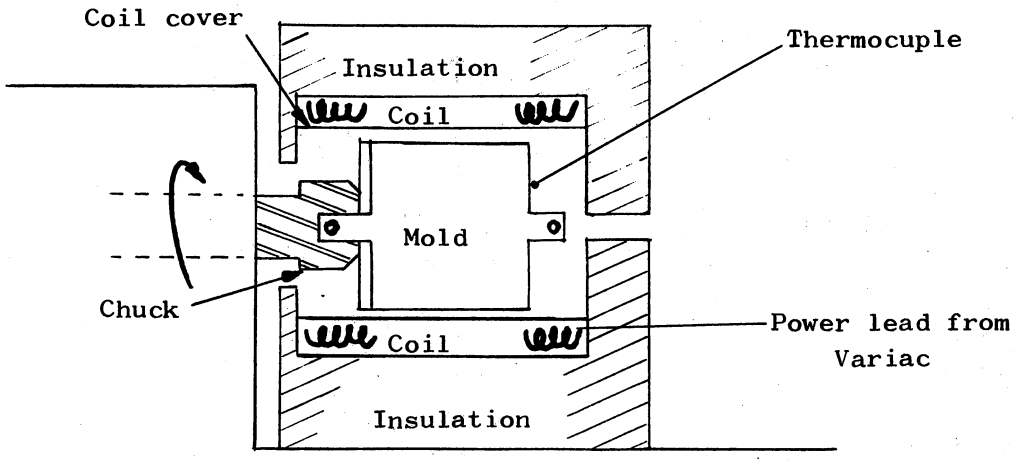

Figure 13. The Apparatus for Turning and Heating the Mold

Before each use the mold was cleaned. A commercial caulking compound (rope caulk) was then used to seal the threads and the other mating surfaces. A sample was prepared by weighing the components (to the nearest 0.5 gram) and melting them together with mixing in a

separate furnace. The molten alloy was then poured into the mold through the opening made when the plug is removed. The plug was replaced, the mold was mounted in the chuck, and the heating coil and insulators were assembled. Then the current to the heating coil was adjusted to achieve a mold skin temperature 100°C above the liquidus of the alloy. The mold and assembly were maintained this way for two hours.

The solidification of the sample was accomplished by selecting the speed of rotation, shutting off the power to the heating coil, and removing the coil and insulators. Cooling proceeded by the forced convection of the mold rotating in room air and through conduction of the heat around the insulators to the turning mechanism. When the sample had cooled to about 50°C the mold was removed and quenched to room temperature in water. Samples formed this way were removed by pressing them out of the mold's cylindrical shell after the mold had been taken apart. The samples were sectioned longitudinally and vertically for polishing, etching, and subsequent microexamination.

Solidification in Glass and Glass Lined Molds

The system for controlling and measuring the thermal cycle of the glass and glass lined molds is shown in Figure 14. Variacs were used to control the temperature in both the heater, a vertical tube furnace, and the stop-bath. The stop-bath was filled with lead-tin eutectic and surrounded by an insulated heating coil. The cooling bath was filled with woods-metal and placed in a cooling-curve furnace. Control of the bath temperature was accomplished by using the Dubuque III Controller in conjunction with the furnace.

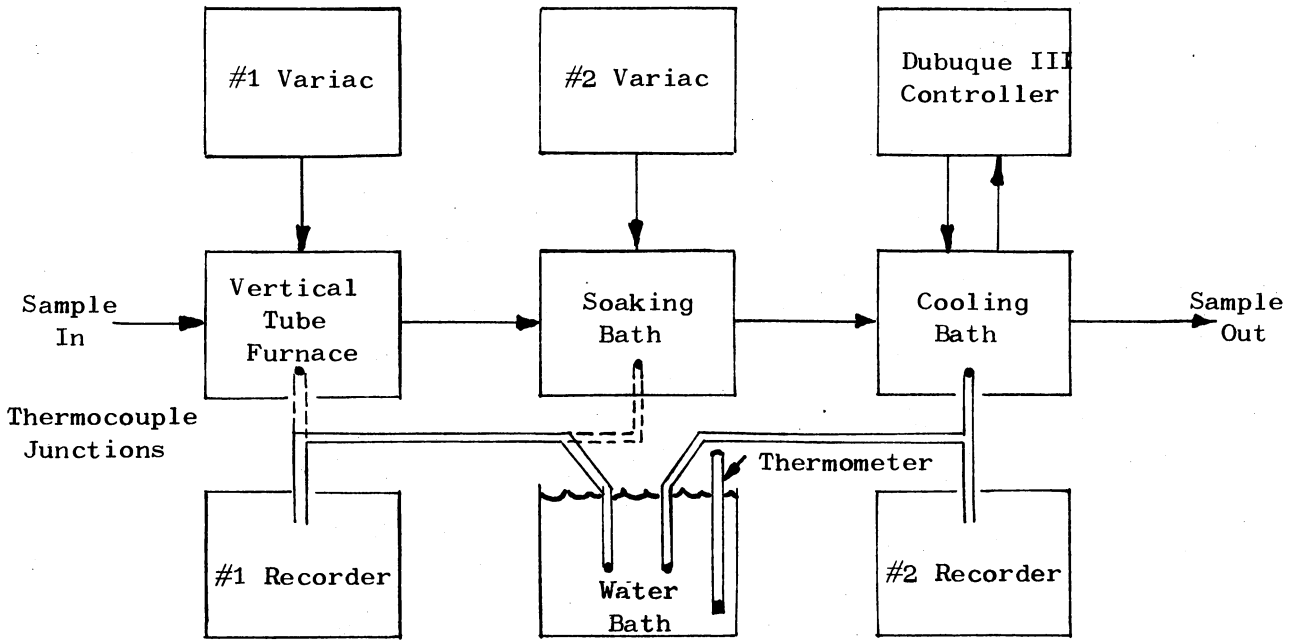

Figure 14. A Block Diagram of the Apparatus Used With the Glass-Lined Copper Mold

Bath temperatures were measured when desired, or recorded. Iron-constantin thermocouples were used with Leeds-Northrup recorders. The thermocouples were encased in a thin pyrex shroud formed by drawing a glass tube out over the junction. The cold junction was placed in a stoppered tube and immersed in a water bath held constant at room temperature or below. This temperature was measured with a conventional mercury thermometer and was not observed to change during the course of an experimental unit.

The thermocouples were calibrated using a melting point technique. The recorders were first calibrated to give a full scale reading for a voltage of 30 mV. The variable zero supression was not used because of a desire to have the thermocouple calibrated over the full range of useful temperatures. Compounds were selected which have melting points

ranging from 70°C to 398°C. These were melted, and the hot junction of the thermocouple inserted. A cooling curve was run until solidification was complete and the compound was reheated. The average of the output (mV) measured during freezing and melting was used. The points were plotted with the thermocouple output as the abscissa and the difference between the temperatures of the hot and cold junctions as the ordinate. A linear regression line was passed through the data and the standard error of the estimate was determined. The accuracy of the temperature measurements was found to be ± 2.5°C over the range from 0 to 400°C. Both the calibration curve and the statistical work can be seen in the appendices.

First preparation of a single metal sample for an experimental unit was done by weighing out the desired amount of metal to 0.1 grams. The metal was then cleaned by agitating it in a solution of 6N HCl for several minutes and then washing it twice in tap water and twice in denatured alcohol. This was followed by a forced air drying step, before the sample was placed into the mold and covered with molten paraffin or dibutyl phthalate.

Alloy samples were prepared in an identical manner. However, it took twice as long. The autectic mixture of the two components was prepared first using the previous procedure. The alloy was melted and mixed before it was poured into cold water. Then the cold eutectic alloy was weighed and mixed with the appropriate amount of primary component to achieve the desired final composition. The mixture was cleaned as before, covered, and then passed once through the specified thermal cycle.

When pyrex test tubes were used for molds, an abbreviated procedure

was used. The mold and sample were heated directly in the soaking bath and cooled by (1) natural convection in air or (2) by quenching in oil or water. Cooling curves for tin samples solidified at each rate are shown in Figure 15.

A glass lined copper mold was constructed to permit the rapid removal of heat from the molten sample and to prevent any contact between the sample and external sites for heterogeneous nucleation. The mold was made from a three inch piece of 3/4" diameter copper stock. The cavity was machined to specification as shown in Figure 16 and lined with glass. (Cleaned copper surfaces were coated with a glass dispersion and fired at 1600°F.) The integrity of the surface was tested by measuring the resistance between a salt solution in the cavity and the mold wall. Commonly, the resistance of the mold wall varied from 10^4 to 5×10^6 ohms. Occasionally, when the wall was mechanically damaged, the resistance dropped to a fraction of an ohm. The surfaces of these molds were redone or the molds were discarded. The variation in acceptable resistivities is attributed to the presence of pinholes formed by oxygen released from the copper during firing. While these permitted limited access of salt ions to the copper surface they do not permit the sample and the copper to touch.

The top surface of the sample was protected from oxidation by a covering of paraffin. The paraffin was melted and poured over the solid sample before the heating cycle was to begin. During the melting and solidification of the sample, the paraffin formed a liquid cover. It in turn was protected from oxidation by sealing the mold top with a copper lid and silicone grease. Samples made under paraffin this way showed the absence of any observable surface oxide.

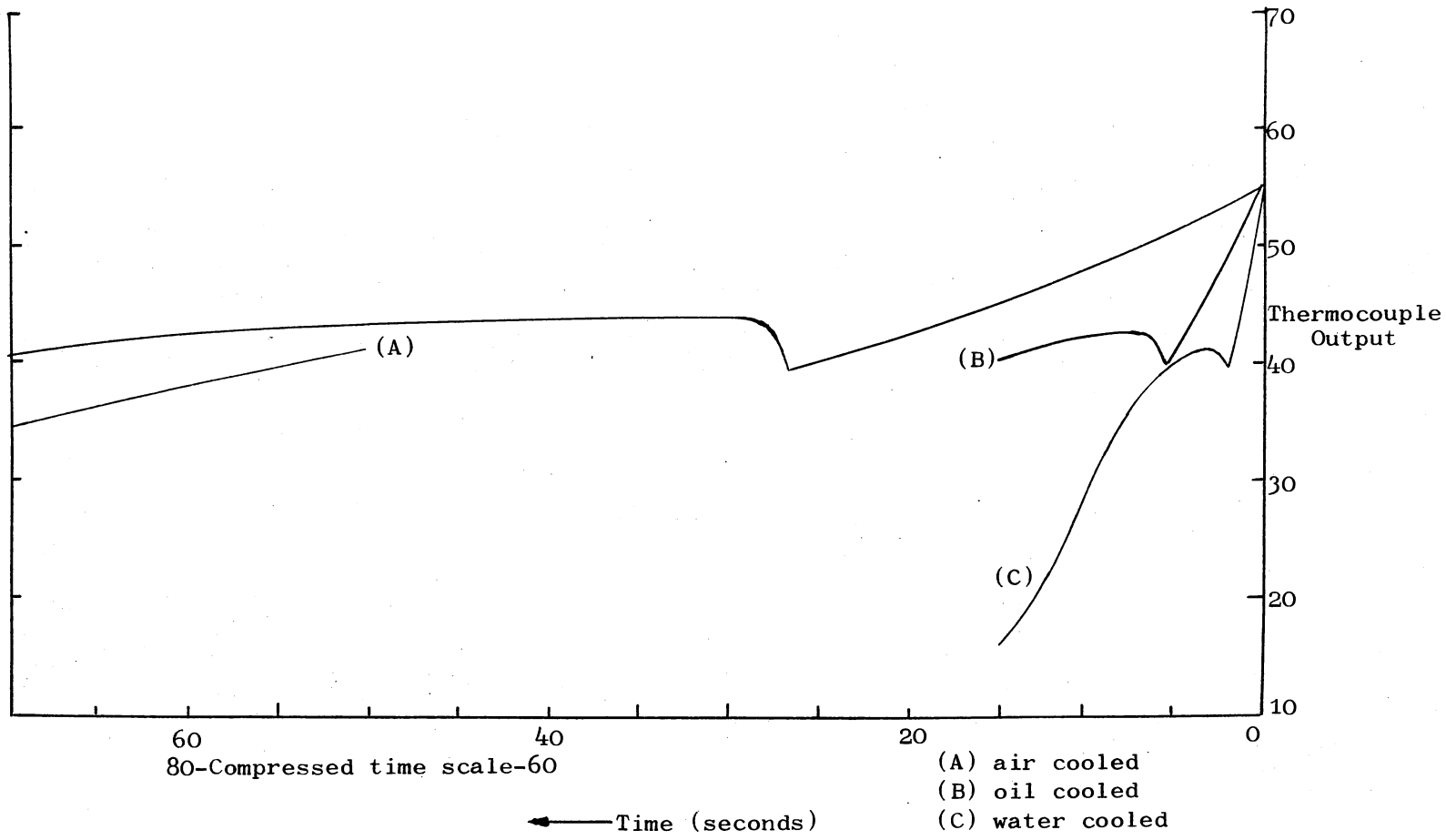

Figure 15. Cooling Curves for Tin-2% Lead Samples in Pyrex Molds

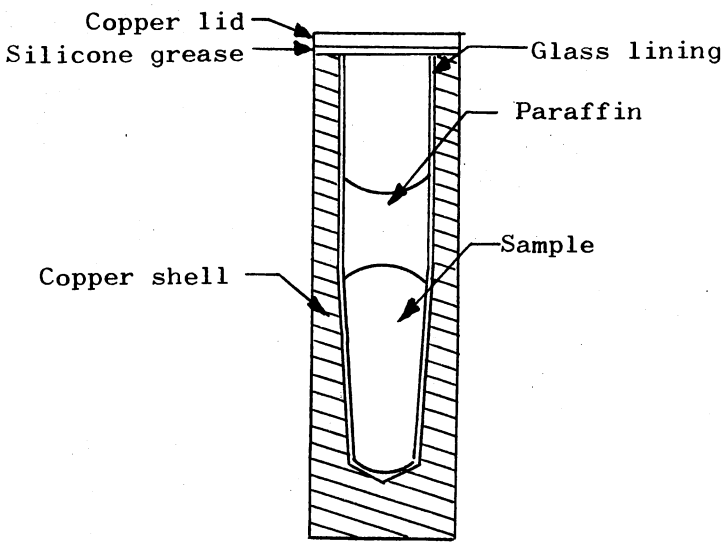

Figure 16. Full Scale Cross-Section of the Glass-Lined Copper Mold

The thermal properties of the mold were determined by running a series of cooling curves for tin. A family of these curves is shown in Figure 17.

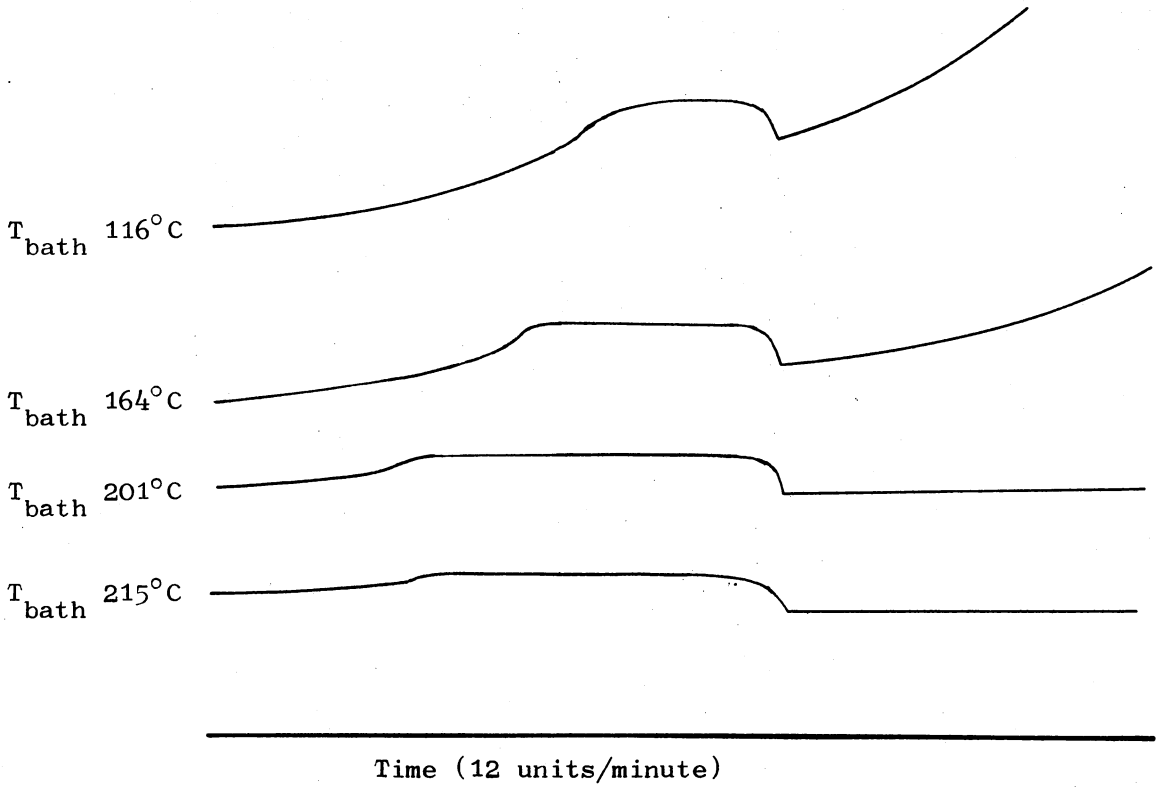

Figure 17. Cooling Curves for the Glass-Lined Copper Molds Resulting From Immersion in a Constant Temperature Liquid Metal Bath

CHAPTER VII

RESULTS OF THE SOLIDIFICATION OF ALLOYS FROM EUTECTIC SYSTEMS IN ROTATING MOLDS

The role of dendrite breakage in promoting the growth of new crystals in the melt ahead of the interface was examined. A two phase alloy was prepared, homogenized and loaded into the mold. It was remelted and then allowed to cool while the mold was rotated at a constant speed, up to 6800 rpm. The basic data for samples solidified this way is given in Table XI and the phase diagram for each alloy system is shown in Appendix B.

TABLE XI

SPEED OF ROTATION FOR SAMPLES SOLIDIFIED WHILE SPINNING

Alloy Composition (w%)	Eutectic Composition (w%)	Speed of Rotation (rpm)	Density Difference Liquid - First Solid (g/cm^3)
Bi-20%Pb	34.5%Pb	6750	0.31
Bi-15%Sn	43 %Sn	3600	- .38
Bi-15%Cd	40 %Cd	3550	- .17
Pb-35%Sn	61.9%Sn	4150	- .89
Sn-15%Pb	38.1%Pb	200	0.57
Sn-15%Pb	38.1%Pb	600	0.57
Sn-15%Pb	38.1%Pb	1800	0.57
Sn-15%Pb	38.1%Pb	3700	0.57
Sn-32%Pb	38.1%Pb	4550	0.57

Bismuth - Pb_2Bi

The results of solidification of the bismuth rich bismuth-lead alloy is considered here first because bismuth forms a faceted phase that can be studied easily. The macrostructure of the sample formed from this alloy is shown in Figure 18 and the microstructure in the following five figures. It consists of a random collection of bismuth crystals near the hollow center of the sample, with closely spaced cellular dendrites of bismuth growing outward. These terminate to form the eutectic structure. Lead dendrites and a few bismuth crystals are found on the very outer edge of the sample.

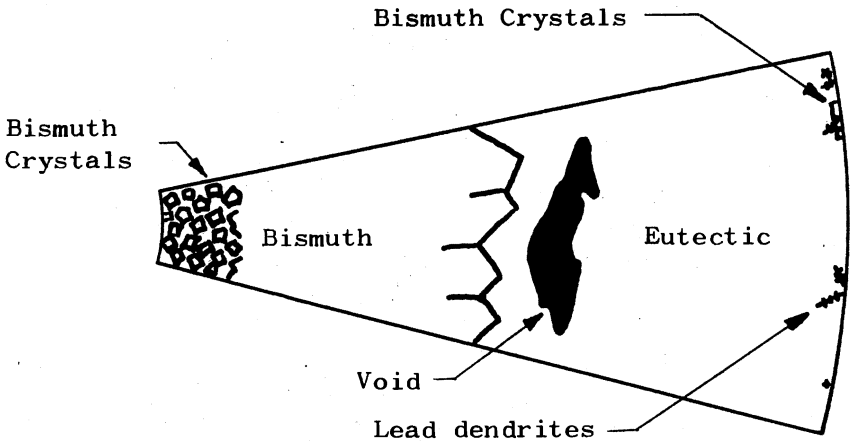

Figure 18. Diagram of the Bismuth - Pb_2Bi Sample Showing Elements of the Macrostructure

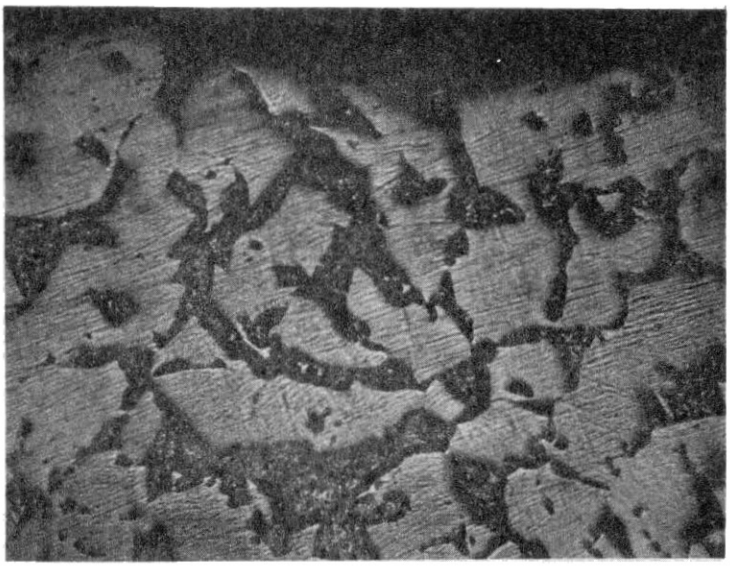

Figure 19. Randomly Packed Bismuth Crystals Found at the Center Surface of the Lead-Bismuth Sample. X60

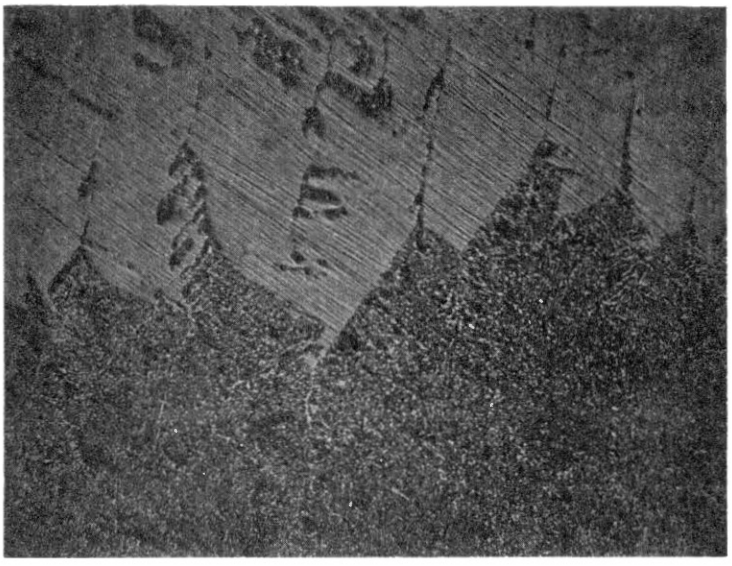

Figure 20. Outward Growing Bismuth Crystals in the Lead-Bismuth Sample. X60

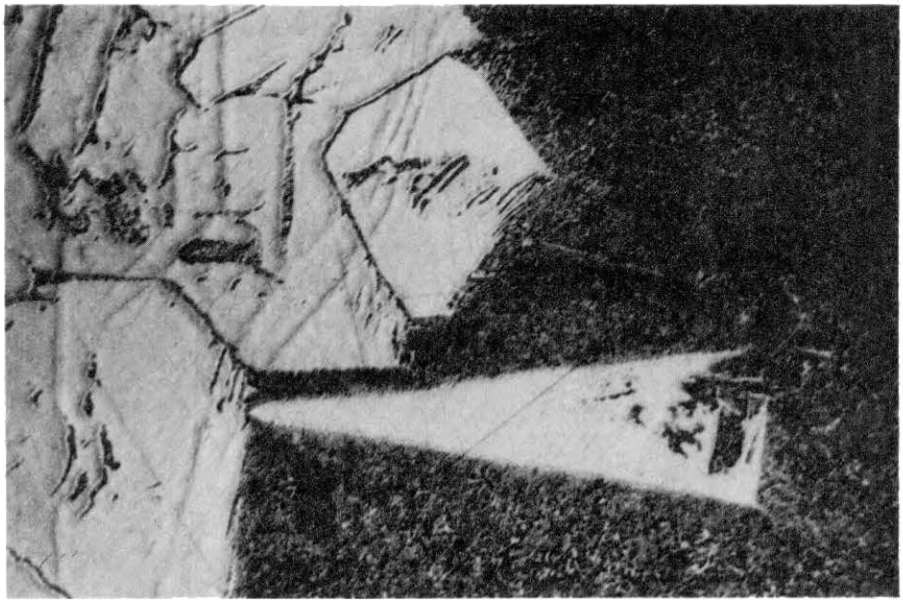

Figure 21. Bismuth-Eutectic Interface Showing an Independent Bismuth Crystal. X60

Apparently the lighter bismuth was nucleated on the outer surface of the sample and the crystals grew to an appreciable size (0.1 to 0.5 mm). At this point the buoyant force created by the rotation was sufficient to separate them from the mold wall and float them to the center. Once there they were packed together randomly. The many sharp corners of these faceted particles and the general lack of cusps on their sides show that only limited remelting occurred. On the contrary, these crystals may have acted as heat sinks as they traveled to the center. They had been cooled physically and by constitutional effects at the perimeter so that their temperature was substantially below the equilibrium temperature of the center liquid. This liquid had remained at its initial composition because Pb_2Bi-rich liquor rejected during the formation of the peripheral bismuth crystals was kept away from the center by the rotational forces.

The movement of the cool crystals to the center causes the radial temperature distribution to be flattened and alters the composition gradient. Cellular dendrites of bismuth grow outward from these first crystals through the adjacent liquid. The heat of fusion is dissipated outward, in the same direction as the growth. At the same time nucleation of more bismuth at the outer surface was being limited by the layer of solute-rich solution there, and only a few more bismuth crystals were formed. One is shown in Figure 21 as it is centrifuged to the center to meet the outward growing dendrites there.

Finally Pb_2Bi was nucleated, both at the bismuth-melt interface where bismuth could serve as a nucleant, and at the outside edge where it was coolest. The Pb_2Bi nucleated at the interface grew along with the bismuth, outward, to form the eutectic. The Pb_2Bi nucleated at the outside edge formed dendrites and began growing inward. This appears to have caused the re-nucleation, or at least renewed growth, of bismuth there. This resulted in the inward growth of eutectic. A shrinkage cavity was formed when the inward and outward growing eutectics came together. The presence of bismuth crystals at the outer surface, Figure 23, and its implications will be discussed later.

Bismuth-Cadmium

In the bismuth-cadmium sample bismuth formed initially on the outside, and being heavier, stayed there. The resultant micro-structure consisted first of columnar dendrites of bismuth growing inward from the mold wall; secondly, of separate bismuth crystals a bit further inside and at the inner surface; and thirdly, of cadmium needles along the bismuth-eutectic interfaces and at the inner surface. Figure 24 is a

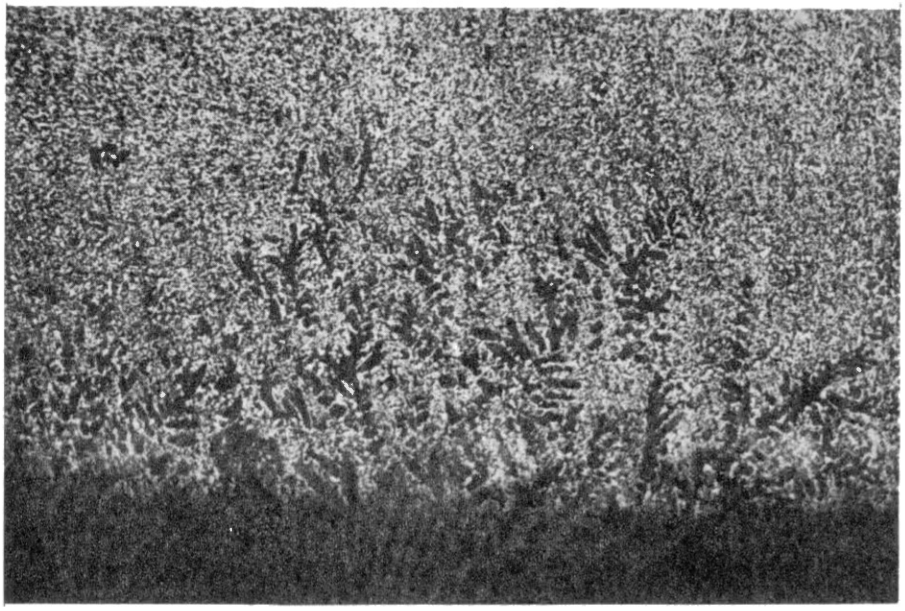

Figure 22. Pb_2Bi Dendrites at the Outer Edge of the Lead-Bismuth Sample. X60

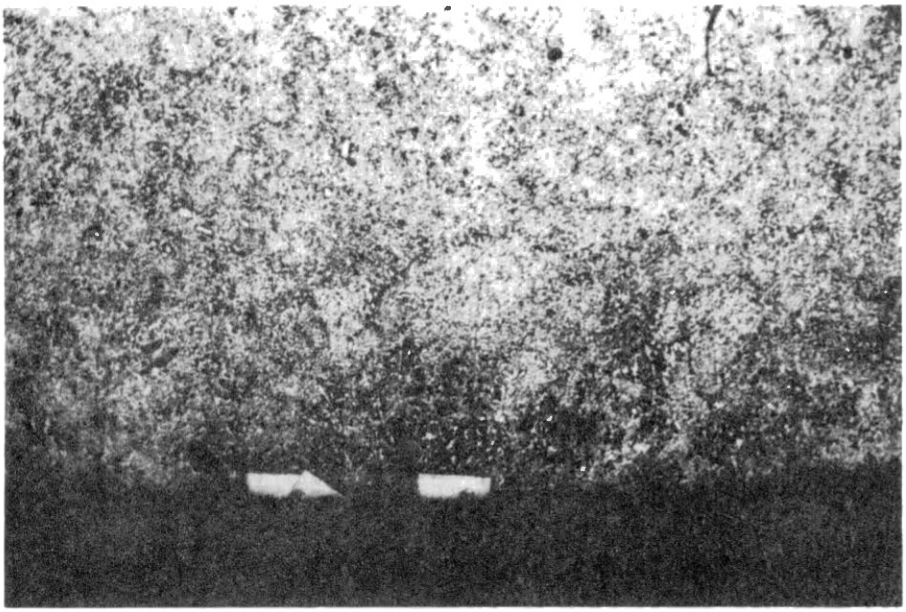

Figure 23. Bismuth Crystals and Pb_2Bi Dendrites at the Outer Edge of the Lead-Bismuth Sample. X60

drawing of the macrostructure of this sample. Micrographs of the structures are shown in Figures 25 through 30.

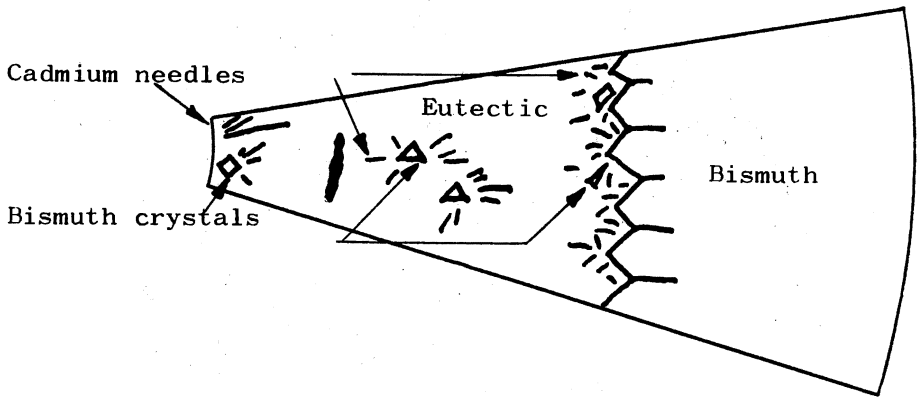

Figure 24. Diagram of the Bismuth-Cadmium Sample Showing Elements of the Macrostructure

During the solidification of this sample cool cadmium-rich liquid, rejected as the bismuth crystals grew inward, was centrifuged to the center. This resulted in the reduction in both the thermal and constitutional gradients, and the nucleation of bismuth in the melt. A few of these bismuth crystals stayed on the inner surface, while others settled outward and were packed up against the columnar crystals. Figure 28 shows two bismuth crystals trapped on their way to the interface by the solidification of the eutectic. Cadmium was eventually nucleated as cooling continued with the bismuth rhombohedrons apparently acting as nucleants. Cadmium grew dendritically for a time and then the growth form changed to the coupled form of the eutectic. As in the

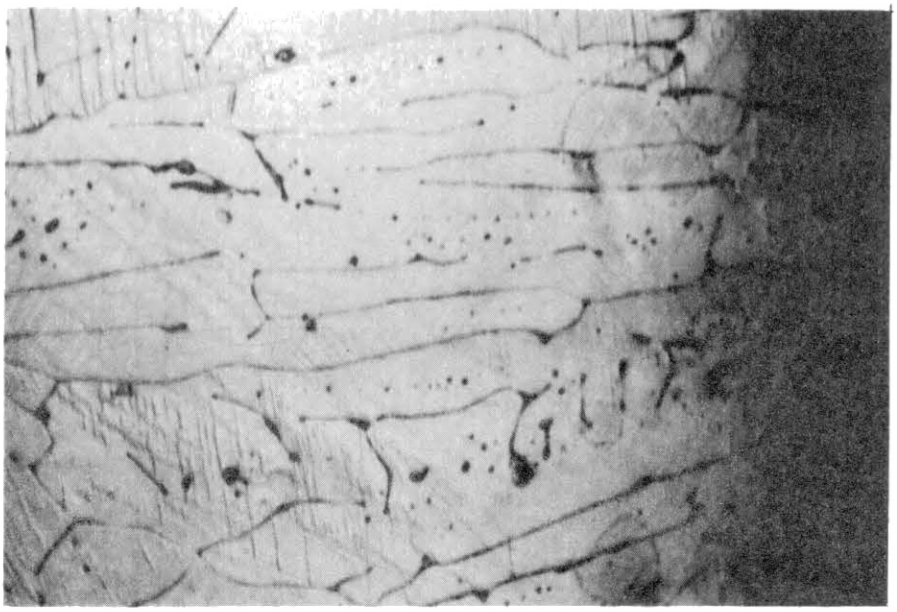

Figure 25. Inward Growing Bismuth Crystals and the Bismuth-Cadmium Eutectic. X60

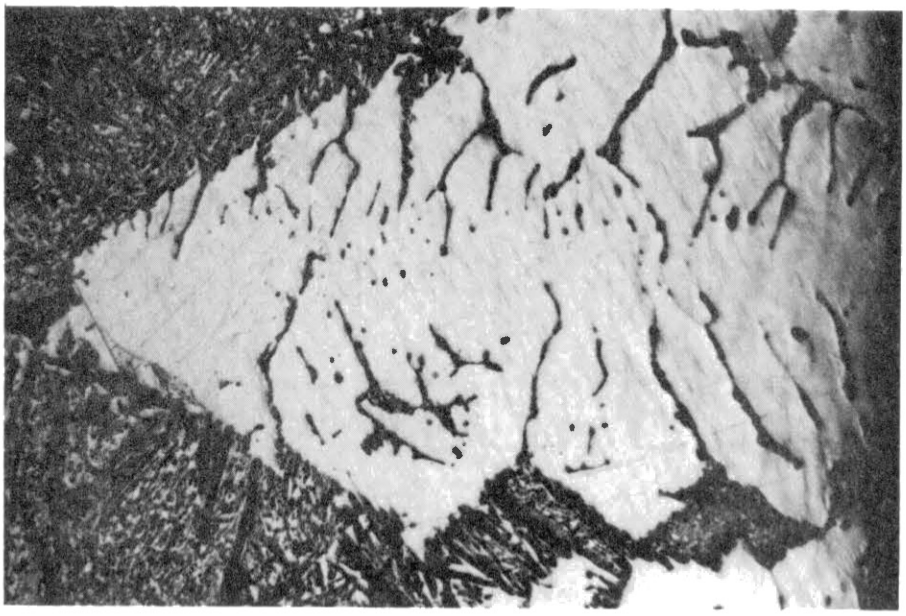

Figure 26. The Bismuth-Eutectic Interface in the Bismuth-Cadmium Sample. X60

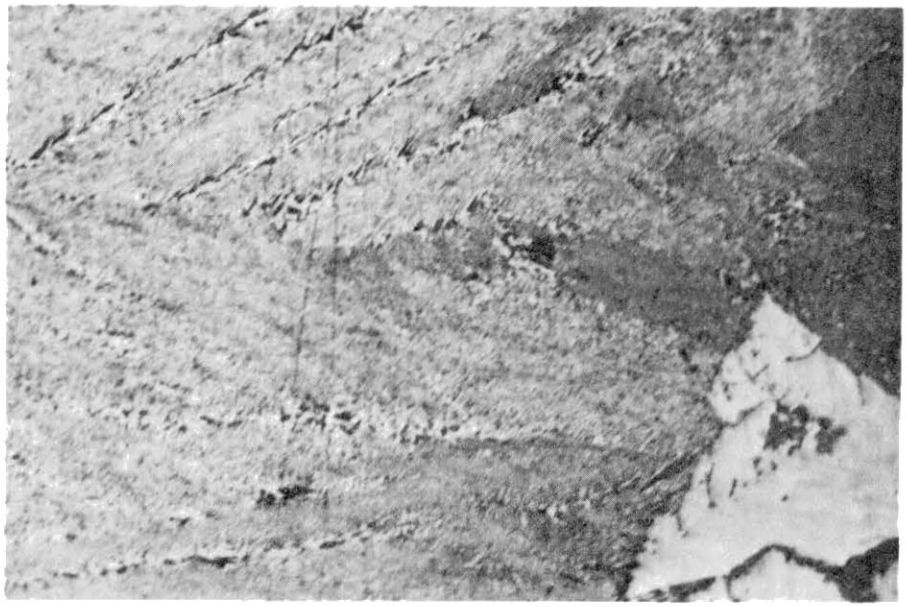

Figure 27. Inward Cellular Growth of the Bismuth-Cadmium Eutectic. X60

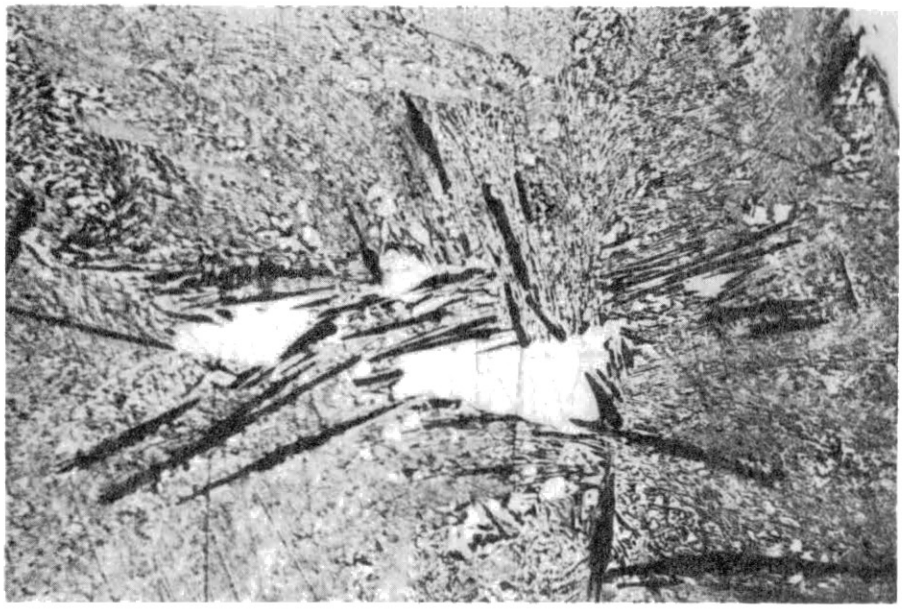

Figure 28. Independent Bismuth Crystals Frozen in the Bismuth-Cadmium Eutectic. X60

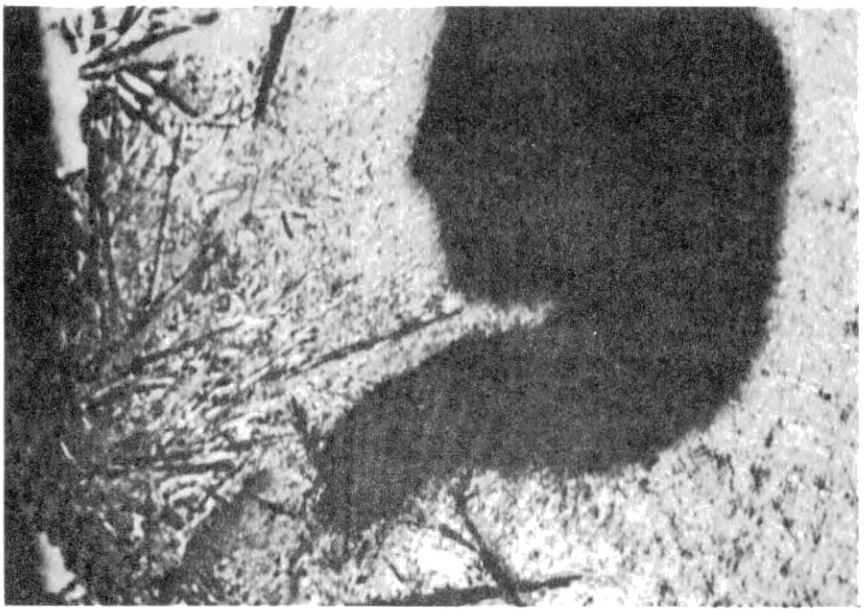

Figure 29. Bismuth and Cadmium Crystals at the Inner Edge Showing a Shrinkage Void. X60

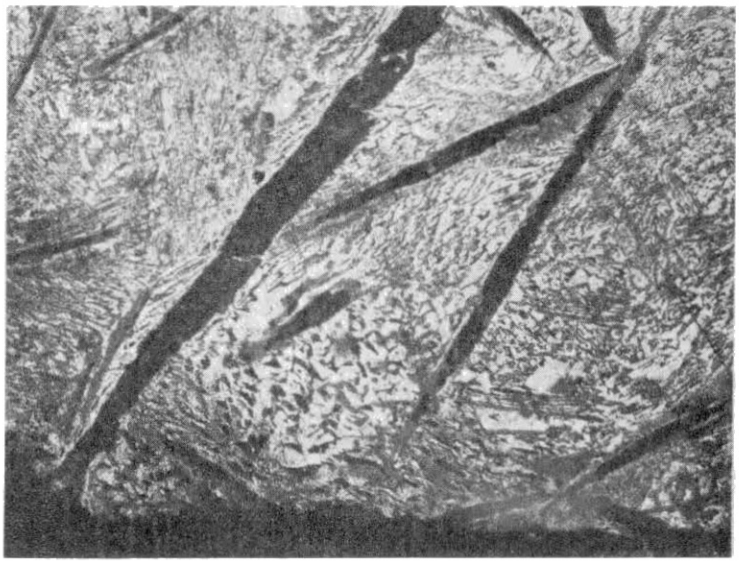

Figure 30. Cadmium Needles at the Inner Edge of the Bismuth-Cadmium Sample. X100

Pb_2Bi-Bi case, eutectic grew both inward and outward forming a void at an intermediate radius.

Bismuth-Tin

Bismuth also formed first in the bismuth-rich Bi-Sn alloy. As it is more dense it stayed along the outside edge. Figure 31 is a schematic of the resultant macrostructure, and Figures 32 through 34 show the sample microstructure. It consists of columnar bismuth crystals at the outside, a few individual bismuth crystals at or near the inner surface, and tin dendrites growing outward from the inner surface.

The formation of this sample was similar to that of the bismuth-cadmium sample. Relatively tin-rich liquid was rejected during the growth of the bismuth dendrites, and centrifuged to the center. The same reduction in the thermal and concentration gradient occurred and bismuth was nucleated in the melt. Then tin was nucleated at the inner surface and independently at the bismuth melt interface. The tin formed at the inside surface grew dendritically at first, and then with bismuth as the eutectic. The tin nucleated at the interface grew immediately as eutectic, coupled with bismuth. No void was seen in this sample. However, a substantial portion of the sample leaked before solidification began and the thickness of the sample was reduced -- so this might be expected.

Lead-Tin

A lead-rich lead-tin alloy was also prepared and solidified in the rotating mold. The lead has a non-faceted structure and offers a

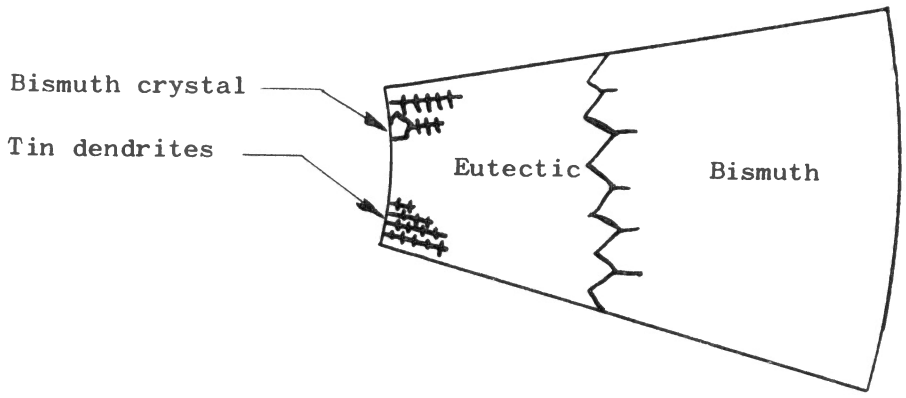

Figure 31. Diagram of the Bismuth-Tin Sample Showing Elements of the Macro-structure

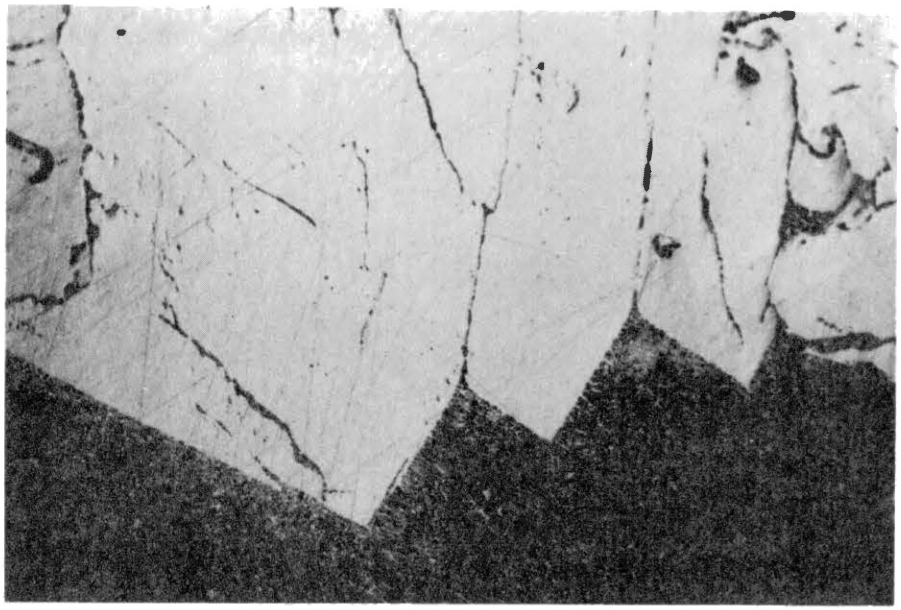

Figure 32. Inward Growing Bismuth Crystals and the Bismuth-Tin Eutectic. X60

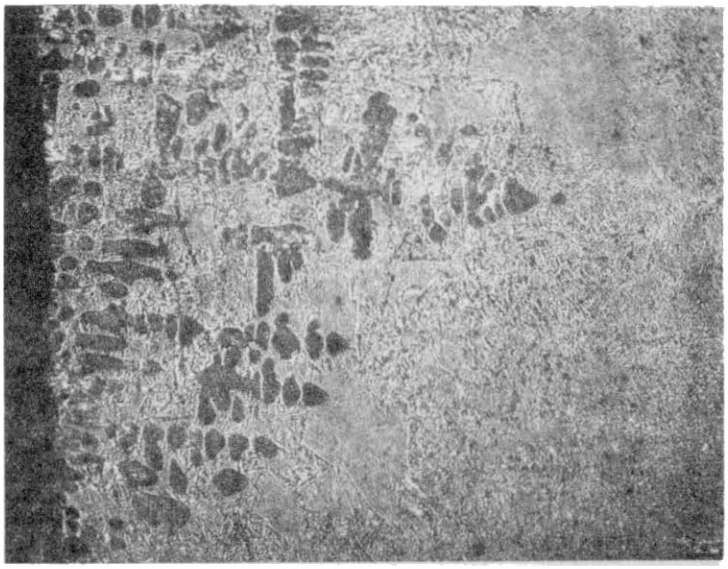

Figure 33. Tin Dendrites at the Inner Surface of the Bismuth-Tin Sample. X100

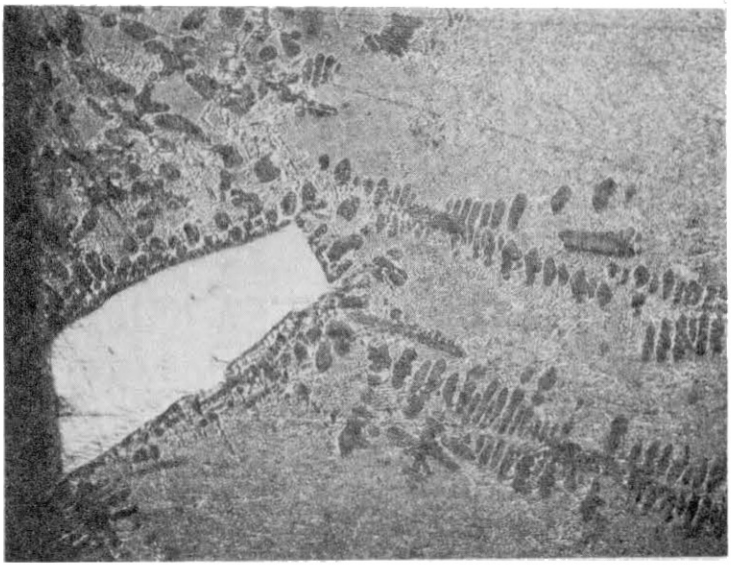

Figure 34. Bismuth Crystal and Tin Dendrites at the Inner Surface of the Bismuth-Tin Sample. X100

contrast for comparison with the alloys of bismuth and cadmium. Figure 35 shows the macrostructure of the lead tin sample, and Figures 36 through 40 show its microstructure.

Lead formed first and presumably grew inward to form a coarse dendritic structure. This is not apparent from the micrograph shown in Figure 36 however. Extensive precipitation of tin occurred in the lead crystals, and deformation of the soft lead dendrites may have destroyed the order characteristic of the dendritic structure.

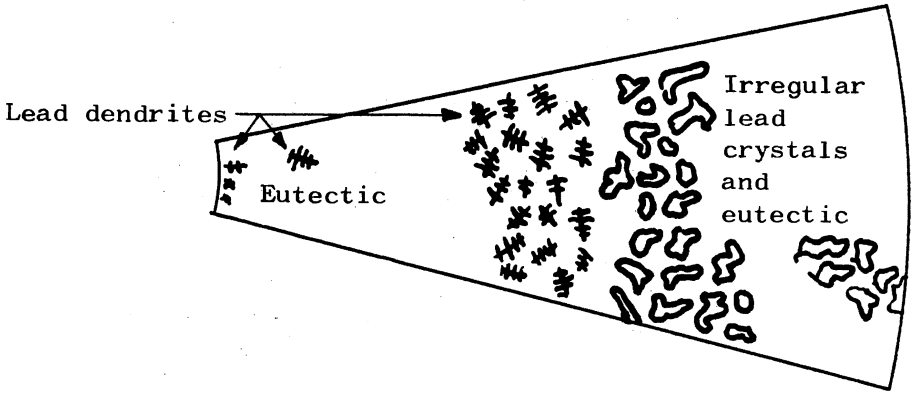

Figure 35. Diagram of the Lead-Tin Sample Showing Elements of Its Macrostructure

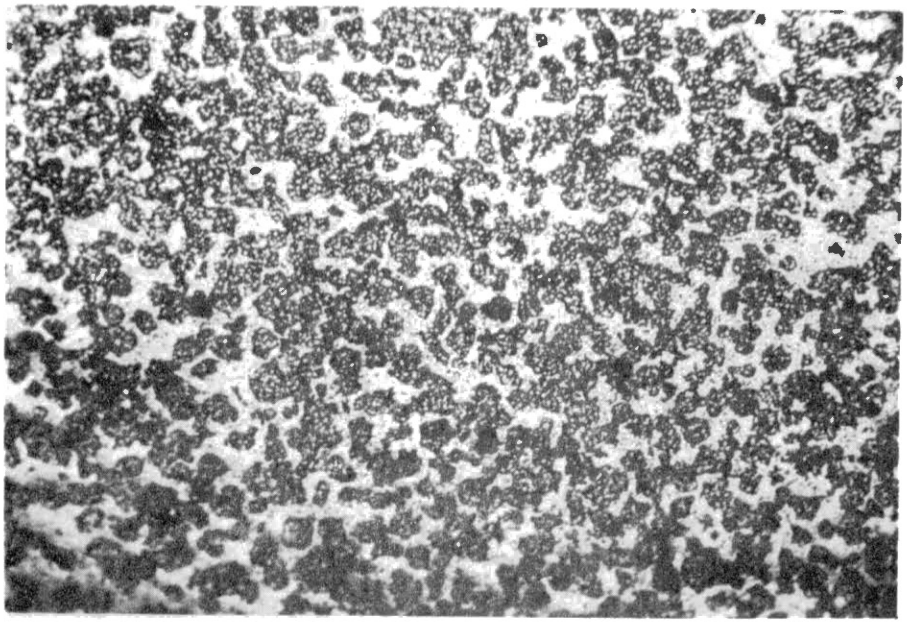

Figure 36. Primary Lead "Dendrites" Formed Near the Outer Edge of the Lead-Tin Sample. X60

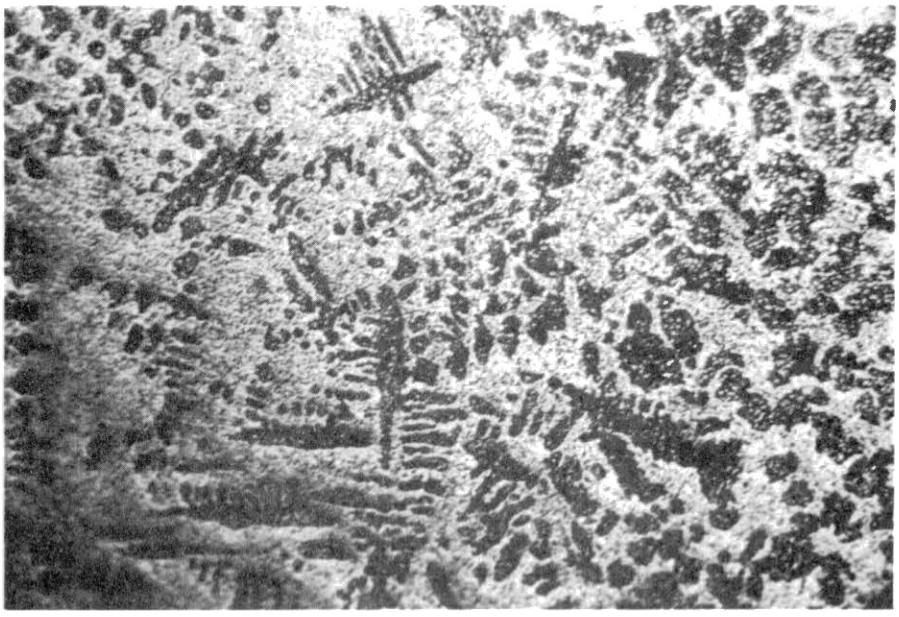

Figure 37. Interface Between the Primary Lead and the Random Lead Dendrites. X60

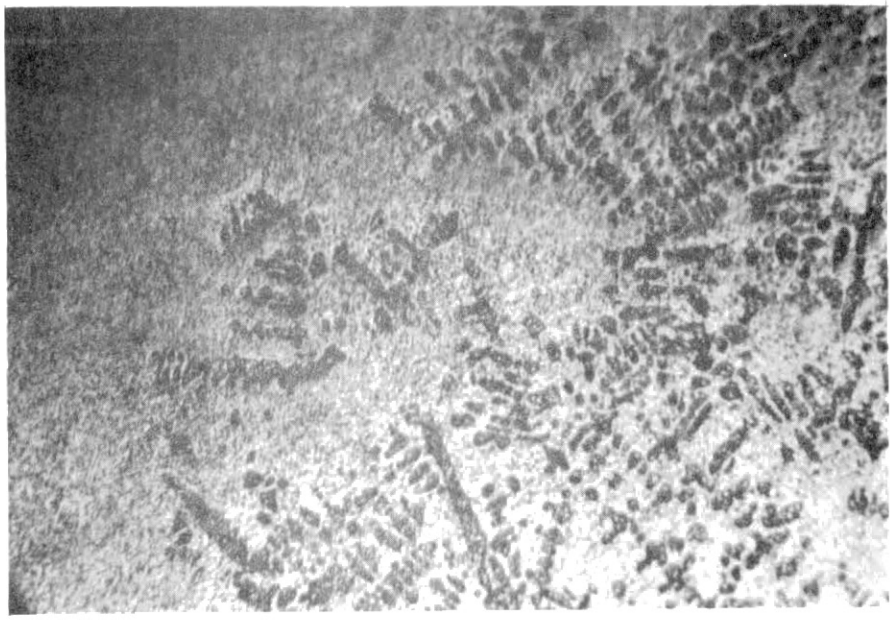

Figure 38. Interface Between the Random Lead Dendrites and the Lead-Tin Eutectic. X60

Figure 39. An Independent Lead Dendrite Frozen in the Lead-Tin Eutectic. X60

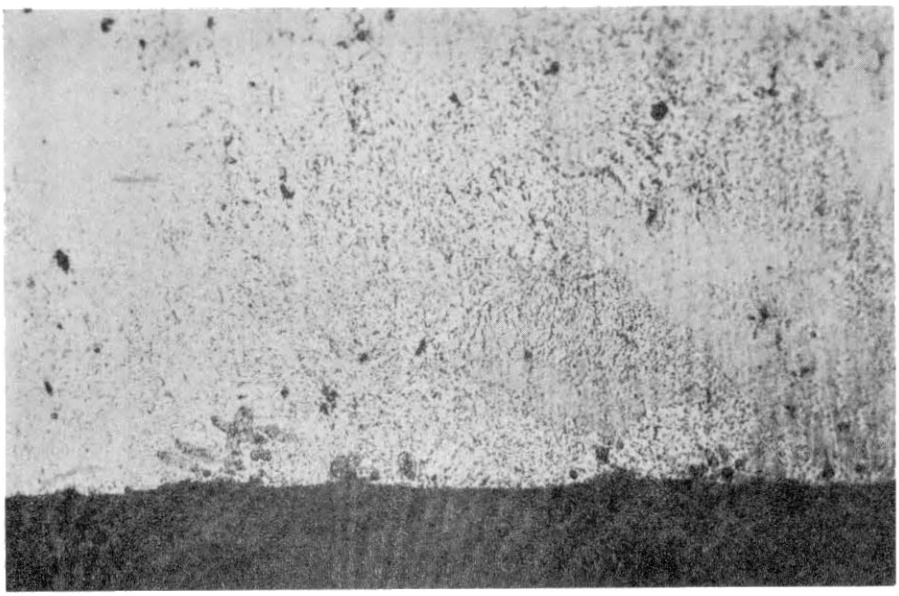

Figure 40. Lead Dendrites Formed at the Inner Surface of the Lead-Tin Sample. X60

Solute rich liquid rejected during the formation of this lead is lighter than the original liquid and was centrifuged rapidly to the center. This motion was reflected in some macrosegregation along the lines of flow; and these were curved because of coriolis acceleration. The inward motion in the liquid caused a flattening of the temperature distribution so that lead crystals were nucleated heterogeneously in it. Figure 40 shows lead dendrites formed this way at the inner surface. As cooling continued these crystals grew until they were about 0.2 to 0.3 mm long. At this point the force from the volume of the liquid they displaced became great enough to separate them from the surface. They floated outward and were packed randomly against the original lead dendrites. This process continued, causing the liquid to become

increasingly tin-rich until tin was finally nucleated. It then grew together with lead as eutectic until solidification was complete. No tin dendrites were found along the inner surface and no voids were observed.

Tin-Lead

The fifth alloy studied, tin-rich tin-lead also has a non-faceted structure. Tin dendrites formed initially, and after reaching lengths of about 0.2mm they were spun to the center. The resultant microstructure consisted of the random packing of these tin dendrites in the center, faint evidences of the outward growth of tin from this area, lead dendrites along the outside surface, and eutectic. Again the eutectic grew both inwards and outwards, leaving a void in the middle. Figure 41 shows the macrostructure typical of the tin-rich samples. Figures 42 through 45 show the resulting microstructures.

The cool tin dendrites that were floated to the center reduced the amount of superheat in the liquid there and served first as the basis for the further growth of tin. Later, lead was nucleated here, too, and the eutectic structure was formed. Lead was also nucleated at the mold wall. This material, in contrast, grew dendritically at first -- until tin was re-nucleated there to form the eutectic. As in two of the previous cases an intermediate void was formed when the two eutectic solid-liquid interfaces approached each other.

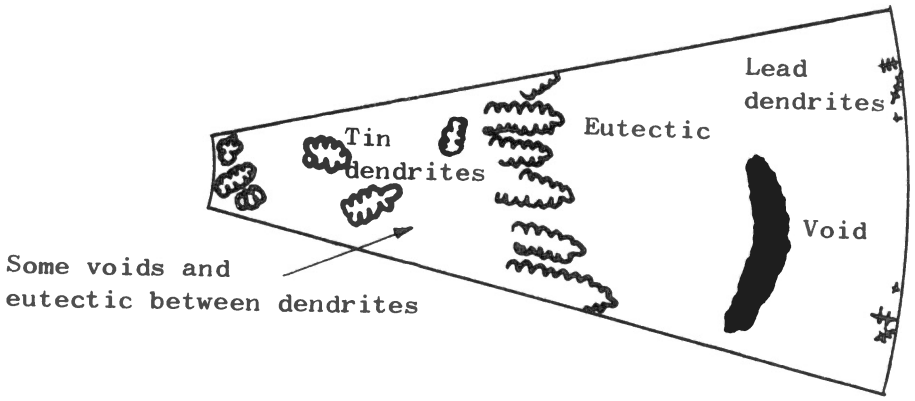

Figure 41. Drawing of a Tin-Lead Sample Showing the Elements of Its Macrostructure

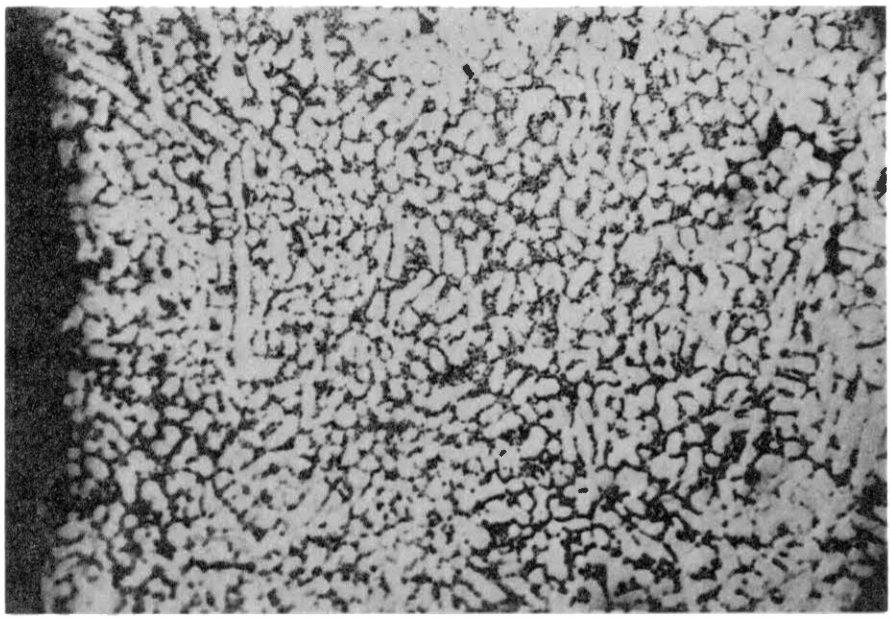

Figure 42. Tin Dendrites Randomly Packed at the Center Showing Shrinkage Voids and Trapped Lead-Tin Eutectic. (3700 rpm) X60

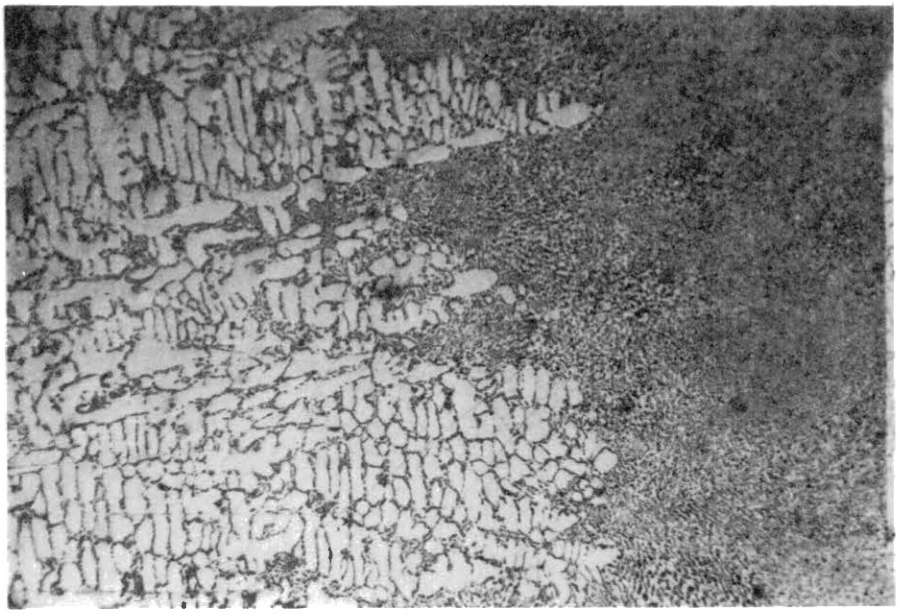

Figure 43. The Tin-Eutectic Interface Showing Outward Growing Tin Dendrites. (4550 rpm) X60

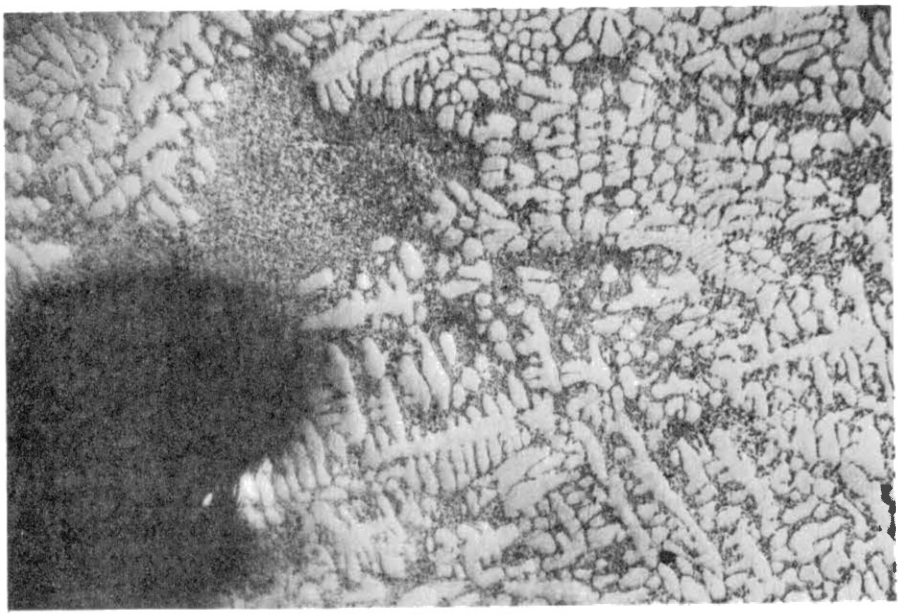

Figure 44. Shrinkage Void in the Lead-Tin Eutectic Near the Outer Edge of the Sample. (3700 rpm) X60

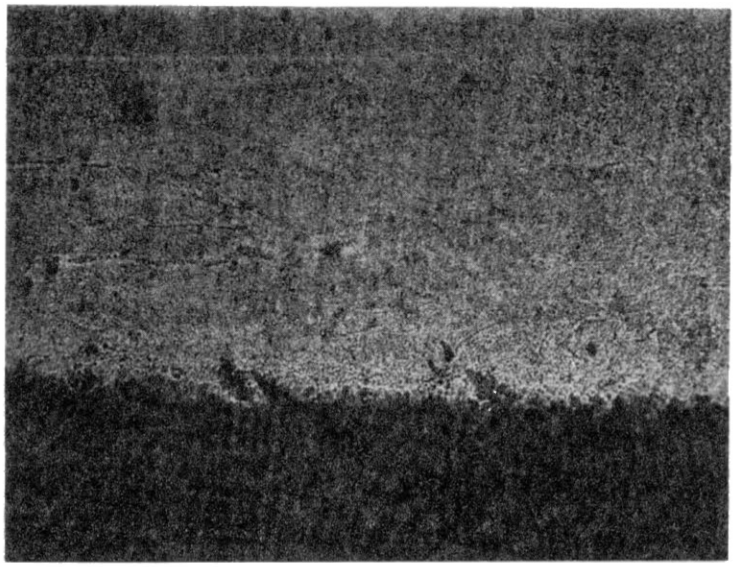

Figure 45. Lead Dendrites at the Outer Edge of a Tin-Lead Sample. (4550 rpm) X50

Variations in Spin Speed

Several samples of tin-rich tin-lead alloy were solidified with different speeds of rotation. The one sample that was solidified without rotation had a uniform structure composed of tin dendrites that were surrounded by eutectic. No differences could be found between this and a sample rotated at 200 rpm. At 650 rpm, however, one could detect some inward motion of dendrites through the appearance of dendrite free areas filled with eutectic. For samples spun at speeds of 1900 rpm and above the tin was completely removed from the outer wall and packed in the center. Lead dendrites were also found, on the outer surface, growing inward in all of these samples. The number of these dendrites was roughly proportional to the speed of rotation.

These effects can be explained in a straightforward way. Without rotation, crystals of tin were nucleated along the outer edge of the sample. Then they grew dendritically inward in a way controlled by the rejection of solute and the resulting constitutional undercooling. The remaining liquid became richer in lead until the eutectic composition was reached. Then the eutectic mixture solidified in the interdendritic spaces.

Rotation only affected this process at moderate or high speeds. With an increase in rotation rate an increased buoyant force is applied to the tin dendrites because of the difference in density between the solid and liquid. The force increases with the volume of the dendrite and toward the later stages of growth (when $\Delta\rho$ is larger). The shear strength of the dendrites and the strength of the bond between the dendrites and the mold wall also increases, but only as the cross-sectional area. Thus, the buoyant force overtakes the bond or shear strength as the speed of rotation is increased. The weakest link, found to be the dendrite-mold bond, breaks and the dendrites float free in the melt.

It is important to note that neither the alteration of the proportion of excess tin nor the speed of rotation resulted in a significant decrease in the final grain or dendrite size. Eutectic lead-tin structures with and without rotation and inward and outward growing were all very similar too. The absence of any change of this kind indicates that the tin dendrites were not easily broken. Hence, the breaking of dendrites is not an important source of secondary nuclei under normal conditions of solidification, and does not figure prominently in the formation of an equiaxed zone in an alloy ingot.

Instead, rotation effects observed in this work point to two other factors as important in the formation of the equiaxed zone. The first is the reduction of the temperature gradient in the liquid by centrifuging cool crystals or rejected solution away from the interface. The second is heterogeneous nucleation in the liquid or at the far surface which results from the flattened temperature gradient.

This is in agreement with a portion of the work of Cole and Bolling (1967, p. 1824) who determined that "the temperature gradient in the liquid is the vital factor. . . ." Their experiments showed that slow rotation (about 100 rpm) suppressed motion in the liquid and that this caused the columnar to equiaxed transition to be delayed. This was attributed to a decrease in the convective heat transfer that kept the temperature gradient in the liquid from decreasing rapidly. The mechanism for nucleation, defined as intricate detail, was largely ignored in their work even though Tiller (1962, p. 457) had predicted mathematically a large increase in the frequency of nucleation with a "decrease in the temperature gradient at the interface." Finally, the recent work of Burden and Hunt (1975) substantiates the importance of the temperature gradient in the melt. They predicted that equiaxed crystals grow in the liquid as soon as the temperature gradient ahead of the interface becomes flat. Then the latent heat they release serves to retard the growth of the columnar interface.

Hypoeutectic Dendrites

In four of the systems examined dendrites of the minor phase were found, at one surface or at the interface between the other component and the eutectic.

A review of the procedures used to prepare the samples shows that there is no mechanism for the formation of inhomogeneities during this procedure that would otherwise account for the results. In each case eutectic alloy was mixed with the primary phase and melted. Heating was continued to a temperature of 50° superheat. Then the sample was stirred and poured into the mold. Finally, the mold and sample both were reheated enough to remelt the primary component. This guaranteed the complete remelting of any solid of near eutectic composition.

Sensitivity of the phase diagram to pressure developed during rotation was also dismissed as a possible explanation because (1) condensed systems do not often show such a sensitivity, and (2) the formation of second phase dendrites occurred twice at the inner surface where the pressure was only slightly greater than atmospheric pressure.

Second phase dendrites can occur, according to one explanation, if the two components in a eutectic liquid supercool different amounts. Then, if the first to solidify does not readily nucleate the second it (the first) will grow dendritically until the undercooling becomes sufficient for nucleation of the second phase (Chalmers, 1964). This can account for the lone Pb_2Bi, lead, tin, and cadmium dendrites which formed from an eutectic solution at the surface opposite from the primary phase.

The independent nucleation of the second phase has been suggested as an alternative explantion. Powell and Hogan (1968) studied both hypo- and hypereutectic alloys of the copper and cuprous oxide system. The solidification of the copper-rich alloy began with the undercooling and nucleation of copper. After recalescense and further undercooling the Cu_2O was nucleated. Partial recalescense followed during the

solidification of the eutectic. However, the oxide-rich alloy solidified another way. The oxide undercooled and nucleated first, recalescense occurred, and the undercooling of copper followed. When copper was nucleated it grew dendritically and a second complete recalescense followed. Formation of the eutectic did not occur until after this second recalescense. This was attributed to different effective nucleants and is summarized as follows: If the first phase nucleates the second the growth is of an eutectic type -- if the second is nucleated independently, growth is dendritic.

In a later work Powell and Cooligan (1970) observed the dependent nucleation in tin-rich Sn-Bi and lead-rich Pb-Sb. Second phase dendrites existing alone in the four samples can be satisfactorily explained by independent nucleation.

Neither unequal undercooling nor independent nucleation can explain adequately the related dendritic structures seen in Figures 23, 29, and 34. With one phase already present as a solid, the dependent nucleation of the second phase should be followed immediately by the onset of coupled growth. This is because coupled growth occurs with a smaller amount of supercooling than the growth of either component separately.

Separation of the components of the eutectic liquid by the combined activity of rejection during solidification and centrifugation is an explanation that can account for the related dendritic structure. It has been shown that slightly superheated eutectic liquids are probably composed of clusters of 10^3 to 10^4 atoms each (Lashko and Romanova, 1961). Furthermore, it is reasonable to assume that there are two kinds of clusters, one component dissolved in the other at the concentration corresponding to that of a saturated solution at the melt

temperature, and vice versa. The growth would deplete the population of one kind of cluster in the immediate area, and centrifuging could remove the rejected material before mixing by convection or diffusion could occur -- if it had a different enough density.

In each of the systems examined, one surface would be expected to have a layer of hypereutectic liquid, the inside surface for Bi-rich Sn-Bi and Bi-rich Cd-Bi or the outer surface for tin-rich Sn-Pb and Bi-rich Bi-Pb. The second phase would be nucleated in this layer by any effective heterogeneous nucleant (including stray first phase crystals) and it would grow dendritically until the melt was returned to the eutectic composition. Unless the first phase was present nearby it would then have to be nucleated locally before the eutectic structure could form.

Other evidence suggests that the eutectic liquid may be separated this way. Vertman, Samarin and Yakobson (1960) observed the formation of lead dendrites when eutectic mixtures were solidified in a centrifuge. Fisher and Phillips (1954) observed anomalies in the viscosities of slightly superheated eutectics, and Danilov and Radchento (1936) found that the x-ray photographs of eutectic liquids are like a superposition of photographs of the two components. Finally, G. M. Bartenev (1970, p. 16) observed the following:

> At present it is generally accepted that full atomic intermixing does not exist in liquid eutectic alloys and they consist of colonies in which a particular component is concentrated. Such a structure of liquid eutectics is called quasi-eutectic. All methods of research into the properties of liquid eutectics confirm this view concerning their structure.

CHAPTER VIII

VARIATIONS IN UNDERCOOLING

Tin and tin alloy samples were prepared and melted under liquid cover to study the effects of process variables on supercooling. The solidification was followed by recording the response of a thermocouple imbedded in the sample. This allowed observation of the sample's thermal behavior after each change of a variable.

Cooling Curves

The cooling curves for samples solidified in the pyrex molds were all very similar to those shown in Figure 15. The point of reversal in the curve was not found to vary for the range of cooling rates investigated, and recalescense to the equilibrium temperature was consistently observed. One sample was heated and cooled repeatedly, and the cooling rate was varied. The temperature of reversal when the cooling rate was fast ($720^{\circ}C$/min) was $198 \pm 2^{\circ}C$. This was not significantly different from the reversal temperature of 199 ± 3 when the cooling rate was slow ($42^{\circ}C$/min).

Recalescense temperatures for a variety of samples, all cooled at the slow rate, are shown in Table XII. In only one case was the recalescense temperature significantly lower than the equilibrium temperature. This sample was the only tin alloy with appreciable lead that was repeatedly cycled, and that displayed much undercooling.

TABLE XII

RECALESCENSE TEMPERATURES OBSERVED

Sample	Number of Samples Measured	Equilibrium Temperature (°C)	Recalescense Temperature (°C)
Tin	27	232	230 ± 3
Tin-1.2% Lead	1	230	231 ± 3
Tin-2.4% Lead	1	228	229 ± 3
Tin-4.8% Lead	7	224	224 ± 2
Tin-9.5% Lead	1	214	210 ± 3
Tin-9.5% Lead	1	214	203 ± 3
Tin- 19% Lead	3	204	204 ± 3
Tin- 38% Lead	1	183	184 ± 3

Superheat Temperature

A thermal cycle was chosen which consisted of heating to temperature in a liquid metal bath, a one-minute soak, and cooling in air. Only the superheat temperature was changed. The resultant changes in supercooling (defined by the point of reversal on the cooling curve) that were found are shown in Figure 46.

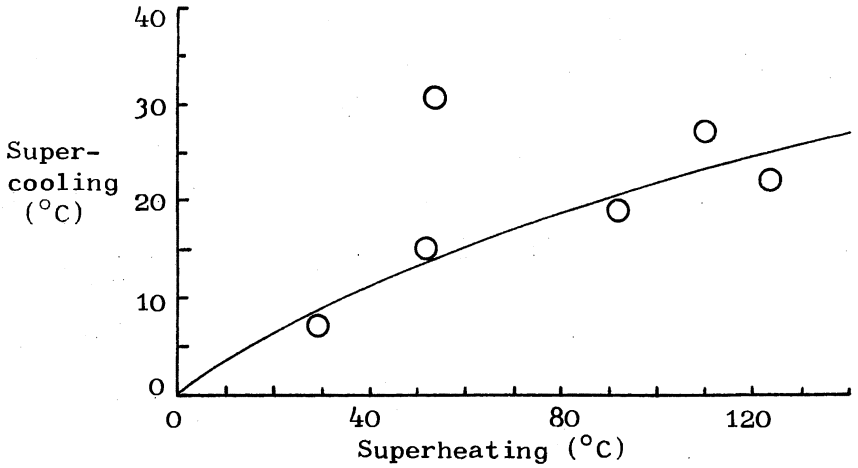

Figure 46. The Variation in the Supercooling of Reagent Grade Tin Caused by Different Superheat Temperatures

Superheat Time and Tin Source

Tin from three sources, Matheson Coleman and Bell, Baker, and Materials Research Corporation was used, and the time at different superheat temperatures was varied. The samples were heated to the desired temperature, soaked for a measured time and then cooled slowly. After recalescense occurred, the samples were reheated to the superheat temperature and soaked for a second (longer) interval. This procedure was repeated until the total time at superheat temperature approximated 330 minutes. Figure 47 shows the effect of superheat time and tin origin on supercooling that was observed.

A sample of Baker tin-19% lead was treated in an identical manner. (The amount of superheating was 53°C.) The supercooling was found to increase with time in much the same way as the supercooling for Baker tin increased for the same absolute superheat temperature. This is illustrated by Figure 48 which shows the two increases superimposed.

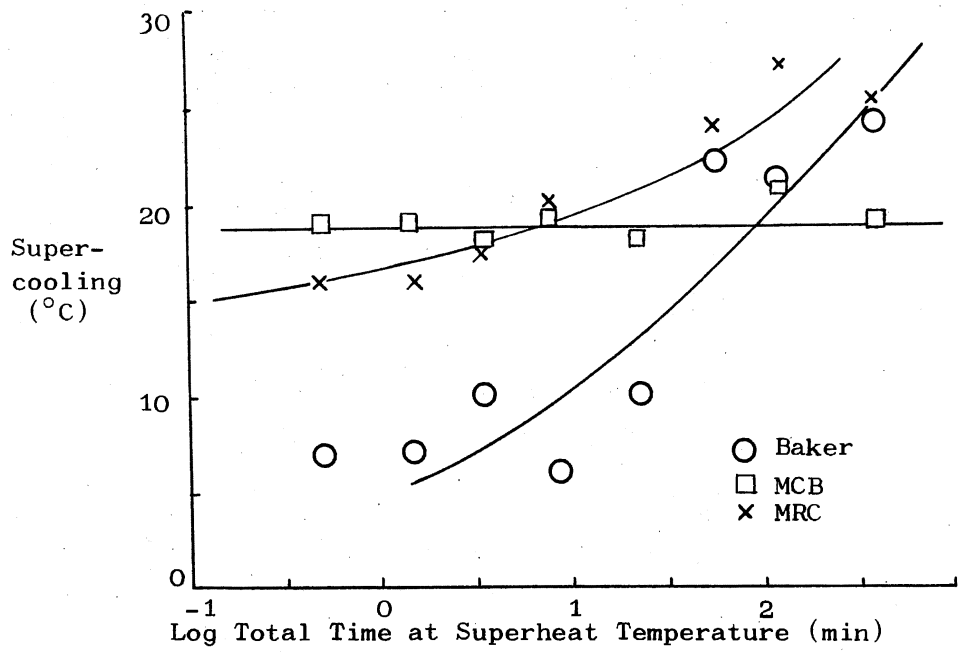

Figure 47. The Supercooling for Single Samples Superheated to 25°C for Increasing Intervals of Time. Three Tin Sources are Compared

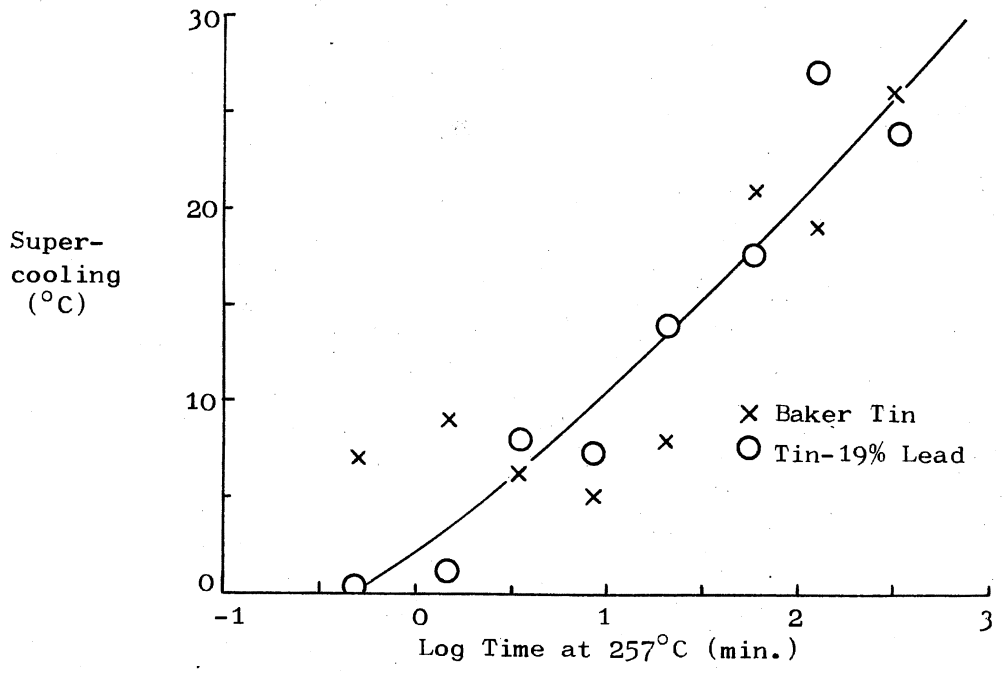

Figure 48. Time Dependent Increases in Supercooling for Tin and Tin-19% Lead

Discussion

Variation is apparent in the amount of supercooling observed for different times and temperatures, and for different sources of tin. It is reasonable to attribute the sources of this variation to two factors, the presence of nucleants of different kinds, and the susceptibility of at least one type to deactivation by heating.

The amount of supercooling observed for Baker and MRC samples increased systematically with increased superheating until a supercooling of about 36°C was reached. The small supercoolings which occurred with little superheat show that very effective nucleants were initially present. These must have been deactivated or destroyed by the increased heating to account for the increases seen.

Efforts to increase the amount of supercooling above 36°C all failed. Takahashi and Tiller (1969) predict such a limitation based on the sample size and the opportunity to form large surface "patches." It is their contention that tin samples would have to be less than 2mm in diameter before a supercooling of 36°C could be obtained. Since the samples studied in this work were 10mm in diameter another explanation is needed. One alternative can be found by assigning the cause for the barrier at 36°C to the presence of a second kind of nucleant, one which is only important when the more effective ones have been destroyed. A second alternative, homogeneous nucleation, is ruled out because that does not occur in tin with supercoolings less than 100°C. Nucleation on the mold wall, a third idea, cannot be ruled out. It is an unlikely candidate however, ceramic type materials are not generally effective nucleants for metals, and because a thin film of the liquid cover probably separated the sample from the pyrex mold wall.

The frequency with which a maximum supercooling of about 36°C is found in the literature (see Table II) is a clue that the cause is common and suggests the first alternative. Oxidies of tin are almost universally present and are considered to be the most likely impurity responsible for the nucleation at 36° undercooling. Oxides were almost certainly present in this work. Samples cleaned in nitric acid exhibited an obvious oxide film, and washing first in water and then ethanol, both with vigorous agitation and shaking, may not have removed all the oxide. This is especially true of the MRC tin since the pieces were cut from an ingot as 1 cm cubes, and the surfaces were more difficult to clean after etching. The oxide Sn_3O_4 is the first one formed with tin at ordinary temperatures, and it is stable above 1000°C (Hansen, 1958).

A second kind of stable nucleant is apparently present in the MCB tin. Undercooling of about 18°C occurs regardless of the time or range of superheat temperatures. The effective nucleant is active at smaller undercooling than the stable species in either the Baker or the MCR tin, and with less than that reported by the several authors cited. The difference is expected to stem from the differences in purity. The analysis of the Baker and MCR tin is given in Table IX for comparison with that of the MCB product. Any of the impurities (or one of their compounds) likely present in MCB tin but not in the others could be the nucleant effective at 18°C undercooling. No further effort was made to identify this nucleant.

The variation in undercooling of Baker tin from 0 to 36°C, depending on superheating time and temperature, is attributed to the deactivation of a nucleant. Glicksman and Childs (1962) report a similar

effect and Tarshis, Walker, and Rutter (1971) report that the amount of undercooling increased two to eight times from that of the initial trial when the samples were repeatedly reheated. This occurred in twelve separate alloys of nickel.

Insight into a mechanism for the deactivation of heterogeneous nucleants can be derived from analysis of data displayed in Figure 49. The half-times for the deactivation of the nucleants were determined for each temperature. This was done by finding the superheat time required to permit a supercooling of 18°C; i.e., the time required to reduce the effectiveness by half. Complete reduction of nucleant effectiveness was assumed to occur when the competing nucleant (effective at 36°C) became the dominant source of nuclei. The Arrhenius equation was chosen to establish the relationship between the several superheat temperatures and the corresponding half-times

$$\ln k = -E_a/R(1/T) + \ln A \qquad (9)$$

since rate constants for chemical reactions conform to it without known exception (Hamill and Williams, 1959). The half times were taken to be equivalent to the reciprocal of the rate constant "k". E_a is the activation energy for the reaction. Figure 50 shows that the experimental data displays the linear relationship predicted by Equation (9).

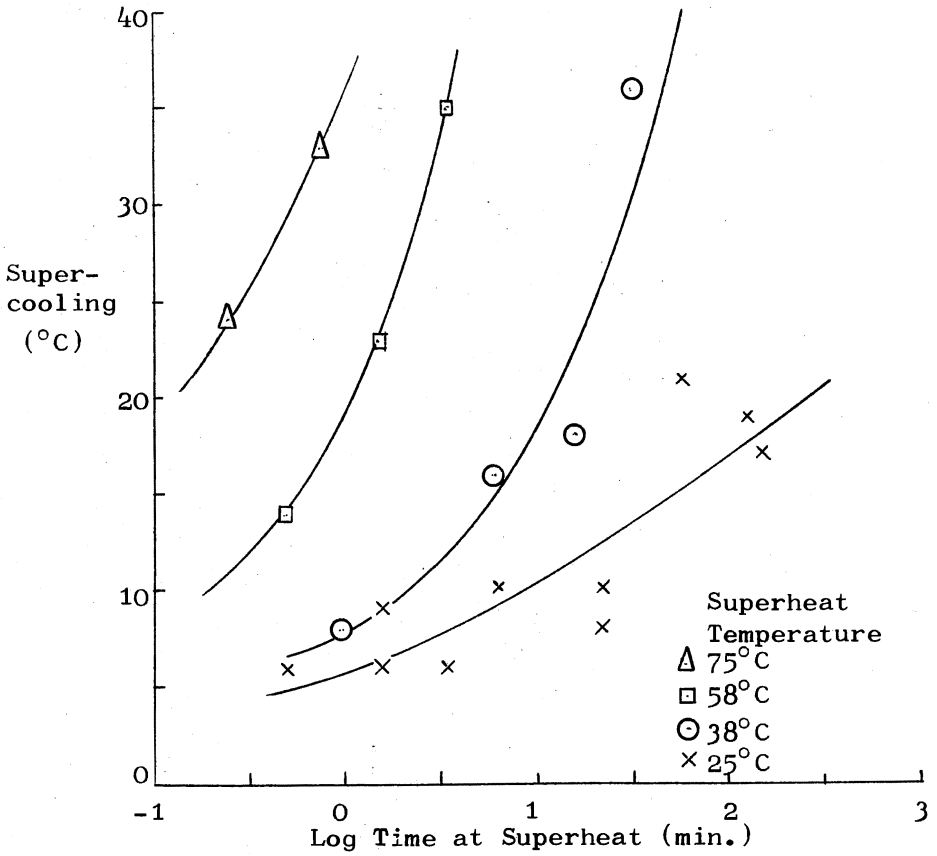

Figure 49. The Influence of the Amount of Superheat and Time at That Temperature on the Degree of Supercooling

The activation energy for the deactivation reaction was found by passing a linear regression line through the data points in Figure 50 and determining its slope. E_a was found to be 36,200 cal/mole or 4.0 eV. This value was surprisingly high, and corresponds in general to the activation energies for chemical reactions. Table XIII gives the activation energies reported for various atomic events for comparison. This high value for the activation energy for the deactivation of the nucleant does not support any of the proposed mechanisms suggested by Crosley and Mondolfo (1971). Rather than the destruction of high order

planes, the motion of lattice defects or vacancies, or the dissolution of the nucleant, the deactivation effect seems truly to be a chemical reaction. One possible reaction which could account for this is the oxidation of an impurity metal as shown in Equation (10). All that this requires is that the metal be more chemically

$$Sn_3O_4 + \text{metal} = \text{metal oxide} + Sn \qquad (10)$$

active than tin.

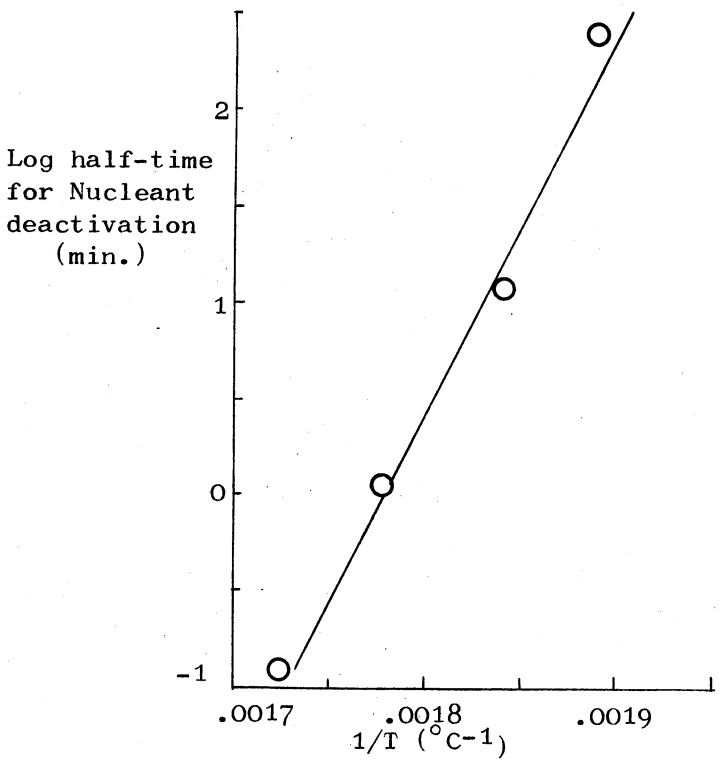

Figure 50. The Relationship Between the Nucleant Deactivation Rate and the Superheat Temperature

TABLE XIII

ACTIVATION ENERGIES FOR VARIOUS REACTIONS

Reaction	Activation Energy eV	cal/mole
Migration of interstitial in Ni (Melvor, Kronmiller, and Seeger, 1965)	1.03	9,280
Migration of vacancies in Ni (Melvor, Kronmiller, and Seeger, 1965)	1.46	13,200
Migration of interstitial in Cu (Manintveld, 1952)	.20	1,810
Migration of vacancies in Cu (Manintveld, 1952)	.88	7,960
Decomposition of Cl_2 (Shaw, 1968)		
$CaO + Al_2O_3 = CaAl_2O_4$	4.79	43,300
$CaO + SnO_2 = CaO \cdot SnO_2$	9.4	85,000
$PbO + PbSiO_3 = Pb_2SiO_4$	6.78	61,300
Deactivation of nucleant in Baker tin	4.00	36,200

CHAPTER IX

RESULTS OF THE SOLIDIFICATION OF TIN AND TIN ALLOYS IN GLASS LINED COPPER MOLDS

Three series of alloys were solidified in glass lined copper molds, tin-only, tin-29% lead, and an unmixed combination of the two. This third combination provided for a gradual change through the sample from one composition to the other.

Tin-Only

The external appearance of the tin-only samples solidified in the glass lined copper molds (GLCM) was similar in many ways to the samples solidified in pyrex ones. The surfaces were smooth and shiny. A slightly darker shade was sometimes seen on the sample top, otherwise the samples were free of apparent oxidation. Numerous circular depressions were found on the sides adjacent to the mold must have resulted from general shrinkage throughout the sample.

One important difference was apparent. There were parallel ridges in the tops of only those samples cooled in the glass lined copper molds. The ridges seemed to form first and become prominent when the freezing liquid contracted away from them. Some samples cooled in the pyrex molds did display porosity in their tops, but without a pattern.

The number of ridges and the spacing between them depended on

the temperature of the cooling bath. When low temperature baths were used the samples had no ridges. Warmer cooling baths produced samples first with raised spots, and then with a few ridges. As the temperature of the cooling baths were made still warmer the number of ridges seen increased. This variation can be seen in part in Table XIV.

TABLE XIV

RIDGES FOUND IN GLCM TIN SAMPLES

Bath Temperature (T_b) (°C)	$T_e - T_b$ (°C)	Number of Ridges
217	15	15
207	25	11
205	27	8
184	48	1

The microstructures of the pyrex and GLCM samples were examined by sectioning and compared. It was found, through continued etching with 2% nital, that a new structure was resolved. This structure occurred in several of the pyrex mold samples and in all but one of the GLCM samples. The most dramatic evidence of this is shown in Figure 51.

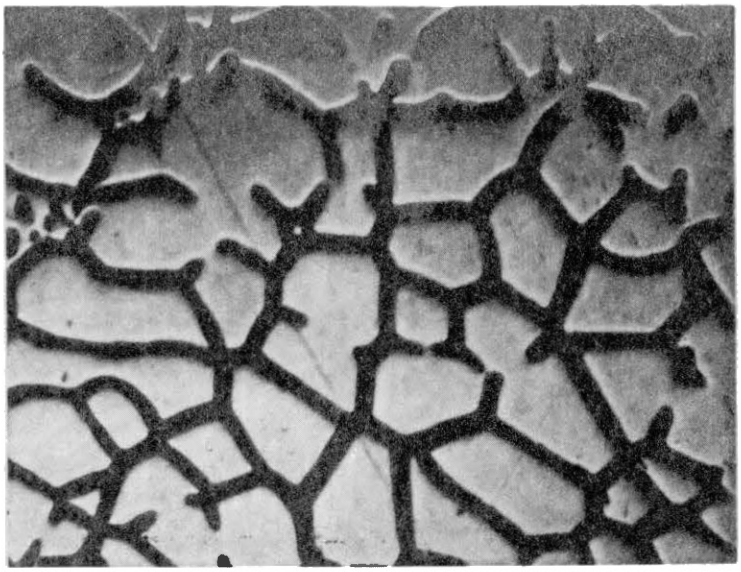

Figure 51. Etched-up Impurities in Tin. A Pyrex Mold Was Used and the Sample Was Treated With $AgNO_3$. Nital Etch. X50

The new structure is attributed to the etching-up of impurities that had collected at the cell boundaries during solidification. The difference between it and the typical structure, shown in Figure 11, occurs because of grain growth following solidification. The influence of impurities is apparent in the GLCM samples as the high purity sample (98% MRC and 2% Baker) was the only one free of this kind of structure. The occurrence of this in the pyrex mold samples was not as easily explained.

A comparison was made of the histories of the pyrex mold samples having and not having the new structure. Many solidification parameters were found that were common to each group. Therefore, superheat, tin source, the type of liquid cover, the cooling rate, the amount of supercooling, and the number of thermal cycles were eliminated as major

factors. However, oxides present in varying amounts depending on the cleaning steps of each individual sample could have been responsible for the differences.

Feest and Doharty (1973) over-etched their nickel-copper samples and were able to reveal the inter-arm dendrite spacing because of the impurity effects of the minor phase. The purer portions appeared bright in contrast to darker regions where impurities rejected during solidification were found. Similarly, the impurity outlines seen in tin were formed during freezing. Then, since there was neither time or temperature enough for them to be dissipated by diffusion, they remain and serve to define the as-cast structure.

The long impurity-bounded dendrites seen in Figures 52 to 55 were typical of those found in the GLCM samples. They formed parallel arrays, and appeared to grow from one surface most of the way across the sample. The orientation of the arrays, diagrammed in Figure 56 seemed to be random, but they were directly related to the ripples on the sample top. Quite possibly the dendrites grew as "flat dendrites" (O'Hara, 1967), since the [1,1,0] direction (the direction of growth for tin (Iyer and Youdelis, 1972)) has no equivalent Z-dependent direction in the body centered tetragonal structure. Growth in the Z direction would be slow. Figure 57 shows the tin crystal structure along with some of the important planes and directions.

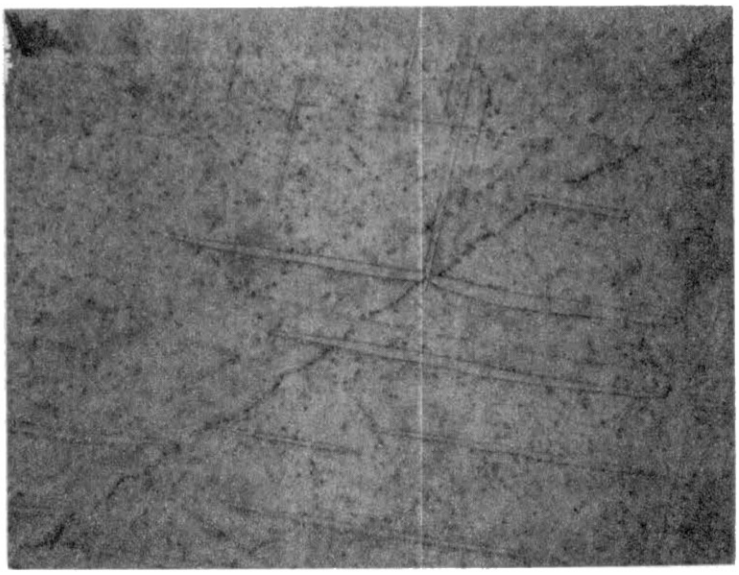

Figure 52. GLCM Tin Sample Showing Long Dendrite-like Structure Outlined by Impurities. T_b = 203°C. X62.5

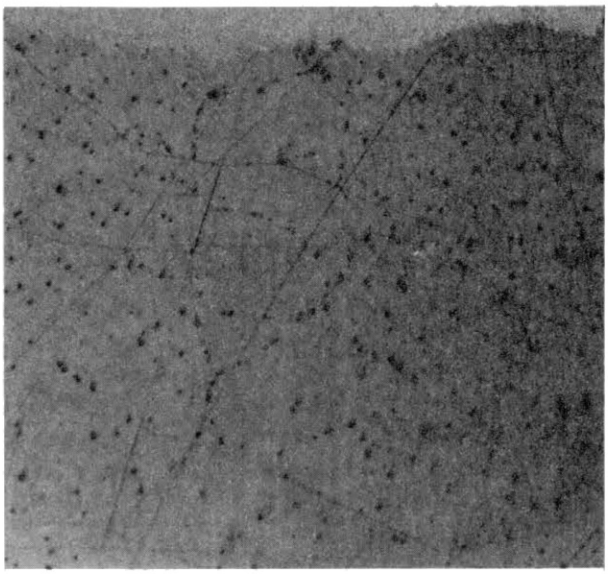

Figure 53. GLCM Tin Sample Showing a Single Linear Dendrite With Segmented Parts. T_b = 118°C. X60

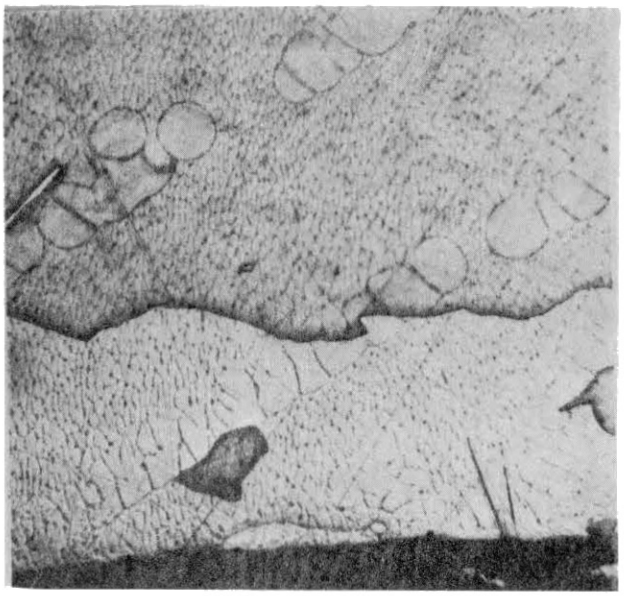

Figure 54. GLCM Tin Sample Showing Parallel Segmented Dendrites. $T_b = 167^{\circ}C$. X60

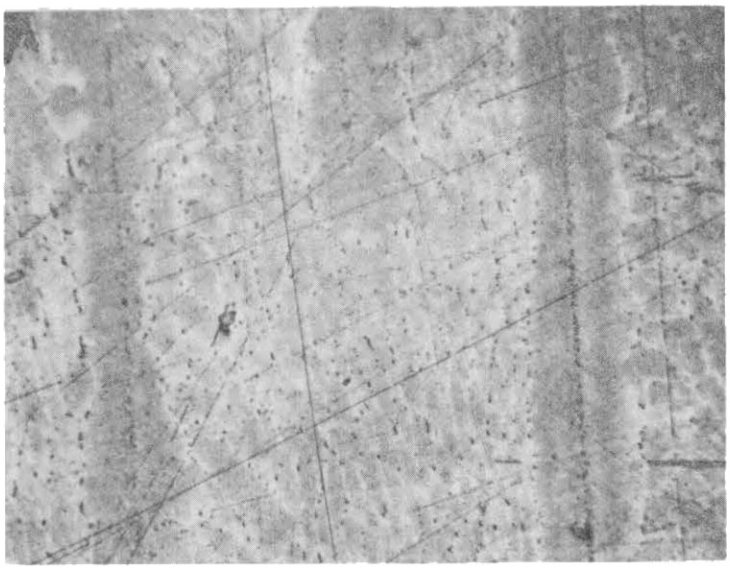

Figure 55. GLCM Tin Sample Showing Continuous Parallel Dendrites. $T_b = 205^{\circ}C$. X50

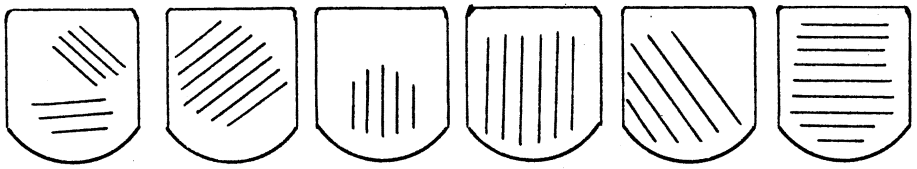

Figure 56. Orientation of Parallel Dendrites

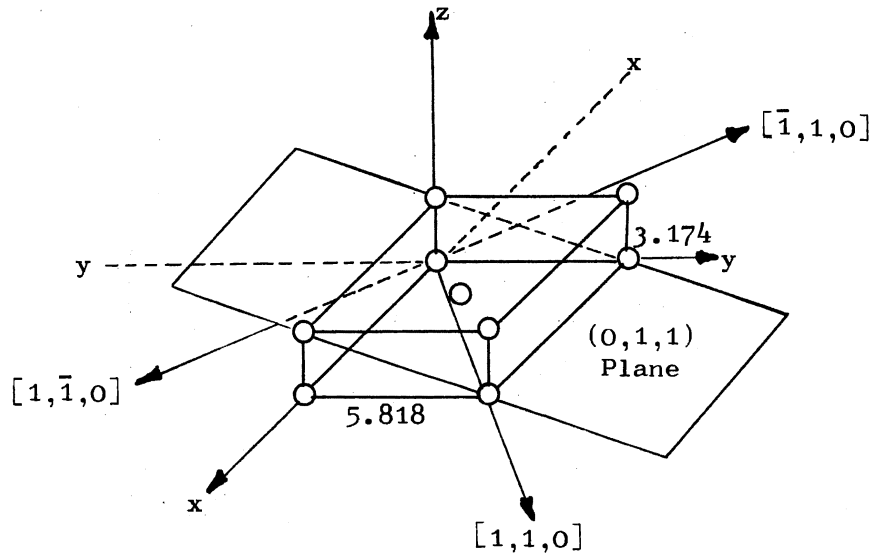

Figure 57. Body Centered Tetragonal Structure for Tin

A "flat dendrite" would form if a primary dendrite growing in the [1,1,0] direction would develop closely spaced side arms in the equivalent [1,$\bar{1}$,0] and [$\bar{1}$,1,0] directions. O'Hara (1967) observed primary dendrites 12° from the [1,1,0] direction and secondary ones also 12° from the expected [1,$\bar{1}$,0] and [$\bar{1}$,1,0] directions. These dendrite forms are consistent since the 12° deviation arises out of O'Hara's crystal pulling technique and the non-isotropic heat flow characteristics of tin. The practice of deliberately sectioning the samples perpendicular

to the plane of the ridges could have caused proposed flat dendrites to appear to be linear.

Differences between these dendrites and the ones found in the pyrex mold samples can be explained by considering the solidification conditions of the GLCM samples. Here the temperature gradient in the liquid was nearly flat at the time of nucleation. Normally an appreciable gradient exists across the liquid at first. The cooling curves (Figures 15 and 17) point this out. For a pyrex mold the slope of the cooling curve is steep, even for the slowest cooling rates. Hence, there must have been a significant gradient in the liquid. The temperature of reversal was determined at various locations in a single sample to verify this and a slope of 25°C/cm was found for the slow cool case.

In contrast, the cooling curves for the GLCM samples at the time of nucleation were almost flat. They remained this way, often for several minutes, while the sample cooled slowly (about 1°/min). Some temperature gradient must have been present in the GLCM samples which were cooled rapidly because the cooling curves are not all flat. Nevertheless, it is a much smaller gradient than in the pyrex mold samples because the rate of heat loss is greater. Only about 15 grams, pyrex mold and all, are being cooled in the first case. In the second the 100 gram glass lined copper mold must be cooled along with the sample. While the cooling curves look the same the solidification of the sample in the GLCM in several times faster.

While growth in both kinds of samples is dendritic, the nature of the growth is quite different. A one dimensional approximation of the temperature gradient ahead of a growing dendrite was made using the method of finite differences. This appears in Appendix D and shows that

the temperature gradient ahead of the dendrite stays much higher if the initial temperature in the liquid is constant, rather than hotter the further in one goes. Heat, therefore, is better transferred away from the growing GLCM dendrite, and control of growth by this factor becomes of less importance. The rate of growth becomes more dependent on the accommodation factor for the competing growth planes, and those with favorable ones experience the more rapid growth.

If one assumes that the accommodation factors vary from a maximum value for the [1,1,0], [1,$\bar{1}$,0], and [$\bar{1}$,1,0] to a low value for any growth having a Z component the high speed growth observed in this work would produce a flat crystal composed of a central primary dendrite with sets of side arms not unlike a feather. Of the three growth directions shown in O'Hara's work (1967), the type which grew 24° up from the primary dendrite occurred less often than the secondary dendrites which grew 88° off to each side.

The feather explanation is consistent with macroscopic observations of the sample tops. A transition was seen from a raised spot to a set of spots to a complete ridge as higher cooling bath temperatures were used. A small temperature gradient exists in the liquid when the cold baths are used and dendritic growth into the sample is slowed. At first only the primary dendrite reaches the surface. Then with warmer and warmer baths the gradient is less, and more of the side-arms reach the surface. Finally, a ridge is formed.

The spacing and parallel character of the "flat dendrites" is the most difficult phenomena to identify and define. Since the spacing decreases when the cooling rate is lower (the bath is warmer), independent nucleation of each dendrite plane cannot be a factor. Further

evidence that the planes must grow dependently is the parallelism observed. No independent or random process can account for it, and yet the planes are relatively far apart (0.5 to 2mm), and there is no apparent connection.

Two mechanisms are suggested that could account for this growth. In one the planes are assumed to be connected by a primary "trunk" dendrite which heretofore has escaped detection. In the second, each additional plane is nucleated by cavitation in the liquid which occurs after the first plane grows.

Factors supporting the first explanation are (1) that discovery of a trunk would not be automatic (see Figure 58), and (2) that the parallelism could readily be explained. In order to simply identify a trunk the section would have to intersect it in a plane coincident with its axis. This is especially unlikely since the trunk would not be expected to grow at right angles to the planes. For example, a growth direction having a Z component might be expected to occur in the [1,0,1] direction. The most likely intersection between an observation plane perpendicular to the dendrite planes would be an ellipse. It is conceivable that such an ellipse is seen in Figure 52. According to this explanation, the [1,0,1] growth direction would accommodate the slow growth of a trunk after the primary dendrite and its side arms had completed one plane. When the trunk extended beyond the area where recalescense had increased the local temperature a second primary dendrite would be formed. This would produce a second parallel plane as the secondary dendrites grew too. For warm baths the flat temperature distribution would enhance the growth of the oblique dendrite and a second plane could form sooner, at a point closer to the initial one. The weakness of this approach is the

failure to establish so far the existence of a trunk.

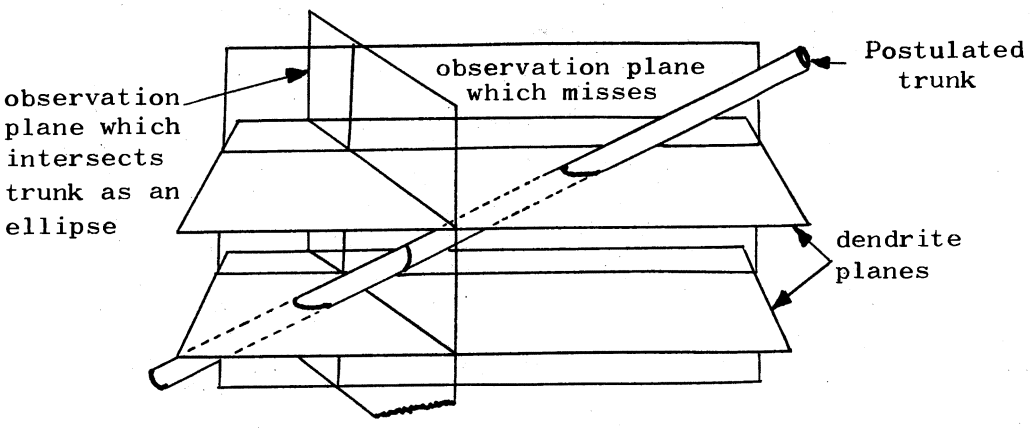

Figure 58. Intersections Between a Postulated Dendrite Trunk and Possible Observation Planes

The cavitation theory is appealing because it would explain how two unconnected planes could be formed in a dependent way. As postulated, the extremely rapid growth of the first plane would cause a large decrease in the pressure immediately adjacent to it. A planar cavity would form momentarily and then collapse causing a plane pressure wave to travel away from the first solid. At the same time heat released during solidification would be conducted away producing a temperature gradient perpendicular to the plane. Figure 59 depicts the suggested gradient and traveling wave. Nucleation would occur some distances away where the effect of the decrease in pressure would offset the local increase in temperature. This idea would explain adequately the different spacings seen for different bath temperatures. The cold bath causes

rapid cooling and results in a temperature gradient in the liquid. The tail of the temperature distribution would be raised and nucleation of the second plane would occur at a greater distance, or not at all. The weakness of this approach is in its failure to provide a mechanism for the orientation of the second plane parallel to the first.

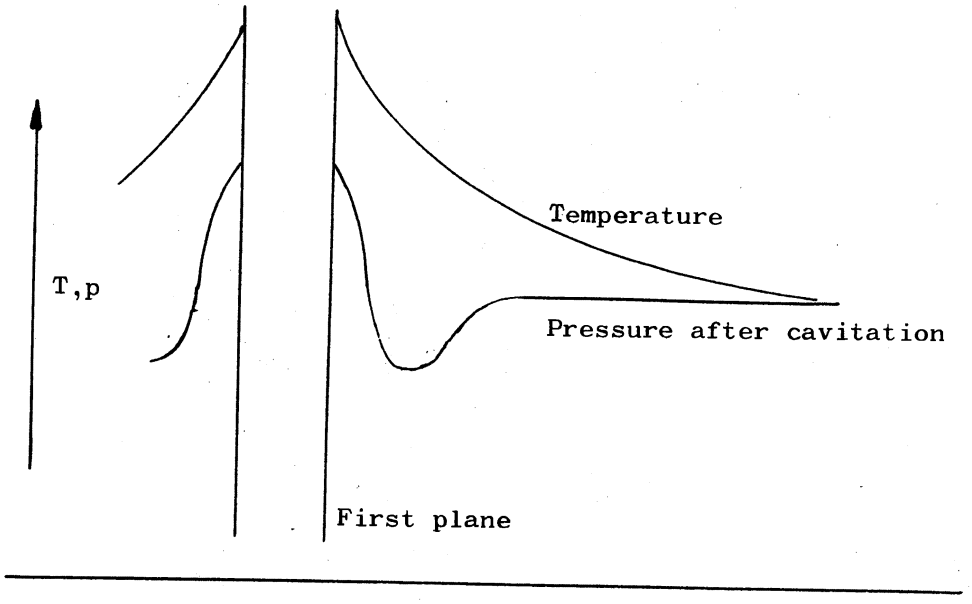

Figure 59. Suggested Temperature and Pressure Changes Caused by Growth of the First Plane

The segmented structures seen in Figures 53 and 54 are probably better representatives of the actual shape of the as-solidified dendrites than the continuous ones. The segmented structures are seen in the samples cooled most rapidly. Where the baths were warmer, annealing of the dendrites to form a platelet would more easily occur. Feest and Doherty (1973) reported such an effect.

The central line of impurities in the "continuous" dendrites may also be the result of the two hour anneal in the cooling bath. Iyer and Youdelis (1972), using an electron probe microanalyzer, have shown that solute content is highest in the center of dendrites solidified from an undercooled melt. Such an area may have acted as an impurity sink during annealing. This was then developed by the thorough etching technique.

One especially curious feature seen best in Figure 54, portraying the most rapidly cooled sample, is the existence of the "rice-grain" structure in the space between the dendrites. This structure is definitely related to the surfaces of the dendrites because the rice grains are all lined up around the edges of them. Again, two possible explanations are apparent. One is that repeated nucleation occurs just ahead of the existing solid because of cavitation. The second, suggested by Leychkis and Mikhaylov (1970) is that nucleation occurs in chain-reaction fashion, each solid crystal serving as a model for the formation of the one next to it. A choice between the two models cannot be made based on this work alone.

One other curiosity is the existence in one sample of unrelated dendrites. While this might have been due to an inadvertant mechanical disturbance, that cannot be established without further work.

Tin - 29% Lead

Five samples of tin - 29% lead alloy were prepared from a single original mixture and solidified in a glass lined copper mold. Two parameters were varied, the amount of time each sample was soaked slightly above its equilibrium temperature, and the temperature of the

liquid metal bath in which it was cooled. Table XV gives these solidification conditions and the results of some microhardness measurement averages.

TABLE XV

SOLIDIFICATION PARAMETERS FOR TIN - 29% LEAD

Sample	Superheat		Soak		Cooling		Indent Diameter*	Vickers Hardness
	Temp °C	Time min	Temp °C	Time min	Temp °C	Time min	μm	Kg/mm^2
127	290	120	212	0.5	115	5	50.4	11.0
128	290	120	212	5	115	5	49.8	11.2
129	290	120	212	50	115	5	50.0	11.1
130	290	120	212	0.5	150	5	48.2	12.0
131	290	120	212	50	150	5	48.0	12.1

*A 50 gm load.

The composition of the alloy was determined by measuring its density by an immersion technique. A check of this value was made by performing a random point count analysis of the resulting eutectic structure. This showed the eutectic composition to be 25.3 ± 4.3 volume or 33.1 ± 4.3 weight percent lead. These values do not disagree beyond the margin of error inherent in the analyses.

Three significant characteristics were seen in the samples, individual lead dendrites, an apparently discontinuous eutectic, and a dendrite free zone at the top of each sample. The microstructures are

shown in Figures 60 and 61. Figure 62 is an enlargement which shows some of the unusual eutectic structure.

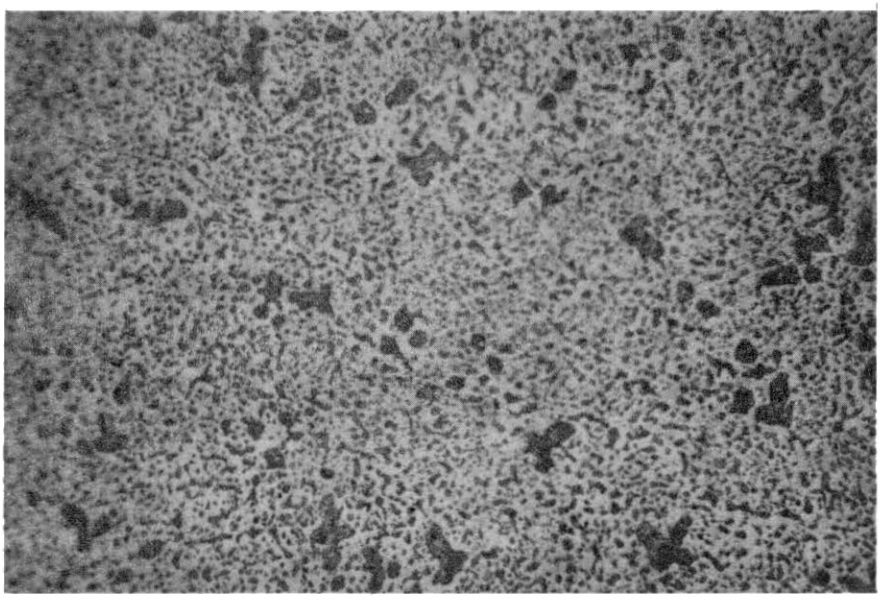

Figure 60. Tin - 29% Lead Sample Showing Lead Dendrites and Anomalous Eutectic. X60

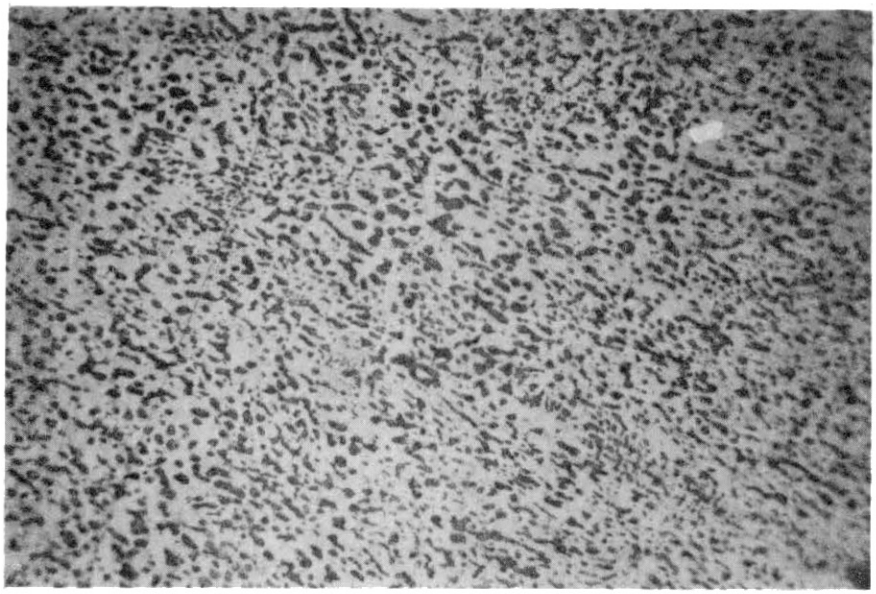

Figure 61. Tin - 29% Lead Sample Showing the Dendrite Free Region Found at the Top. X60

The formation of lead dendrites in a tin-rich alloy (the eutectic composition is 38.1 weight percent lead) can occur if the tin supercools substantially and the lead does not. The alloy would cool until it reached an extension of the lead liquidus. Then lead would be nucleated. The assumed undercoolings do apply in this case, as Baker tin undercooled 36°C after substantial superheating, and the lead did not supercool at all.

Following this line of reasoning, shown in Figure 63, the lead is nucleated at point A and grows dendritically as the composition of the melt changes to point B. The solution becomes even more rich in tin and the undercooling increases until tin is nucleated. Coupled eutectic growth follows as Powell and Hogan (1967) predicted it would if the first phase had acted as a nucleant.

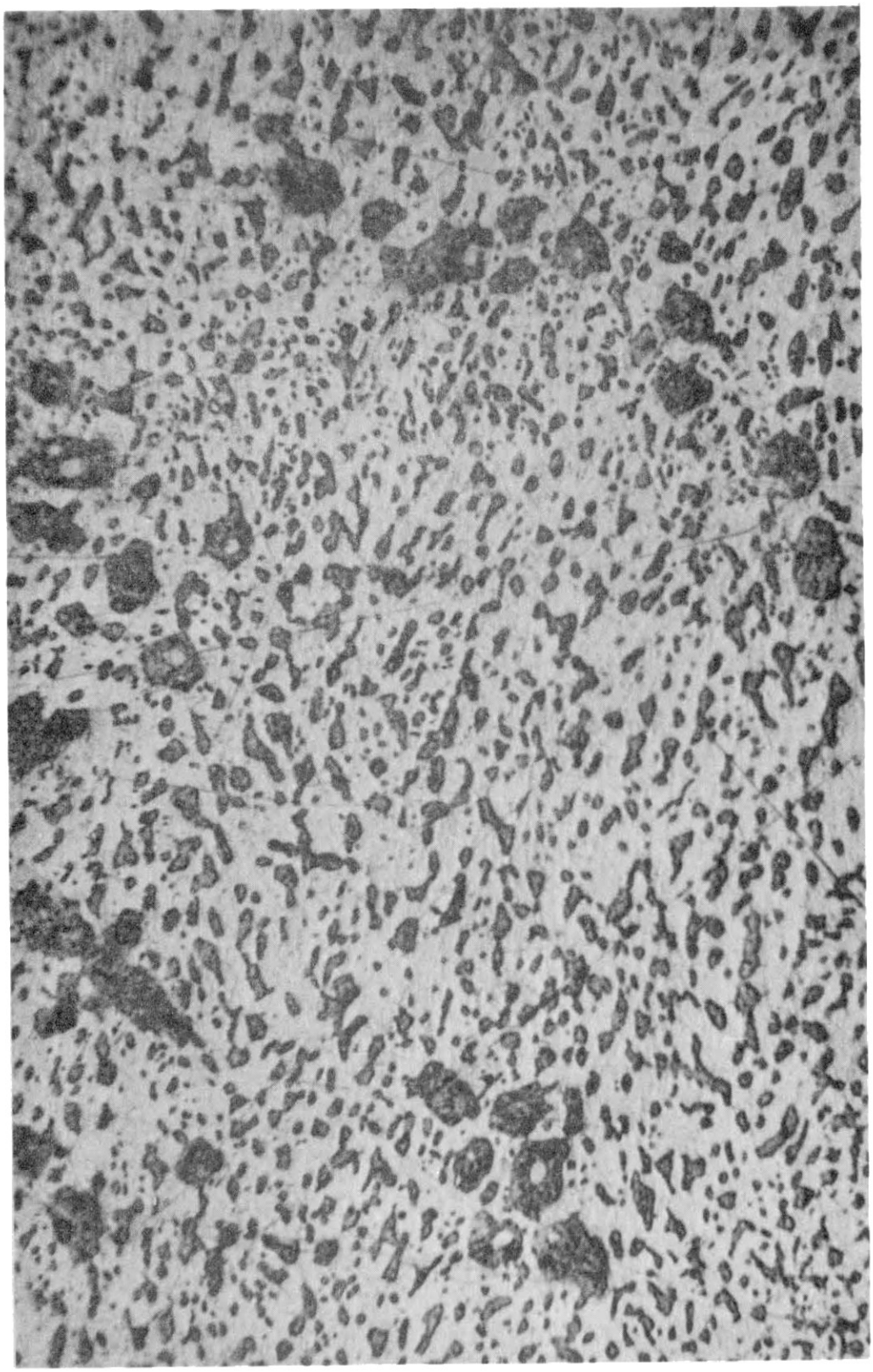

Figure 62. Enlarged View of Tin - 29% Lead Sample.
X60 enlarged 2.7 times

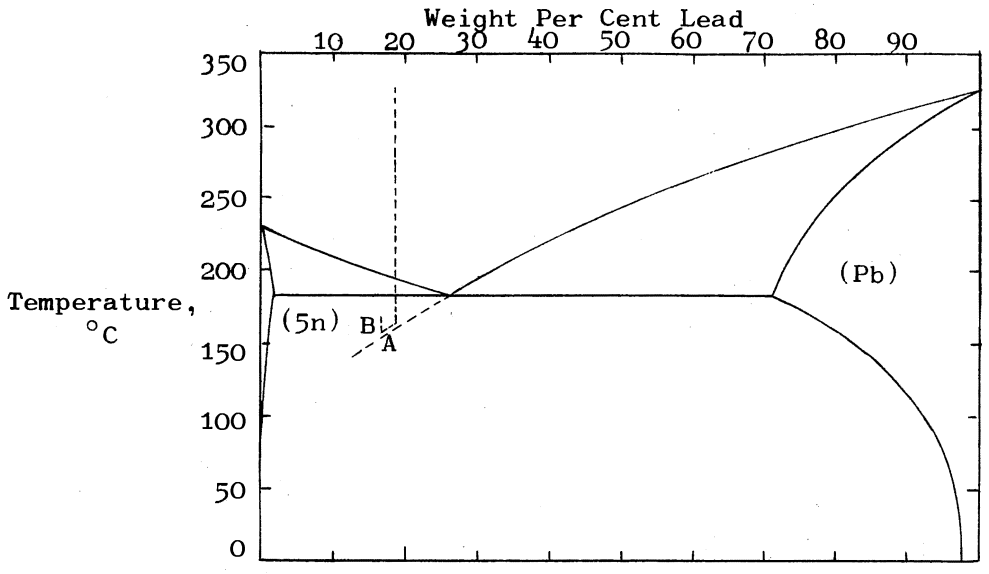

Figure 63. Mechanism for the Formation of the Tin - 29% Lead Samples

By taking repeated photographs of the same locality, identified by a microhardness indent, after polishing off 5 to 10 micrometers and re-etching with 2% nital, it was shown that the dendrites were connected locally. No long range relationship could be seen this way however, and the lack of a consistent orientation is further evidence that the dendrites are independent.

The complete dendrite size is estimated to range from 75 to 150 μm and the number density was determined to vary from 20 to 80 per cm^3. Since nucleation of lead was obviously heterogeneous, this latter number also corresponds to the number density of nucleants effective at the nucleation temperature.

For comparison, three eutectic samples were solidified in a pyrex test tube inside of a copper mold. Three different cooling programs

were used, pouring the melt into a room temperature mold, pouring into a hot mold and then air cooling, and pouring into a hot mold and following with a furnace cool. This variation in cooling rate had several effects. First, the size of the lead dendrites varied from 10 to 10^2 to 2×10^3 μm for the furnace cooled sample. Secondly, the number of nuclei varied in an opposite way, from about 1.5×10^2 to 9×10^7 to 3000 per cm^3. Finally, there was a significant change in the structure across the first two samples, varying from coarse along the mold walls to fine in the center. In all three cases, the eutectic in the center formed a cellular structure. Figures 64, 65, and 66 show the microstructure of these three samples.

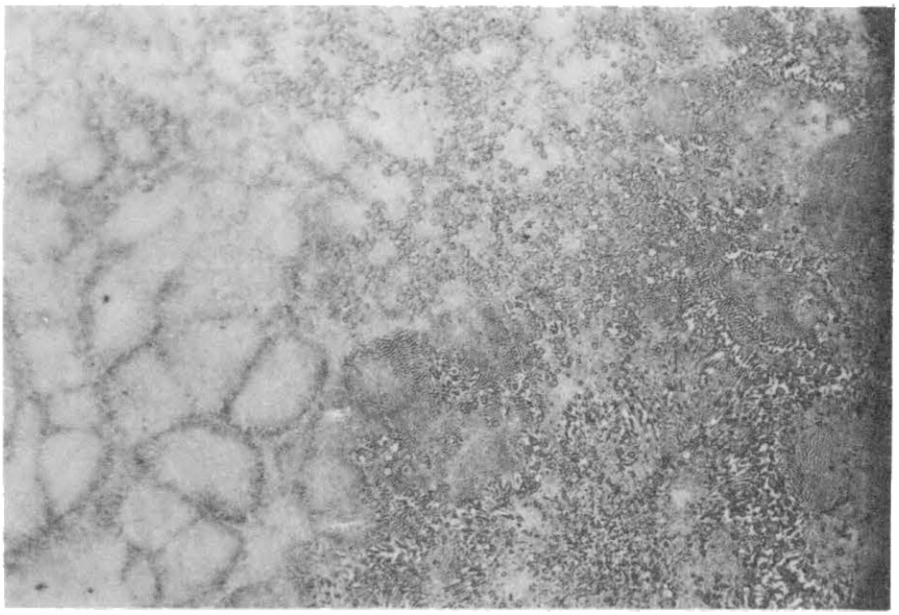

Figure 64. Eutectic Lead-Tin Sample Poured Into a Cold Mold. X60

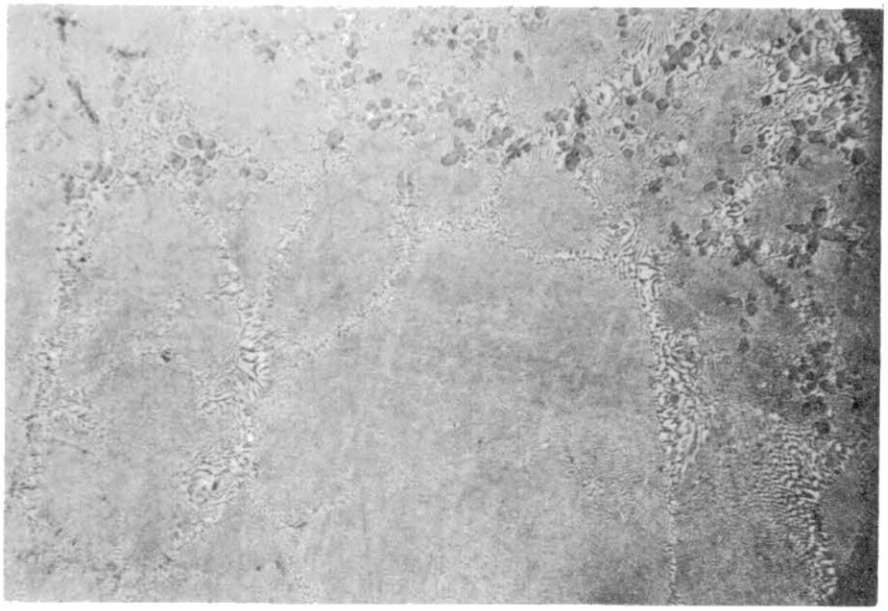

Figure 65. Eutectic Lead-Tin Sample Poured Into a Hot Mold and Air Cooled. X60

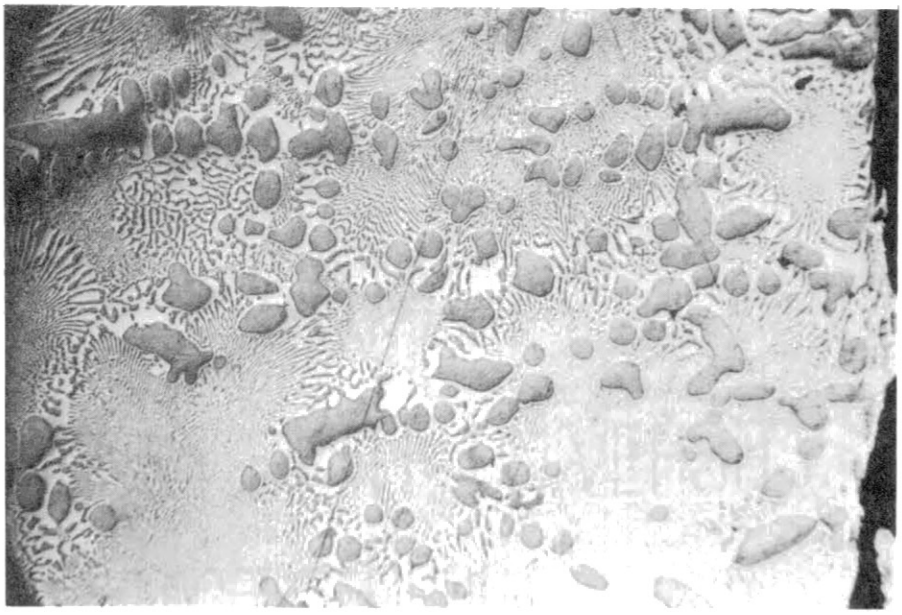

Figure 66. Eutectic Lead-Tin Sample Furnace Cooled. X60

These three samples reinforce the solidification model presented in Chapter II and show the effect of the temperature gradient in the liquid at the time of nucleation. In the furnace cooled sample the lead was nucleated at or near the surface. The slowness of the cooling permitted the lead to grow extensively with little supercooling so that comparatively few nucleants became effective. Even though the temperature gradient was very small the inward growth of the first lead dendrites was limited by the rate of heat removal and the outward diffusion of lead. The continued growth of lead caused more undercooling of tin until it was nucleated too.

At the intermediate cooling rate the growth of the first lead crystals was not fast enough to suppress further cooling and more nucleants became effective. Again, the lead grew dendritically until the tin was nucleated. However, this nucleation and growth was limited to the coolest areas in the sample. The center stayed hot and was completely free of lead crystals. A direct comparison between samples shown in Figures 60 and 65 show a much greater density of lead dendrites in the eutectic sample (while the dendrite sizes are comparable). This would be expected since the eutectic sample, 9% richer in lead would have to proceed farther along the extended lead liquidus before nucleation of tin could occur.

Large numbers of very fine lead crystals were formed in the sample poured into a cold mold, again because of the cooling rate over-ride. The initial dendrite growth had been too slow to reverse the cooling trend. Tin nucleation occurred early, before the center of the sample had cooled to the eutectic temperature, and as a result, no lead crystals are found there.

The existence of the dendrite free region at the top of the GLCM samples can be explained in a parallel way by referring to Figure 65. The hottest part of this sample had no lead dendrites so, by analogy no dendrites would be expected in the hottest part of the GLCM samples. Figure 67 which shows the macrostructure of a GLCM shows the direction of growth to be inward and upward, thus the hottest part and the last to solidify is the top. The variation in size of the dendrite free region from about 2 mm in depth for samples cooled quickly to 6 mm for the slowly cooled ones is consistent with this explanation. Heat transferred from the liquid cover, which acts as a heat source, is more effective in keeping the sample top hot when the cooling rate is slow.

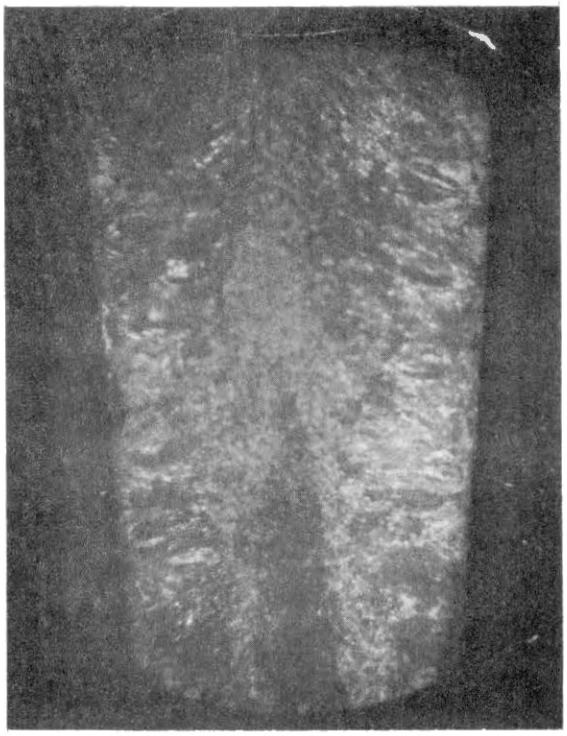

Figure 67. The Macrostructure of a Tin-29% Lead Sample. X5

The eutectic in the GLCM samples is unusual. Its microstructure is coarse and anomalous, and no cellular growth pattern is evident. The taking of successive photographs after polishing gives evidence that the lead particles in the eutectic are not independent as they appear to be. Powell and Colligan (1969) reported this structure in SnBi and PbSb systems, and Kattamis and Flemings (1970) established the continuity of the minor phase. Successive sections shown in Figure 68 show that the lead portion of the eutectic is continuous, as expected in anomalous eutectics.

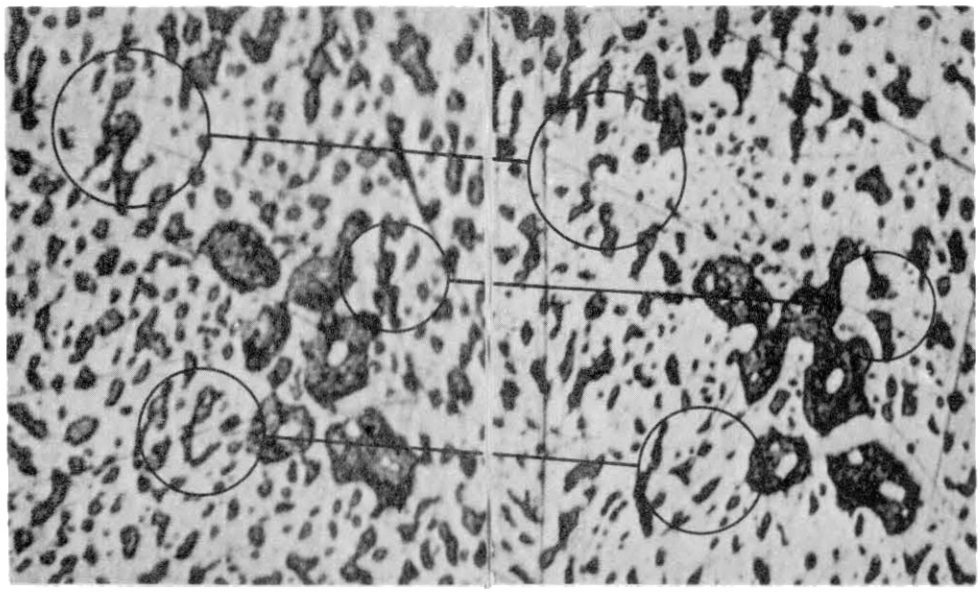

Figure 68. Successive Sections of Tin-29% Lead Sample Showing Local Continuity of the Minor Phase in the Eutectic. X60 enlarged 2.7 times

The unusual structure is attributed to an inequality in the growth

rate of the two components. The slower growing phase is lead which is growing essentially at its liquidus, while tin is highly supercooled. This slow growth of lead cannot accommodate all the solute-rich liquid rejected by the fast growing tin. The growth of tin is slowed as a result so that lethargic diffusion processes can take up part of the slack caused by the slow growth of lead.

The difference in eutectic structure between Figures 60 and 65 may be explained if the areas where the solution is tin-enriched are assumed to be local. Such areas, appearing in the second figure next to the lead dendrites are similar in structure to the GLCM eutectic and any differences may be accounted for by differences in the cooling rate. Apart from these areas however, the bulk of the GLCM sample is 9% tin enriched, and the eutectic sample is not enriched at all. Here the GLCM sample is much coarser, even though the cooling rate is faster, and no cellular structure is seen.

The first effect arises from the need to have increased interface supercooling for eutectic solidification, mentioned earlier, and the second from different rates of solidification. The cellular structure seen in Figures 64 and 65 is attributed to a decrease in the local growth rate at the end of the solidification process. Such a decrease occurs when the balance between the release of the heat of fusion and the rate of heat removal is upset. In the pyrex-cooled samples where the heat loss was slower, the release of heat during the late stages of growth had a relatively large effect. In the GLCM on the other hand, the rate of heat removal was several times faster and the heat of fusion could be removed effectively without causing the growth rate to slow.

In summary, large portions of the tin-29% lead samples cooled

31° to the extended lead liquidus, and lead was nucleated at about 162°C. The lead grew dendritically until local areas became enriched in tin and were effectively supercooled as a result (i.e., the liquidus is higher for richer tin solutions). Tin was eventually nucleated and grew with the lead to form an anomalous eutectic structure. The additional diffusion required to accommodate the solubility of each component in the other caused the structure to be fairly coarse. Finally, the sample top, which had never cooled to the extended lead liquidus, solidified as eutectic only.

Unmixed Combination

Mixtures of tin and tin-29% lead were made by adding the former to the latter and melting in the GLCM. The two hour heating time was not sufficient to allow for diffusion to achieve complete mixing, and the heaviest liquid was on the bottom. As a result, the samples had a vertical composition gradient. Two initial mixes were made using 85% and 95% tin, the balance being Tin-29% Lead. Cooling was done at four temperatures. The results shown in Figures 69 through 71 show tin dendrites growing through a solute poor zone at the top, down through regions increasingly richer in lead. Solidification ended at the mold bottom where some interdendritic porosity was found. Although not apprent in these pictures, the dendritic structure continued to the top of the sample and could be revealed by continued etching.

These samples were different on all points from both the tin-only and tin-29% lead series. The lack in these samples of any of the distinctive features found in the other alloys is attributed to two factors, the constitutional undercooling of the tin rich liquid, and

insufficient undercooling of tin to allow lead to nucleate first. Constitutional effects prevent the growing dendrites from seeing a flat temperature distribution ahead, and the presence of lead, according to O'Hara (1967), increases the chances for the formation of additional grains.

Tin must have been nucleated first. The top of the sample was composed of almost lead-free tin (with a T_3 of near 232°C), while the bottom was 29% or less lead. Nucleation of the lead here, which would be expected to occur near 162°C, should not be considered credible. It would require the top part of the sample to be ~~cooled nearly~~ 70°C or the temperature gradient in the sample to be steep. Neither of these cases were observed in this work.

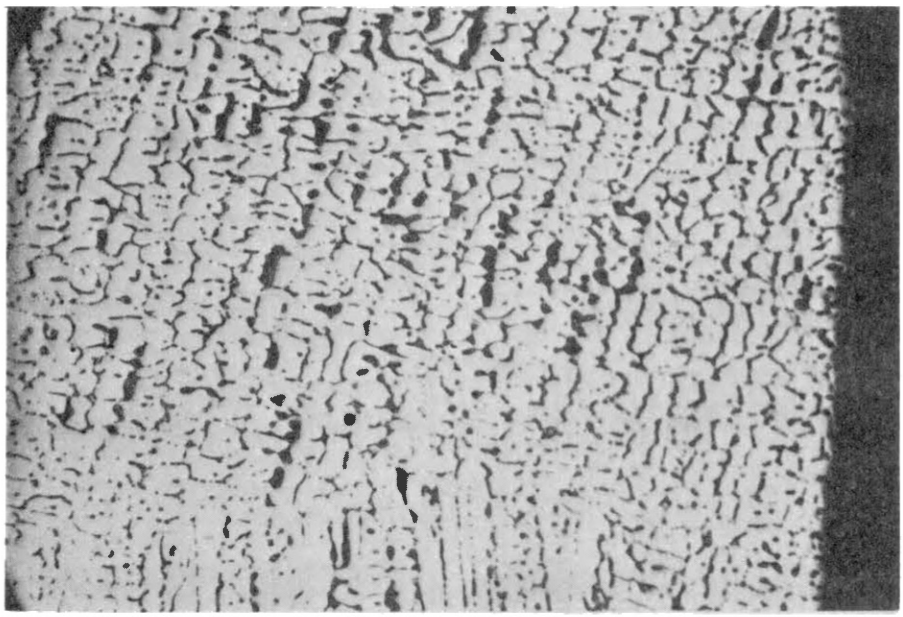

Figure 69. A Middle Section of a Sample of the Lead-tin Mixture. T_b = 180°C. X60

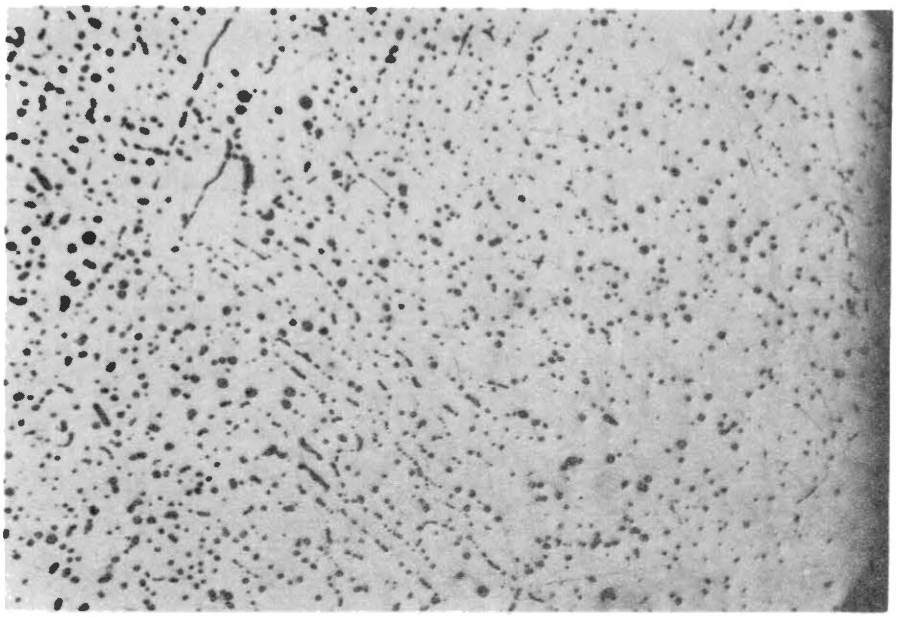

Figure 70. Top Section of a Sample of the Lead-Tin Mixture Showing Reduced Lead Composition There. $T_b = 180^\circ C$. X60

Figure 71. Middle Section of a Sample of the Lead-Tin Mixture Showing the Finer Structure Resulting From More Rapid Cooling. $T_b = 128^\circ C$. X60

CHAPTER X

CONCLUSIONS AND RECOMMENDATIONS

The examination of samples solidified in the rotating mold led to the following conclusions:

(1) Dendrite breakage was not observed in this study. Motion of crystals was only observed to occur after the crystals had grown to macroscopic sizes, and then only by virtue of overcoming the adherence between the crystal and the mold wall or the sample surface. Hence, it is doubtful that dendrite breakage plays an important part in the formation of the equiaxed zone under normal conditions of solidification.

(2) Flattening of the temperature gradient in the liquid by convection (enhanced by rotation in this work) increases the likelihood of heterogeneous nucleation away from the solid-liquid interface.

(3) The growth of minor phase dendrites can occur through the combined effects of solute rejection and centrifugation during solidification.

Conclusions arising from the study of samples solidified in pyrex and glass-lined copper molds follow:

(1) Etching-up of impurity outlines can be used to determine the as-cast structure of samples when, as in the case of

tin, substantial grain growth occurs just after solidification.

(2) Solidification in a uniformly undercooled melt begins with the rapid formation of a dendrite framework throughout the sample. The intermediate spaces are then filled in as cooling continues.

(3) In eutectic alloy systems nucleation of the minor phase can occur first, on an extension of the liquidus. This happens if the major phase experiences substantial undercooling and the minor phase does not. When the major phase is finally nucleated growth of an anomalous eutectic results. Its composition is significantly different from that of eutectic formed under equilibrium conditions.

Suggestions for Further Work

There are a number of areas where a follow-up of this work appears to have value. They are enumerated as follows:

(1) The range of the rotating mold data could be expanded, by providing for intermediate quenching of the sample and by testing pairs of alloys on opposite sides of a eutectic.

(2) The technique for driving off oxygen by heating the sample under a glass slag could be applied to tin to try to achieve bulk undercoolings greater than 36°C and to identify the nucleation catalyst effective there.

(3) A technique could be developed for measuring, and then

controlling the effective nucleant distribution. An alloy similar to the tin-29% lead alloy used in this work could be employed since the first phase to solidify is the minor one.

(4) The small uniform crystals found in the as-cast tin-only samples (described as rice grains) could be studied to determine the mechanism for their formation. Solidification parameters could be varied, and the change in size and orientation observed.

SELECTED BIBLIOGRAPHY

Barker, N. J. W., and A. Hellawell.

1974 "The Peritectic Reaction in the System Pb-Bi." Metal Science, VIII (October), 353-356.

Bartenev, G. M.

1970 The Structure and Properties of Inorganic Glasses. Groningen, Netherlands: Walters Noordoff.

Bradshaw, F. J., M. E. Gasper, and S. Pearson.

1958 "The Supercooling of Gold as Affected by Some Catalysts." Journal of the Institute of Metals, LCCCVII, 15.

Burden, M. H., and J. D. Hunt.

1975 "A Mechanism for the Columnar to Equiaxed Transition in Castings or Ingots." Metallurgical Transactions A, VI (January), pp. 240-241.

Cech, R. E., and D. Turnbull.

1951 "Microscopic Observation of the Solidification of Cu-Ni Alloy Droplets." Journal of Metals (March), 242-243.

Chalmers, Bruce.

1964 Principles of Solidification. New York: John Wiley and Sons, Inc.

Chell, M. F., and H. W. Kerr.

1972 "Anomalous Structures in Eutectic Alloys." Metallurgical Transactions, III (July), 2002-2004.

Chernov, A. A.

1973 "Crystallization." Annual Review of Materials Science, III 397-454.

Cline, H. E.

1967 "Lamellar Stability in Lead-Tin Alloys." Transactions of the Metallurgical Society of AIME, CCXXXIX (October), 1489-1492.

Cline, H. E., and J. D. Livingston.

1969 "High Speed Directional Solidification of Sn-Pb Eutectic Alloys." Transactions of the Metallurgical Society of AIME, CCXXXXV (September), 1987-1992.

Cole, G. S., and G. F. Bolling.

1967 "Enforced Fluid Motion and the Control of Grain Structures in Metal Castings." Transactions of the Metallurgical Society of AIME, CCXXXIX (November), 1824-1835.

Crosley, P. B., A. W. Douglas, and L. F. Mondolfo.

1968 "Interfacial Energies in Heterogeneous Nucleation." Iron Steel Institute, 110, 10-17.

Crosley, P. B., and L. F. Mondolfo.

1971 "Heterogeneous Nucleation." The Metallurgical Society of AIME, Paper F71-4.

Crossley, F. A., R. D. Fisher, and A. G. Metcalfe.

1961 "Viscous Shear as an Agent for Grain Refinement in Cast Metal." Transactions of the Metallurgical Society of AIME, CCXXI (April), 419-420.

Danilov, V. I., and I. V. Radchenko.

1936 "Structure of Liquid Metals." Physik Z Sowjehunion, X, 260.

Dehoff, R. T., and F. N. Rhines.

1968 Quantitative Microscopy. New York: McGraw-Hill Book Company.

Doherty, R. D., E. A. Feest, and K. Holm.

1973 "Dendritic Solidification of Cu-Ni Alloys: Part I. Initial Growth of Dendrite Structure." Metallurgical Transactions, IV (January), 115-124.

Feest, E. A., and R. D. Doherty.

1973 "Dendritic Solidification of Cu-Ni Alloys: Part II. The Influence of Initial Dendrite Growth Temperature on Microsegregation." Metallurgical Transactions, IV (January), 125-136.

Fisher, H., and A. Phillips.

1954 "Viscosity and Density of Liquid Lead-Tin and Antimony-Cadmium Alloys." Transactions AIME, CC, 1060.

Frawley, J. J., and W. J. Childs.

1968 "Dynamic Nucleation of Supercooled Metals." Transactions of the Metallurgical Society of AIME, CCXXXXII (February), 256-263.

Fredriksson, H., and M. Hillert.

1972 "On the Formation of the Central Equiaxed Zone in Ingots." Metallurgical Transactions, III (February), 565-569.

Glicksman, M. E

1965 "Dynamic Effects Arising From High-Speed Solidification." Acta Metallurgica, XIII, 1231.

Glicksman, M. E., and W. J. Childs.

1962 "Nucleation Catalysis in Supercooled Liquid Tin." Acta Metallurgica, X (October), 925-933.

Hamill, W. H., and R. R. Williams, Jr.

1959 Principles of Physical Chemistry. Englewood Cliffs, N. J.: Prentice-Hall, Inc.

Hansen, Max.

1958 Constitution of Binary Alloys. 2nd ed. New York: McGraw-Hill.

Holloman, J. H., and D. Turnbull.

1953 "Nucleation." Progress in Metal Physics, IV, 333-388.

Hunt, J. D., and J. P. Chilton.

1963 "An Experimental Investigation of the Undercooling at the Solid/Liquid Interface of the Lead-Tin Eutectic." Journal of the Institute of Metals, XCII, 21-25.

Hunt, J. D., and K. A. Jackson.

1966 "Nucleation of Solid in an Undercooled Liquid by Cavitation." Journal of Applied Physics, XXXVII, 254.

Iyer, S. P., and W. V. Youdelis.

1972 "Effect of Cooling Rate on Supercooling." Journal of the Institute of Metals, C, 372-373.

Jaffey, D.

1975 "The Importance of Solute-Induced Interdendritic Fluid Flow in Macrosegregation." Metal Science, IX (January), 13-17.

Jakob, Max, and Georga A. Hawkins.

1957 Elements of Heat Transfer. New York: John Wiley & Sons, Inc.

Johnston, M. H., and D. H. Baldwin.

1974 "The Influence of Acceleration Forces on Nucleation. Solidification, and Deformation Processes in Tin Single Crystals." Metallurgical Transactions, V (November), 2395-2399.

Jones, B. L.

1971 "Growth Mechanisms in Undercooled Eutectics." Metallurgical Transactions, II (October), 2950-2951.

Jordan, R. M., and J. D. Hunt.

1972 "Interface Undercoolings During the Growth of Pb-Sn Eutectics." Metallurgical Transactions, III (June), 1385-1390.

Kattamis, T. Z., and M. C. Flemings.

1970 "Structure of Undercooled Nickel-Tin Eutectic." Metallurgical Transactions, I, 1449-1451.

Kattamis, T. Z., and R. Mehrabian.

1974 "Highly Undercooled Alloys: Structure and Properties." Journal of Vacuum Science Technology, XI (Nov./Dec.), 1118-1121.

Kehl, George L.

1949 The Principles of Metallographic Laboratory Practice. New York: McGraw-Hill, Inc.

Langenbert, F. C., G. Pestel, and C. R. Honeycutt.

1961 "Grain Refinement of Steel Ingots by Solidification in a Moving Electromagnetic Field." Transactions of the Metallurgical Society of AIME, CCXXI (October), 993-1001.

Lashko, A. S., and A. V. Romanova.

1961 "X-Ray Investigation of the Structure of Liquid Alloys in Eutectic Systems." Izrest. Akad. Nauk. SSSR, Met. 1 Topl, 135-138.

Leychkis, D. L., and N. V. Mikhaylov.

1970 "Physiochemical Features of Crystallization of Metallic Melts in a Vibration Field." Physics of Metals and Metallography, XXIX, 91-97.

McLeod, A. J., B. L. Jones, and G. M. Weston.

1971 "Dendrite Remelting in Relation to Grain Refinement." Journal of the Australian Institute of Metals, XVI (June), 124-126.

Manintveld, J. A.

1952 "Recovery of the Resistivity of Metals After Cold Working." Nature, CLXIX (April), 623.

Mascre, C.

1971 "Supercooling and Solidification Nuclei in Metals and Alloys." Mem. Sci. Rev. Met., LXVIII (April), 131-142.

Melvor, H., H. Kronmiller, and A. Seeger.

1965 "The Recovery of Nickel Above Room Temperature." Physics Status Sol., X (August), 728.

Miroshnichenko, I. S., and G. P. Brekharya.

1970 "Influence of Cooling Rate on the Supercooling of Metal Melts." Physics of Metals and Metallography, XXIX (March), 233-234.

Morrison, R. T., and R. N. Boyd.

1960 Organic Chemistry. Boston: Allyn and Bacon, Inc.

O'Hara, S.

1967 "Controlled Growth of Tin Dendrites." Acta Metallurgica, XV (February), 231-236.

Orrok, T.

1958 "Dendritic Solidification of Metals." (Unpublished Ph.D. Thesis, Harvard University.)

Powell, G. L. F.

1965 "The Undercooling of Silver." Journal of the Australian Institute of Metals, X, 223.

Powell, G. L. F., and G. A. Colligan.

1969 "Nucleation in Undercooled Ag-Bi, Pb-Bi, and Sn-Bi Alloys." Transactions of the Metallurgical Society of AIME, CCXXXV (September), 1913-1915.

Powell, G. L. F., and L. M. Hogan.

1968 "The Undercooling of Copper and Copper-Oxygen Alloys." Transactions of the Metallurgical Society of AIME, CCXXXXII (October), 2133-2138.

1969 "The Influence of Oxygen Content on the Grain Size of Undercooled Silver." Transactions of the Metallurgical Society of AIME, CCXXXXV (February), 407-412.

Richards, R. S., and W. Rostoker.

1955 "The Influence of Vibration on the Solidification of an Aluminum Alloy." Presented at the 37th Annual Convention of the American Society of Metals, October 17 to 21.

Rosenberg, A., and W. C. Winegard.

1954 "The Rate of Growth of Dendrites in Supercooled Tin." Acta Metallurgica, II, 342.

Samuels, L. E.

1971 Metallographic Polishing by Mechanical Methods. New York: American Elsevier Publishing Co., Inc.

Scripov, V. P., V. P. Koverda, and G. T. Butorin.

1972 "Kinetics of Crystal Growth in Small Volumes." Mechanism i. Kinetika Rosta Crystallizatsii. Erevan: VSES Sovesh Chanie Rostu Kristallov, 4th Conference, 1, 74-77.

Shaw, Kenneth.

1968 Principles of Solid State Chemistry. London: MacLaren and Sons, ltd.

Southin, R. T.

1966 "The Influence of Low-Frequency Vibration on the Nucleation of Solidifying Metals." Journal of the Institute of Metals, LXXXIV, 401-407.

Strangman, T. E., and T. Z. Kattamis.

1973 "Gravity Segregation During Remelting of Dendritic Alloys." Metallurgical Transactions, IV (September), 2219-2221.

Streat, N., and F. Weinberg.

1972 "Pipe Formation in Pb-Sn Alloys." Metallurgical Transactions, III (December), 3181-3184.

1973 "Authors Reply." Metallurgical Transactions, IV (October), 2474-2475.

1974 "Macrosegregation During Solidification Resulting From Density Differences in the Liquid." Metallurgical Transactions, V (December), 2539-2548.

Sundquist, B. E., and L. F. Mondolfo.

1961 "Heterogeneous Nucleation in the Liquid-to-Solid Transformation in Alloys." Transactions of the Metallurgical Society of AIME, CCXXI (February), 157-164.

Swartzbeck, G., and T. Z. Kattamis.

1973 "Fatigue Behavior of Aluminum-Copper Alloy Exhibiting a Duplex Dendritic Structure." Metallurgical Transactions, IV (November), 2667-2669.

Takahashi, T., and W. A. Tiller.

1969 "The Supercooling Dependence for Nucleation of Some Metals on the Liquid Drop Size." Acta Metallurgica, III (May), 647.

Tarshis, L. A., J. L. Walker, and J. W. Rutter.

1971 "Experiments on the Solidification Structure of Alloy Castings." Metallurgical Transactions, II (September), 2589-2597.

Tiller, W. A.

1962 "Grain Size Control During Ingot Solidification. Part II: Columnar-Equiaxed Transition." Transactions of the Metallurgical Society of AIME, CCXXIV (June), 448-459.

Trivedi, R.

1970 "Growth of Dendritic Needles From a Supercooled Melt." Acta Metallurgica, XVIII (March), 292.

Turnbull, D.

1950 "Correlation of Liquid-Solid Interfacial Energies Calculated From Supercooling of Small Droplets." Journal of Chemical Physics, XVIII, 769.

1952 "Kinetics of Solidification of Supercooled Liquid Mercury Droplets." Journal of Chemical Physics, XX (March), 411-424.

Turnbull, D., and R. E. Cech.

1950 "Microscopic Observation of the Solidification of Small Metal Droplets." Journal of Applied Physics, XXI (August), 804-810.

Vertman, A. A., A. M. Samarin, and A. M. Yakobson.

1960 "The Structure of Liquid Eutectics. Izzvest. Akad. Nauk. SSSR, 3, 17-21.

Vonnegut, B.

1948 "Variation With Temperature of the Nucleation Rate of Supercooled Liquid Tin and Water Drops." Journal of Colloid Science, III (September), 563-569.

Winegard, W. C.

1964 An Introduction to the Solidification of Metals. London: The Institute of Metals.

Yesin, V. O., G. M. Pankin, and R. S. H. Nasyroo.

1971 "Procedure for Studying Dendrite Growth Kinetics at the Free Surface of a Supercooled Tin Melt." Physics of Metals and Metallography, XXXII (May), 121.

Youdelis, W. V., and S. P. Iyer.

1973 "Effect of Alloy Composition on Supercooling." Journal of the Institute of Metals, X (June), 176-178.

APPENDIX A

THERMOCOUPLE CALIBRATION

The melting points of five compounds were used to calibrate the thermocouple

TABLE XVI

LINEAR REGRESSION CALCULATION FOR THERMOCOUPLE CALIBRATION

Material	Thermocouple Output	ΔT	ΔT_p	$\Delta T-\Delta T_p$	$(\Delta T-\Delta Tp)^2$
$K_2G_2O_7$	82.4	375.2	378.0	-2.8	7.84
Biphenyl	10.3	48.2	47.2	1.0	1.00
N_aNO_3	62.1	284.0	284.8	-0.8	.64
$Cu(NO_3)_2 \cdot 3H_2O$	19.2	91.3	87.0	4.3	18.49
NH_4NO_3	32.2	146.8	147.8	1.0	1.00
Total	206.2	945.5			28.97

The conversion from thermocouple output to temperature was found to be $4.59^{\circ}C/mV$; and the standard error of the estimate was $2.38^{\circ}C$.

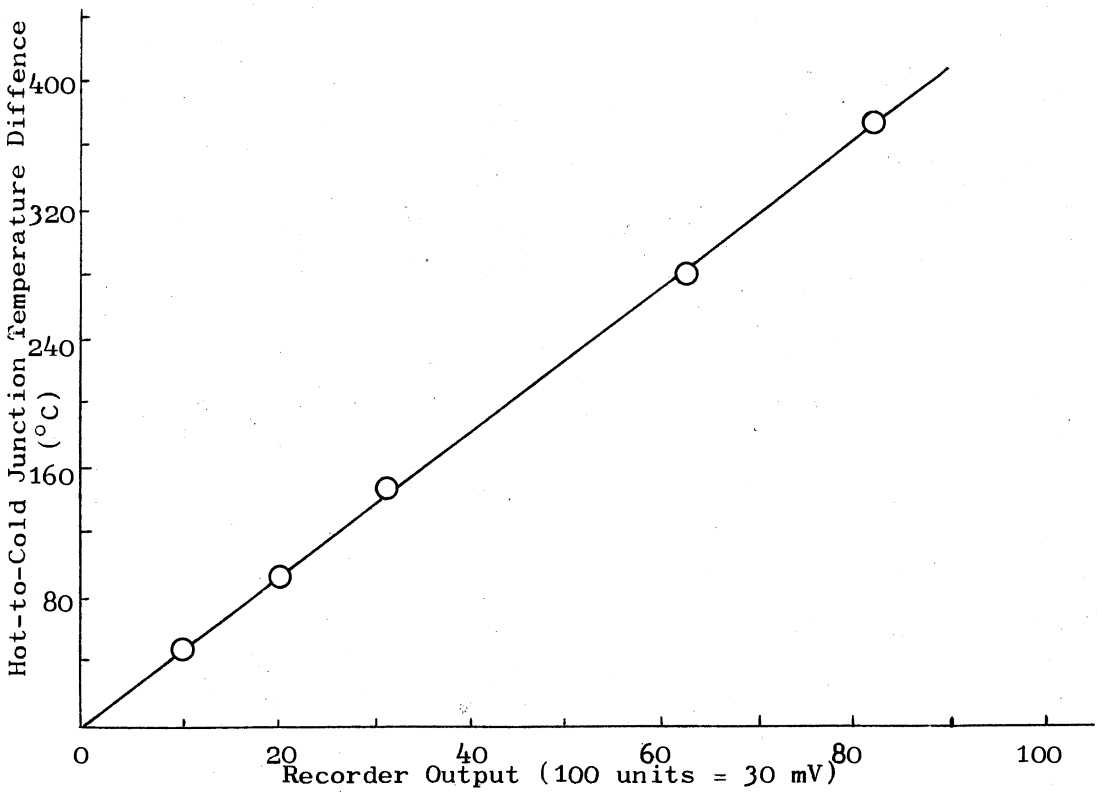

Figure 72. Thermocouple Calibration Curve

APPENDIX B

PHASE DIAGRAMS FOR SYSTEMS STUDIED

Pb-Sn

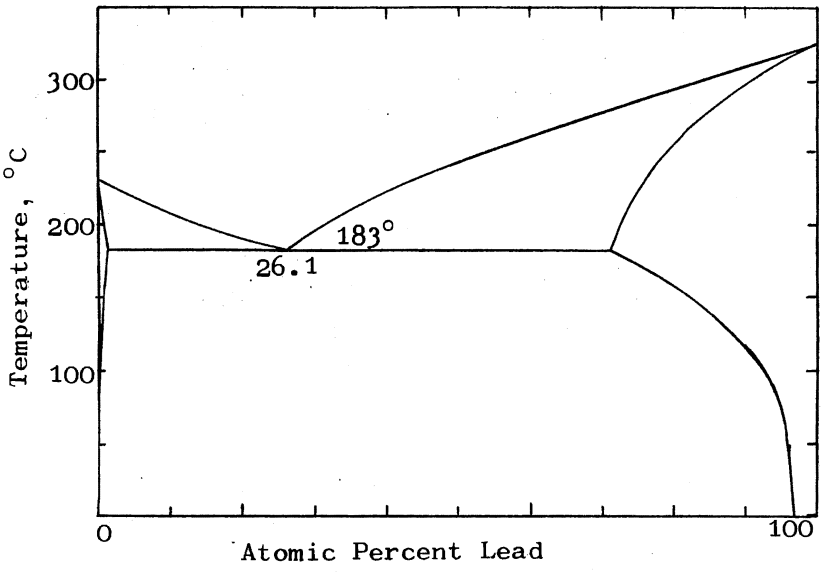

Figure 73. Pb-Sn Phase Diagram

Bi-Cd

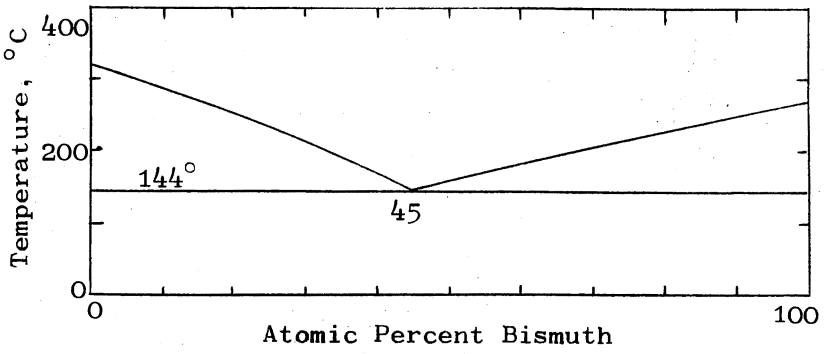

Figure 74. Bi-Cd Phase Diagram

Bi-Sn

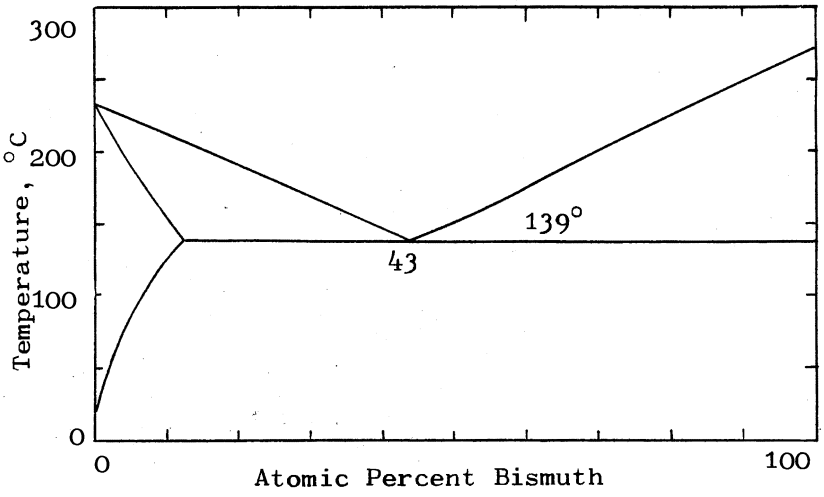

Figure 75. Bi-Sn Phase Diagram

Bi-Pb

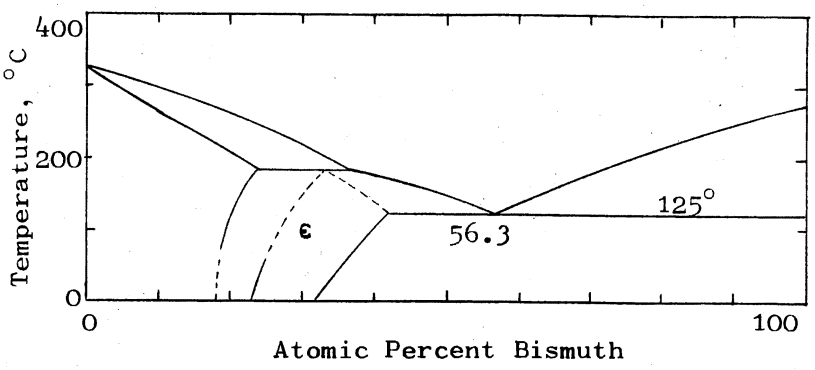

Figure 76. Bi-Pb Phase Diagram

Sn-O

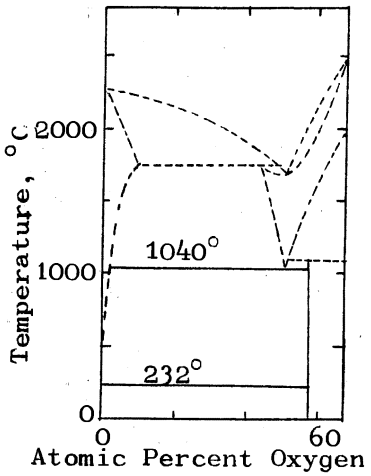

Figure 77. Sn-O Phase Diagram

Note: All phase diagrams taken from Max Hansen, Constitution of Binary Alloys (New York), 1958.

APPENDIX C

COMPUTATION OF ACTIVATION ENERGY

A linear regression equation was determined for the temperature and half-time data displayed in Figure 50.

TABLE XVII

DETERMINATION OF ACTIVATION ENERGY USING LINEAR REGRESSION

$K=1/T$	$P=\log t_{1/2}$	$K-\bar{K}$	$P-\bar{P}$	$K-\bar{K}(P-\bar{P})$	$(P-\bar{P})^2$
1.899E-3	2.15	1.65	8.8E-5	14.52E-5	7.74E-9
1.842E-3	.95	.45	3.1E-5	1.39E-5	.96E-9
1.777E-3	- .05	- .55	-3.4E-5	1.87E-5	1.16E-9
1.725E-3	-1.1	-1.6	-8.6E-5	13.76E-5	7.40E-9
				31.54E-5	17.26E-9

The slope of the equation was found to be 18,300; and the activation energy which resulted was 36,200 cal/gram-mole.

APPENDIX D

MODEL FOR GRADIENT DEPENDENT DENDRITE GROWTH RATE

Two one-dimensional solutions of the heat transfer equations were made using the method of finite differences. In one case the growth was assumed to be directed into a uniformly supercooled melt. In the second the growth was assumed to be into a constant but increasing gradient. The interface temperature was assumed to stay constant at a T_e of 100 and the slope of the temperature distribution at T_e at each time was used to determine the amount of growth.

Figures 78 and 79 show the temperatures profiles for the two cases for the odd iterations, and Figure 80 shows the temperature gradients at the interface for the two cases with time as the independent variable.

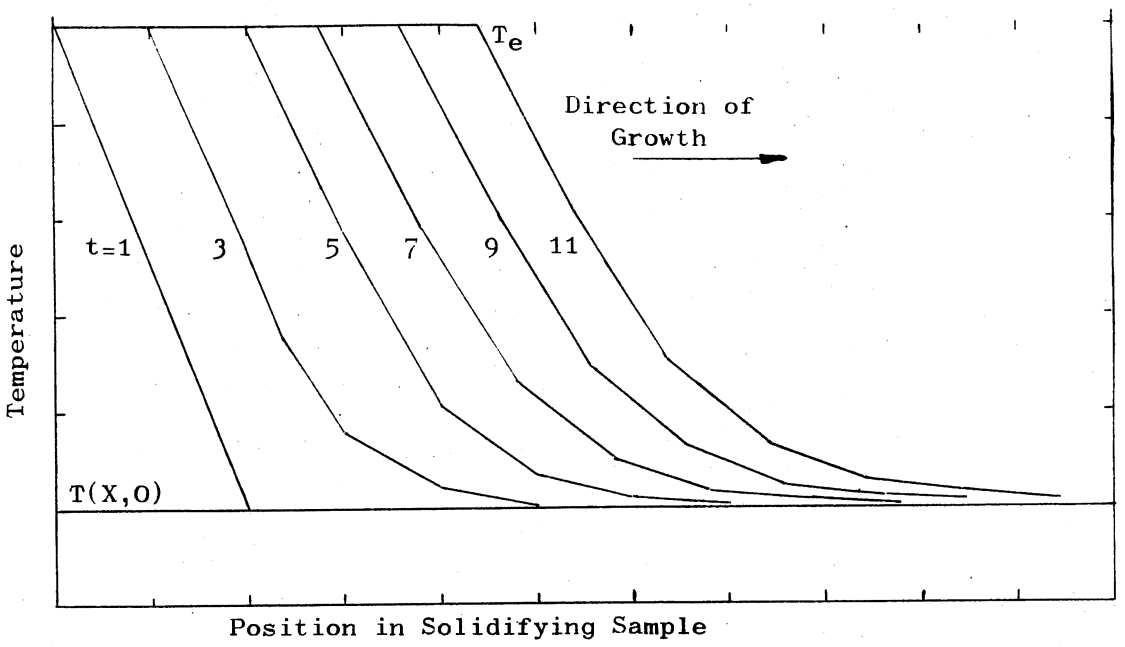

Figure 78. Temperature Profiles for Case 1

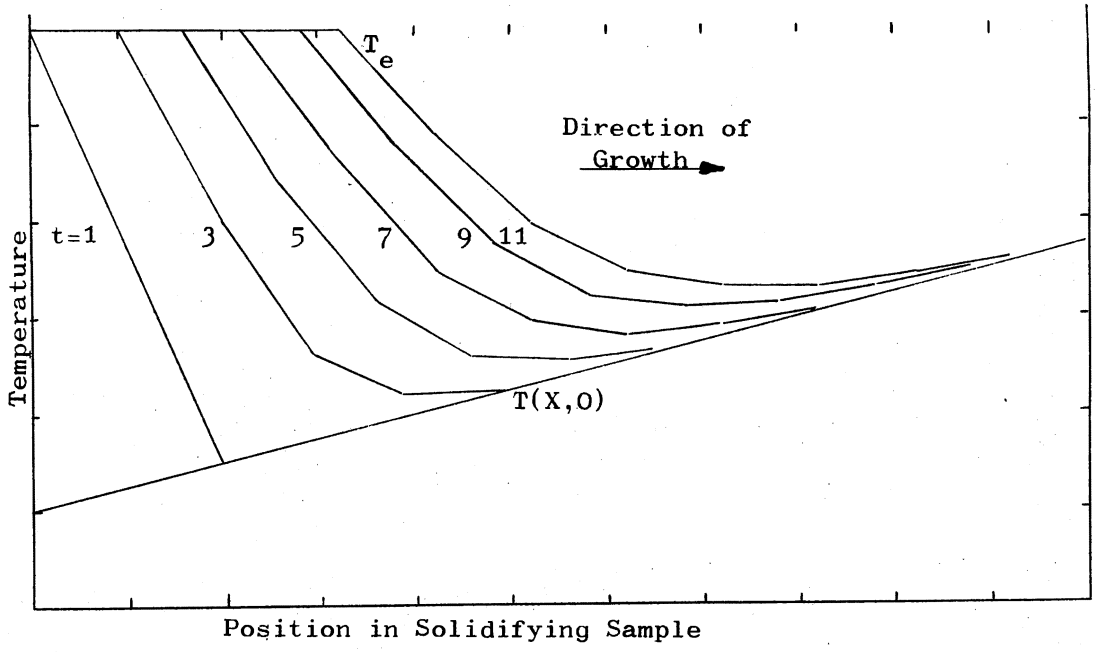

Figure 79. Temperature Profiles for Case 2

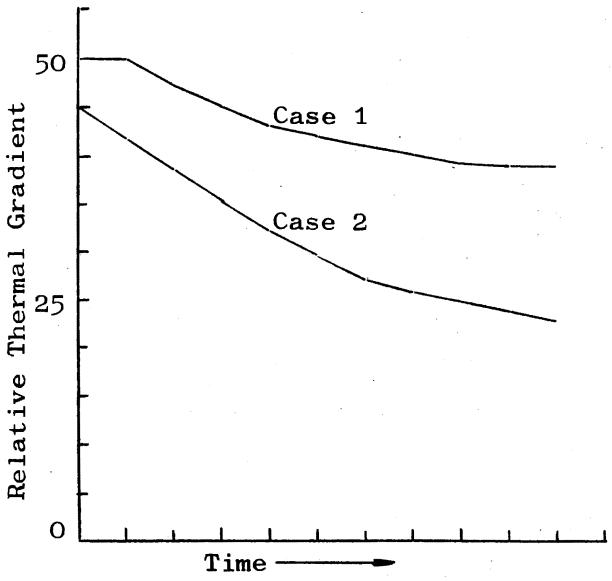

Figure 80. Comparative Thermal Gradients for Case 1 and Case 2

VITA

Kenneth John Eger

Candidate for the Degree of

Doctor of Philosophy

Thesis: RELATIONSHIPS BETWEEN PROCESS VARIATION, NUCLEATION, AND THE MICROSTRUCTURE OF CASTINGS

Major Field: General Engineering

Biographical:

Personal Data: Born in Cincinnati, Ohio, June 4, 1940, the son of Mr. and Mrs. J. L. Eger.

Education: Graduated from Western Hills High School, Cincinnati, Ohio, in June, 1958; received Chemical Engineering degree from the University of Cincinnati, in June, 1963; received Master of Science degree, majoring in Nuclear Engineering, from the University of Cincinnati in June, 1965; completed requirements for the Doctor of Philosophy degree at Oklahoma State University in May, 1976.

Professional Experience: Co-operative Engineer, Inland Manufacturing Division, G. M., 1959-63; Instructor, School of Technology, Oklahoma State University, 1965-67; Assistant Professor, School of Technology, Oklahoma State University, 1967-70; Assistant Professor and Head, Department of Radiation and Nuclear Technology, School of Technology, Oklahoma State University, 1970-73; Senior Engineer, Plant Safety and Environs Monitoring, General Electric-Midwest Fuel Recovery Plant, 1973-74; Senior Engineer, Plant Safety and Licensing, General Electric-Morris Operation, 1974-76. Member, American Nuclear Society, Health Physics Society, Certified Health Physicist, June, 1972, and Registered Professional Engineer, Illinois, 1975.